Drug Delivery Device for Bladder Disorders

by

Heejin Lee

B.S., Mechanical Engineering
Seoul National University, 2002

M.S., Mechanical Engineering
Massachusetts Institute of Technology, 2004

Submitted to the Department of Mechanical Engineering
in Partial Fulfillment of the Requirements for the Degree of

Doctor of Philosophy in Mechanical Engineering
at the
Massachusetts Institute of Technology
February 2009

Signature of Author.....
Department of Mechanical Engineering
January 9, 2009

Certified by.....
Michael J. Cima, Ph.D.
Sumitomo Electric Industries Professor of Engineering, Thesis Supervisor

Certified by.....
Ioannis V. Yannas, Ph.D.
Professor of Polymer Science and Engineering, Thesis Reader

Certified by.....
Robert S. Langer, Sc.D.
Institute Professor, Thesis Committee Chair

Accepted by.....
David E. Hardt, Ph.D.
Ralph E. and Eloise F. Cross Professor of Mechanical Engineering
Chairman, Departmental Committee on Graduate Students

Drug Delivery Device for Bladder Disorders

by

Heejin Lee

Submitted to the Department of Mechanical Engineering
on January 5, 2009 in partial fulfillment of the requirements for the degree of
Doctor of Philosophy in Mechanical Engineering

ABSTRACT

Several pathologies associated with the bladder have wide impacts on society. Overactive bladder (OAB) and interstitial cystitis/painful bladder syndrome (IC/PBS) are chronic urological conditions characterized by pain, urinary frequency, and urgency with or without urinary incontinence. The estimated prevalence of OAB and IC/PBS is more than 34 million people in the U.S. alone. The American Cancer Society estimated a total of 68,810 new bladder cancer cases and 14,100 deaths from bladder cancer in the U.S. in 2008. Treatment options include oral medications, transdermal patches and intravesical instillations of therapeutic solutions. Direct intravesical instillation is considered an effective option, especially for those who remain refractory to oral and transdermal formulations due to intolerable side effects and skin irritations, respectively. Intravesical treatment, however, requires repeated instillations due to rapid drug voiding by urination, and the frequent urinary catheterizations involve risk of urinary infection and patient discomfort.

An alternative, site-specific local delivery approach was created using a reservoir-based drug delivery device. This novel passive device was designed to release drug in a pre-determined manner once inside the bladder. The device also possesses a retention feature to prevent accidental voiding. The device can be implanted into and retrieved from the bladder by a non-surgical cystoscopic procedure. *In vivo* tests using lidocaine, a local anesthetic used for IC/PBS treatment, showed that a sustained and local treatment to the bladder can be achieved with the device. The lidocaine bladder tissue concentration was found to be a thousand-fold higher than the lidocaine plasma concentration at three and six days in a rabbit model. The device approach has the potential to achieve localized therapy to the bladder while minimizing side effects. Future studies may use the device for other therapeutic agents in the treatment of OAB, IC/PBS, and bladder cancer.

Thesis Committee
Prof. Michael J. Cima (Thesis Advisor)
Prof. Ioannis V. Yannas (Thesis Reader)
Prof. Robert S. Langer (Committee Chair)

Acknowledgements

I am grateful to my thesis supervisor, Professor Michael Cima for his guidance and generous support throughout my research project. His endless curiosity about the unknown and passion for the research has motivated me to make greater efforts. Your enthusiasm and excitement have always impressed me. I am also indebted to Professor Robert Langer and Professor Ioannis Yannas for their support and priceless advice with their supreme expertise.

I would like to thank Dr. Alison Hayward, Katie Madden, Sylvia Lesnikowski, Chris Autieri, and Catrina Wong for being helpful, patient, and supportive of me during the many hours in the animal facilities.

I would like to thank the members of Convergence Products Research Research Laboratory at MIT: Grace Kim, Hong Linh Ho Duc, Karen Daniel, Christophoros Vassiliou, Yoda Patta, Noel Elman, Dan Wesolowski, Alex Scott, Byron Masi, Irene Tobias, Yibo Ling, Lenny Rigione, and Barbara Layne. In particular, Grace Kim thankfully proofread my thesis carefully. I also should mention three summer UROP students, who contributed to the research: Mario Castillo, Lydia Marshall, and Daniel Macaya. I would also like to extend my appreciation and apologize to the experimental animals. Their sacrifice contributed to scientific knowledge and experience I gained throughout this project.

Finally, I would like to thank my family and friends for their support, understanding, and encouragement in my many moments of stress. I thank my parents for their emotional support and encouragement they have given me throughout the years. I also thank my friends, Yeunwoo Cho, Jongmin Shim, Jungik Kim, Hyungsuk Lee, Chiwon Kim, Sunho Park, and Kyung-yon Na.

Table of Contents

List of Figures

List of Tables

Chapter 1 Introduction

1.1 Background and motivation

1.1.1 Interstitial cystitis/painful bladder syndrome (IC/PBS) and overactive bladder (OAB)

Interstitial cystitis/painful bladder syndrome (IC/PBS) and overactive bladder (OAB) are chronic urological conditions characterized by pain, urinary frequency, urgency with or without urinary incontinence, and variable degrees of sexual dysfunction. IC/PBS affects about 1 million people in the US alone with 90% of them women. The quality of life of IC/PBS patients is comparable to end stage renal failure. The estimated prevalence of OAB in the US is about 33 million with the occurrence rising with age [1-4]. Patients with OAB symptoms tend to restrict their social activities to avoid public embarrassments, and the social isolation caused by OAB often leads to depression symptoms [5, 6].

Recent studies concerning IC/PBS have suggested that an inhibition of normal bladder epithelial cell proliferation leads to a loss of epithelial barrier integrity with subsequent exposure of sensory nerve cells in the bladder wall to toxic and irritating urinary constituents [7, 8]. However, there is no known cure for IC/PBS, and so current treatments are targeted to relieve symptoms. A major challenge in the treatment of IC/PBS is to deliver the appropriate medication to the bladder. The FDA-approved oral medication for IC/PBS, pentosan polysulfate sodium (PPS), is thought to help replenish the defective and denuded bladder wall. However, the bioavailability of PPS is as low as 3% [9], and recent studies have reported questionable results about the significant benefit for IC patients provided by orally administered PPS [10].

Oxybutynin is a frequently prescribed medication for OAB although orally administered oxybutynin often causes side effects. A large pre-systemic, first-pass metabolism of oxybutynin results in an oral bioavilability of only 6%. Oxybutynin metabolites appear to contribute largely

to dry mouth [11, 12], the most common side effect with oxybutynin, which is unfortunate for the patients because their desire to drink is countered by a desire to manage their urinary incontinence. A transdermal patch (OXYTROL) has been recently introduced to avoid first-pass metabolism although skin irritation leads to its low acceptance rate [13]. Skin irritation is due to the high concentration of oxybutynin required to achieve sufficient flux through the skin. The plasma level of the active metabolite N-desethyloxybutynin, the main cause of dry mouth, to its parent compound oxybutynin was 1.3:1 compared to 11.9:1 for an orally administered dose. Thus, an alternative route of administration can reduce the production of oxybutynin metabolites and, thus, can decrease the incidence of dry mouth.

Intravesical instillation of therapeutic solutions for bladder disorders is considered an effective treatment option especially to those who remain refractory to oral formulations due to intolerable side effects. A measured amount of drug solution is instilled into the bladder through a catheter, and the drug solution is held inside the bladder usually less than an hour before patients void the solution. The procedure is performed every week or repeated as needed. If the bladder is the site of the problem as in the case of IC/PBS, intravesical administration of drug solutions can diminish undesirable side effects which are commonly found in oral drug treatment for bladder disorders.

A recently introduced treatment for IC/PBS is intravesical delivery of a lidocaine solution [14, 15]. The solution contains lidocaine, heparin, and sodium bicarbonate and demonstrated immediate symptom relief as well as the sustained relief of pain and urgency with 90% effectiveness [15]. This "therapeutic cocktail" has been shown to be effective in managing pain in IC/PBS patients, but its limited duration requires frequent intravesical boluses of drug, such as three treatments per week for two weeks. While the site-specific, local delivery approach of

intravesical instillation is desirable, frequent intravesical instillation accompanied by urinary catheterization should be avoided to minimize the risk of infection and patient discomfort.

1.1.2 Superficial bladder cancer

The American Cancer Society estimates that 68,810 men and women will be diagnosed with and 14,100 will die of cancer of the urinary bladder in 2008 [16]. 70-80% of bladder tumors are non-muscle invasive tumors [17]. Recurrence following endoscopic resection of the superficial disease will occur in 50 to 70% of these cases if not followed by chemotherapy. Chemotherapeutics are administered in solution as an intravesical bolus. The patient must retain the bolus for a period of about an hour as the majority of the agent is eliminated during urination. The procedure is repeated weekly for five to six weeks. Agents include mitomycin C, ethoglucid, thiotepa, doxorubicin, epirubicin, and valrubicin [18]. The short exposure times require that the drug concentration be made as high as possible in the intravesical formulation. *In vitro* experiments with human bladder cancer cell lines have shown that concentration and exposure time are equally important. That is, the same cytotoxicity was achieved for mitomycin C, thiotepa, epodyl, and adriamycin when the exposure was 30 minutes for a given concentration or 120 minutes at one fourth the concentration [19]. Thus, the normal chemotherapeutic doses of 20 to 30 mg could be significantly lowered if the exposure time could be lengthened to days from the current thirty to sixty minutes. In addition, there is clinical evidence that current exposures are not optimized and should be increased. Patients receiving six weekly 40 mg mitomycin C administrations had twice the recurrence-free fraction at five years than patients receiving 20 mg doses [20].

1.2 Thesis objectives

The goal of this research is to develop a drug delivery device that can replace treatments requiring frequent intravesical instillations of drug solutions for patients with IC/PBS and OAB. The proposed approach is to fabricate passive, non-resorbable release devices that can be deployed and retrieved by a conventional catheterization, which is a simple nonsurgical outpatient procedure. The size of the device should be small enough to minimize patient discomfort and have a retention feature to avoid accidental voiding of the device. The objectives pertaining to developing an intravesical drug delivery device are as follows:

1) Fabricate a device that can be non-surgically implanted into the bladder (Chapter 2).

2) Perform *in vitro* drug release studies to determine parameters affecting drug release rate (Chapter 2).

3) Investigate device retention features to prevent its accidental voiding (Chapter 3).

4) Characterize drug absorption into the bladder wall (Chapter 4).

5) Perform *in vivo* drug exposure studies (Chapter 5).

6) Obtain design equations for the device for human application (Chapter 6).

Chapter 2 Device fabrication and *in vitro* drug release studies

2.1 Design concept

The drug delivery device was designed to fulfill multiple criteria. Primarily, the device must be inserted into and retrieved from the bladder through the urethra cystoscopically. This means that the device must pass through a narrow tubular path. The outer diameter of the urethral catheter for adult humans is about 14-16 Fr (4.7-5.3 mm). The device should also reduce patient discomfort and trauma to the bladder. The size of the device was minimized. The outer surface of the device, furthermore, should be soft and smooth without sharp edges or tips. It is desired that the device has a density less than urine or water so that it can float inside the bladder to keep the device from touching the sensitive trigone region near the bladder neck. The device should have a retention feature to avoid its accidental voiding during urination over the treatment period. A design that features a material with a certain elastic limit and modulus allows the device to be introduced into the bladder in a collapsed shape but then spring open once inside the bladder. A sufficient elastic modulus would prevent the device from collapsing into a linear shape and accidentally being expelled from the bladder during urination or contraction of the detrusor muscle.

One of the simplest design options is a loop-shaped device shown in Figure 1 where the device has multiple drug release orifices. The feasibility of a loop-shaped device depends on the availability of such elastic, biocompatible materials. A, large deformation will occur at two folded spots during cystoscopic insertion, and the device will return to its original loop shape after insertion for the retention of the device in the bladder.

The device may contain both multiple orifices and multiple reservoirs to release more than one type of drug. Orifices can be generated by laser ablation or drilling on a polymeric tube

wall. Figure 2 shows a device with multiple reservoirs and orifices. Spherical objects can be inserted into the tubing to create partitioned reservoirs. The elastic nature of the tubing material enables the insertion of the snugly-fitted spherical objects, whose diameter is slightly larger than the inner diameter of the tubing to create a seal between two adjacent reservoirs. The mechanism of drug release from the device is that of an osmotic pump [21]. Water (or urine) permeates through the walls of the polymer tube (semi-permeable membrane) and pushes drug particles or solution out through a micro-orifice on the polymer wall. The surface area, wall thickness, and water permeability of the tube are key factors for the drug release.

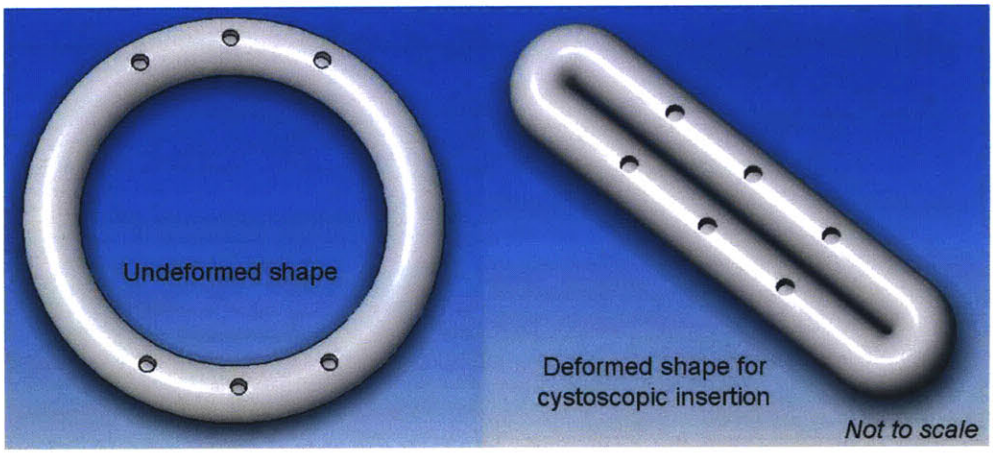

Figure 1. A loop-shaped device with multiple drug release orifices. Undeformed shape of the device after being deployed in the bladder (left). Deformed shape during cystoscopic implantation through the urethra (right).

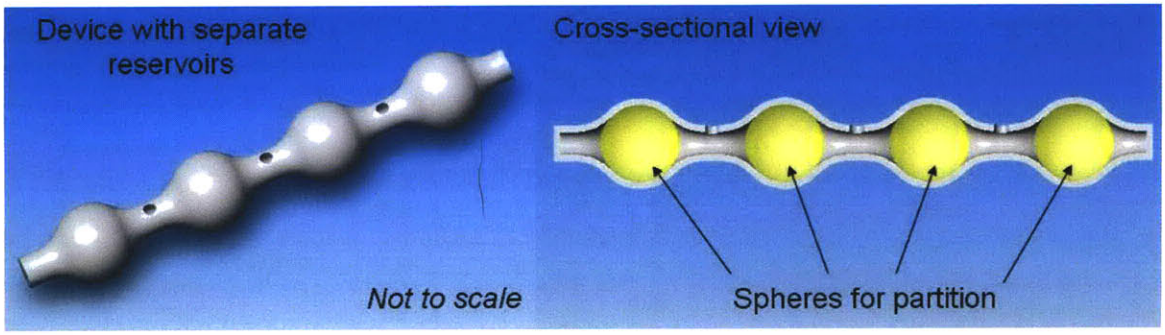

Figure 2. A device containing multiple reservoirs and orifices (left). Cross-section view of elastic polymer tubing with spheres inserted for compartmentalization of reservoirs (right).

2.2 Device fabrication methods

A solid form of drug, instead of liquid form, was loaded into the device to maximize the payload within a given volume. Chondroitin 6-sulfate or chondroitin sulfate C (CSC) is a sulfated glycosaminoglycan (GAG), and the site of sulfation is carbon 6 of the GalNAc sugar. CSC is used for the treatment of IC/PBS [22-26]. CSC (Chondroitin 6-sulfate sodium salt from shark cartilage, Sigma-Aldrich, St. Louis, MO) was cast into a cylindrical form by a solution filling and evaporation method. Silicone is highly permeable to water as the scale decreases [27, 28]. Thin-walled silicone tube (0.012"x 0.020", ID x OD, Invotec International, Inc.) was first filled with CSC aqueous solution, and then the solution was allowed to dry at room temperature while keeping the tube straight. The length of the tube filled with CSC solution decreased while evaporation of water proceeded. Figure 3 shows the final product obtained after the evaporation procedure. The length of the cast CSC depends on the initial length of tube filled with CSC solution and the solution concentration.

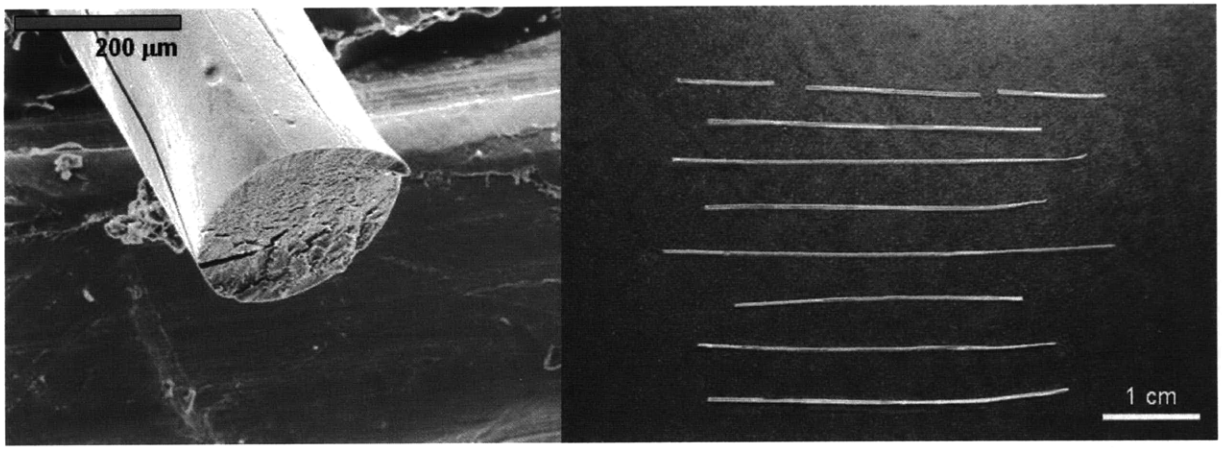

Figure 3. Cast form of chondroitin sulfate C (CSC). (Left) SEM picture of cast CSC (Courtesy of Lenny Rigione and Hong Linh Ho Duc). (Right) macro image of cast CSC.

Lidocaine and lidocaine hydrochloride (HCl) were both purchased from Sigma-Aldrich (St. Louis, MO). Lidocaine base form has a very low solubility (~ 4 mg/mL) in comparison to that of lidocaine HCl (~680 mg/mL) [29]. The HCl form was used to make aqueous lidocaine HCl solution. Tube filling followed by evaporation was performed as described for CSC. The length of the tube filled with the lidocaine solution decreased while water evaporated, but a solid lidocaine cast was not obtained at the end. Lidocaine remained as a gel form instead of a solidified form. Crystallization step for lidocaine was further introduced to the saturated lidocaine after the evaporation step [30]. A lidocaine seed crystal was inserted into either end of the tube after evaporation, and the tube was stored at 4 °C. Crystallized lidocaine was brittle compared with CSC, resulting in crystallized pieces that were less than 1 cm (Figure 4).

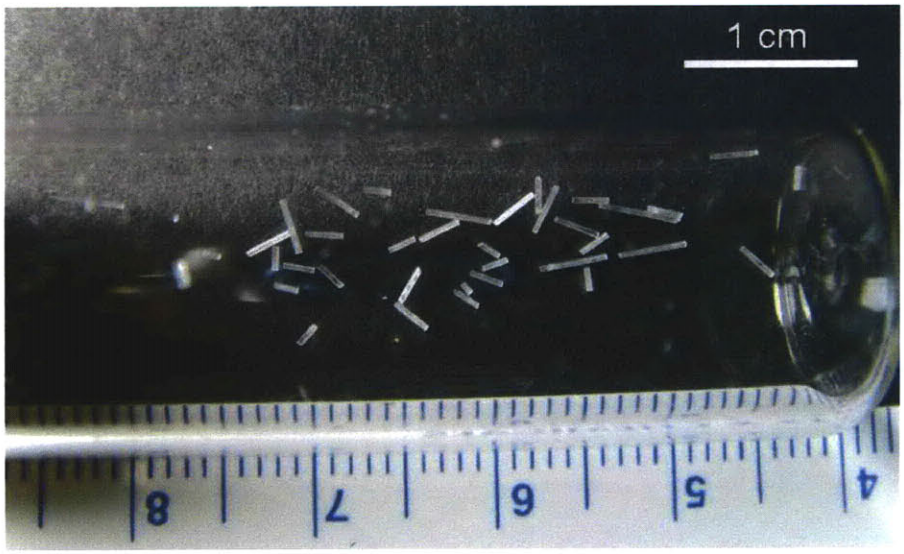

Figure 4. Crystallized lidocaine in a cylindrical form.

In vitro drug release studies were performed using silicone tube of 1 cm or 2 cm in length. The same size tube as the one where drug was cast or crystallized was used for each drug. A single piece of cast CSC was inserted into the silicone tube since long cast CSC were produced. A longer length of CSC rod was cut to 1 cm or 2 cm with a razor blade. Several pieces of crystallized lidocaine, however, were inserted into the tube to fill 1 cm or 2 cm in length. One piece of CSC rod or several pieces of lidocaine rods were pre-weighed before insertion into the tube. A drug release orifice on each silicone tube was generated by laser ablation (Spectralytics Inc., MN, and Teosys Engineering, MD) before inserting the drug rod piece(s). Figure 5 shows silicone tubes filled with crystallized lidocaine pieces. Lidocaine pieces were inserted piece by piece using tweezers and stainless steel wire. Stainless steel microballs with a diameter of 0.024" (SS316, Salem Specialty Ball Company, Inc., CT) were inserted to seal both ends. The elastomeric nature of the silicone tube enables the balls larger than inner diameter of the tube to snugly fit into the tube. The laser drilled orifice with a diameter of 50 μm was positioned in the middle of two sealing balls. Additional stainless steel wires (Stainless Steel 304V Wire .022"OD,

Small Parts, FL) were inserted to fix the tube in a vial for *in vitro* release study. UV curable epoxy (Medical Device, 1-20542, Dymax Corporation, CT) with UV system (ADAC Cure Spot 50 Systems, Dymax Corporation, CT) was used to anchor the drug loaded tube to a vial.

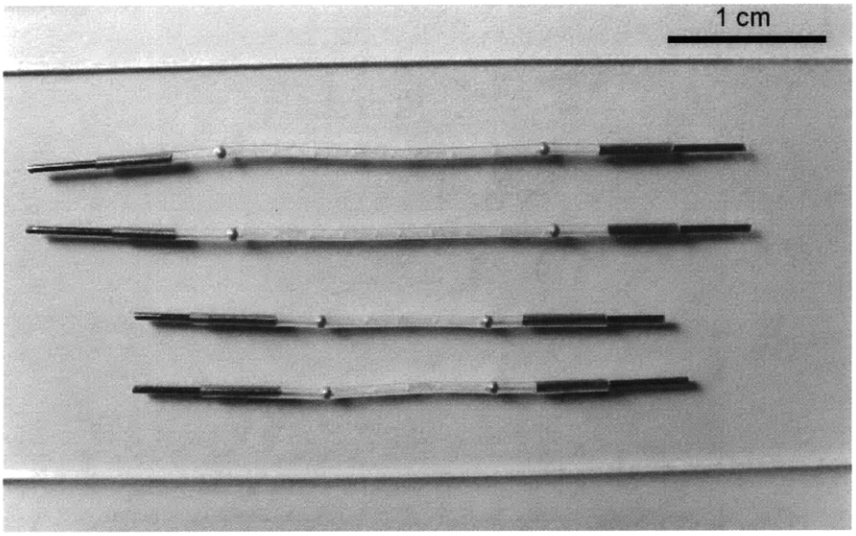

Figure 5. Silicone tubes (0.012" x 0.025", ID x OD) containing crystallized lidocaine pieces. Each tube was sealed with stainless steel microballs at both ends. Stainless steel wires inserted at the ends were used to fix the tube in a vial for *in vitro* release study. Laser drilled orifice is located in the middle between two microballs for each tube.

Polyurethane tube (Micro-Renathane, 0.025" x 0.040" (ID x OD), Braintree Scientific, Inc., MA) was used to cover some portion of the silicone tube to reduce water permeation of the device. Half the length of 2 cm length device was covered with the polyurethane tube. Two 0.5 cm sheaths made of polyurethane tubes were used for a 2 cm device shown in Figure 6. Silicone tubes shown in Figure 6 do not have stainless steel wires inserted at the ends. Two sheathes were located near the orifice to prevent the drug located far from the orifice from being isolated during the process of the water permeation and drug release. The results from *in vitro* release studies using the drug-loaded silicone tubes will be shown in the next section.

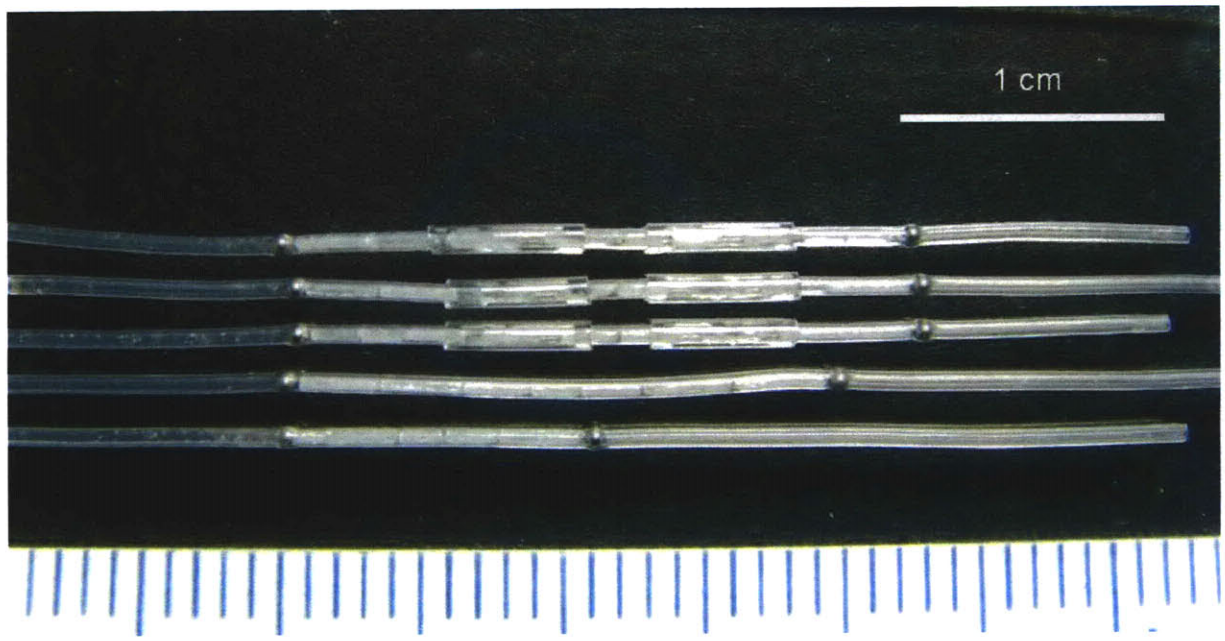

Figure 6. Silicone tubes (0.012" x 0.025", ID x OD) filled with crystallized lidocaine pieces. First three tubes from the top have an additional polyurethane sheath to minimize water permeation at the covered locations. Laser drilled orifice is located at the middle between two microballs for each tube.

The drug-loaded silicone tube was used to construct the intravesical drug delivery device. Figure 7 shows various types of prototype device such as a device with medical silicone adhesive (Silastic Medical Adhesive, silicone type A, Dow Corning, MI), device with monofilament nylon suture (Ethilon, monofilament nylon, size 1, 4.0 metric, Ethicon, inc.), and device connected by stainless steel ball with a diameter of 1/32". The device with suture was tested for preliminary *in vivo* toleration test with a rabbit. The device, however, was urinated out soon after implantation. This result indicated that a device should be equipped with better retention feature to avoid accidental voiding.

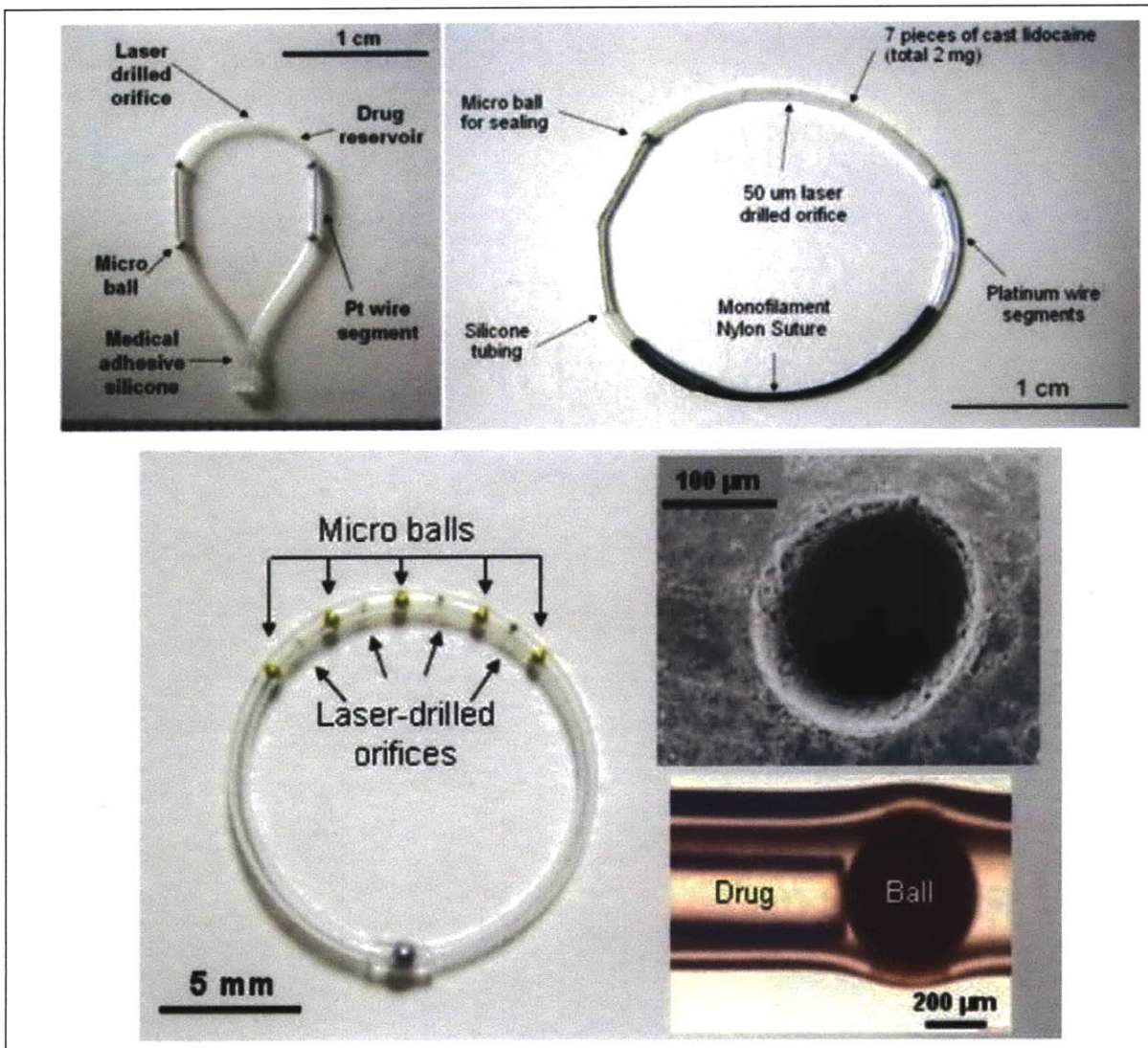

Figure 7. Various types of prototype device made of silicone tubing. (Top left) device with medical silicone adhesive. (Top Right) device with monofilament nylon suture. (Bottom) device with multiple reservoirs and orifices, SEM images of laser drilled hole, and microscopic image of inserted cast rod and microball into the silicone tubing.

Superelastic wire was introduced to improve the retention of the device. Superelastic nitinol wire (0.009" O.D., Small Parts Inc. FL) was formed into a pretzel shape by heat treatment. A new shape was imparted by restraining the wire in the pretzel shape and heating it to a temperature above 500 °C for over five minutes. More details about the shape will be discussed

in Chapter 3. Figure 8 shows the shaped wires after heat treatment and the drug loaded silicone tube connected to the superelastic structure made of nitinol wire.

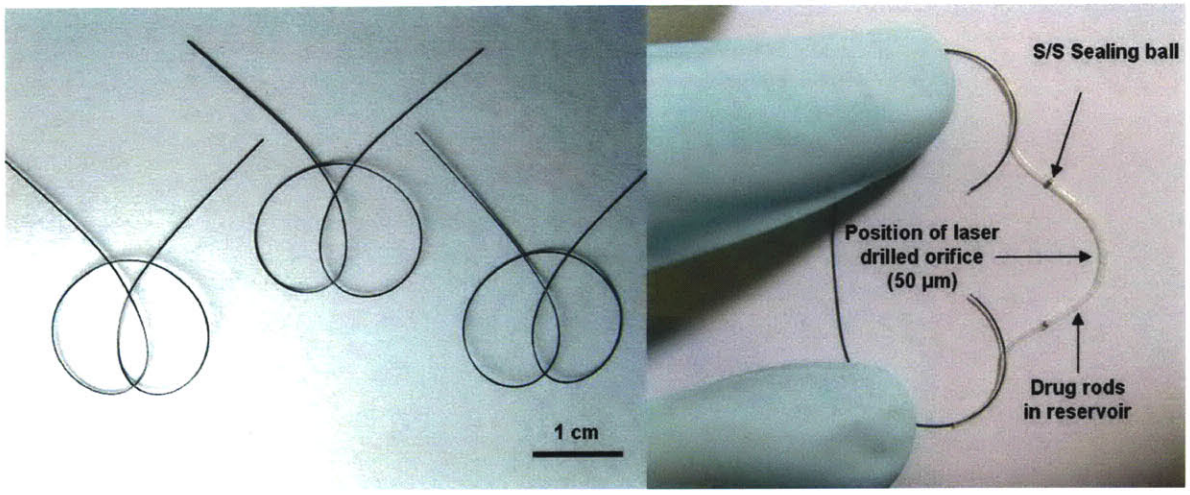

Figure 8. Shaped nitinol wires after heat treatment (left). Drug filled silicone tube connected with a shaped nitinol wire (right). Shaped nitinol structure has a superelastic property.

Additional steps were required to complete device fabrication for *in vivo* studies, and Figure 9 shows a completed form of the device. End portions of the nitinol structure were cut, and the silicone tube (0.020" x 0.037", ID x OD, Invotec International, Inc.) was covered at either end. UV curable epoxy was used to smoothen both ends of the device before covering with the silicone tube. Platinum wire (Platinum wire, 0.010" O.D., Omega Engineering, Inc., CT) can be optionally wound around either end of the nitinol wire structure before applying UV curable epoxy (Figure 9) to improve radio-opacity for x –ray imaging although nitinol itself shows radio-opacity to some extent.

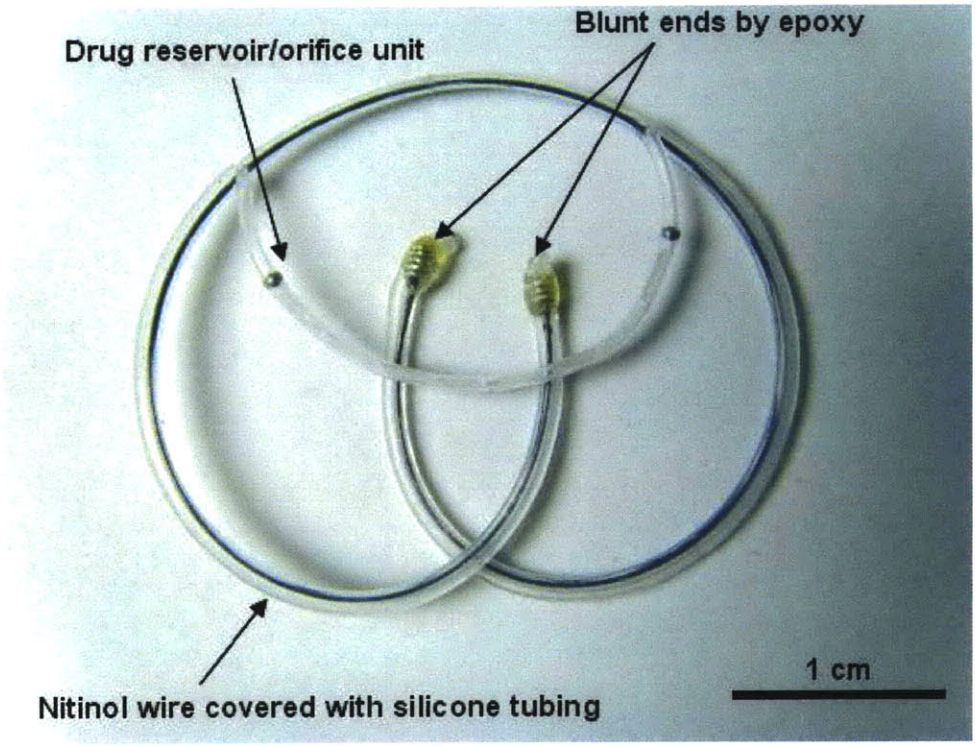

Figure 9. Completed form of the device. Both ends of the arms can have platinum wires wound around the tips (optional), and the ends are embedded with UV curable epoxy to make the tips blunt and smooth.

The device functions as a spring due to the superelastic nitinol while still having a smooth and soft outer surface due to the outer silicone surface. Figure 10 shows the sequence of the device compression. The device is designed to have more resistance to the compression as the compression proceeds to prevent the collapse of the device due to detrusor muscle contraction during urination. Measurement of the device spring constant during compression will be discussed in Chapter 3. The device returns to the original shape after compression once the load is removed.

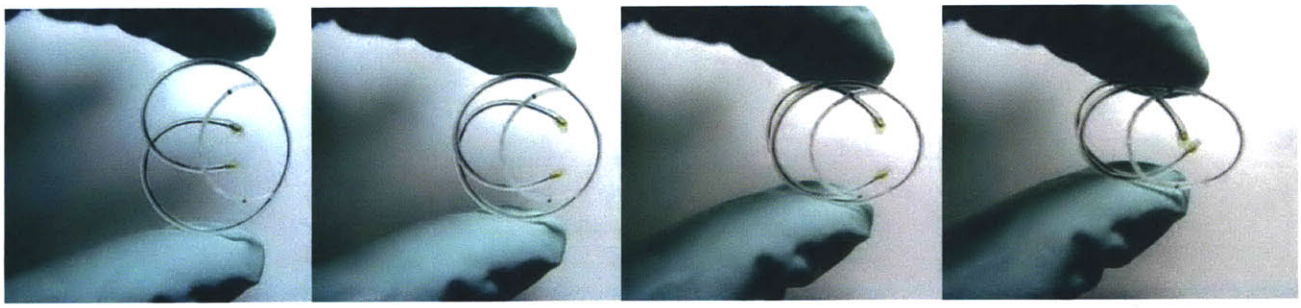

Figure 10. Sequence of the device compression. The resistance increases once the three sub-circles overlap. The device returns to the original shape immediately after the compression is removed.

2.3 *In vitro* drug release studies

2.3.1 *In vitro* release study with chondroitin sulfate C

A spectrophotometric 1,9-dimethylmethylene blue (DMMB)-based GAG assay was used to quantify concentrations of CSC for *in vitro* release study [31, 32]. A dye solution was made by adding 5.5 mg of DMMB powder (1,9-Dimethyl-Methylene Blue, Sigma-Aldrich, MO) to 500 mL of 0.05 M sodium acetate trihydrate ($CH_3COONa \cdot 3H_2O$, pH 4.75) buffer. The dye solution was stored at room temperature in an airtight brown glass bottle no longer than 1 month. 20 μL of samples from *in vitro* CSC release study in water as well as standard dilutions (0 to 80 μg/mL) were transferred to each well in a 96-well plate, and 200 μL of the dye solution was added to each well. The optical density of each well was measured using a micro-plate reader (SpectraMax plus384, Molecular Devices) at a wavelength of 520 nm.

The effect of orifice size on the drug release rate was investigated with the use of precision ruby orifices (synthetic ruby orifice, Bird Precision, Inc., MA). The ruby orifices offer extremely round and sharp edges hole with tight tolerance (+0.0002"/-0.0000") compared with a hole generated on the silicone tube wall by laser ablation. Ruby discs with drug release orifices

with a diameter of 10, 15, 20, or 50 μm and silicone tubes with a laser-ablated hole of 50 or 150 μm were compared. Figure 11 shows silicone tube (0.012"x 0.020", ID x OD, Invotec International, Inc.) with a ruby disc and a microball (diameter of 0.024", SS316, Salem Specialty Ball Company, Inc., CT) inserted at either end. A CSC rod with a length of 1 cm was loaded between the ruby disc and the microball. The ruby disc was tightly inserted into the silicone tube, and only the portion near a hole was exposed (Figure 11).

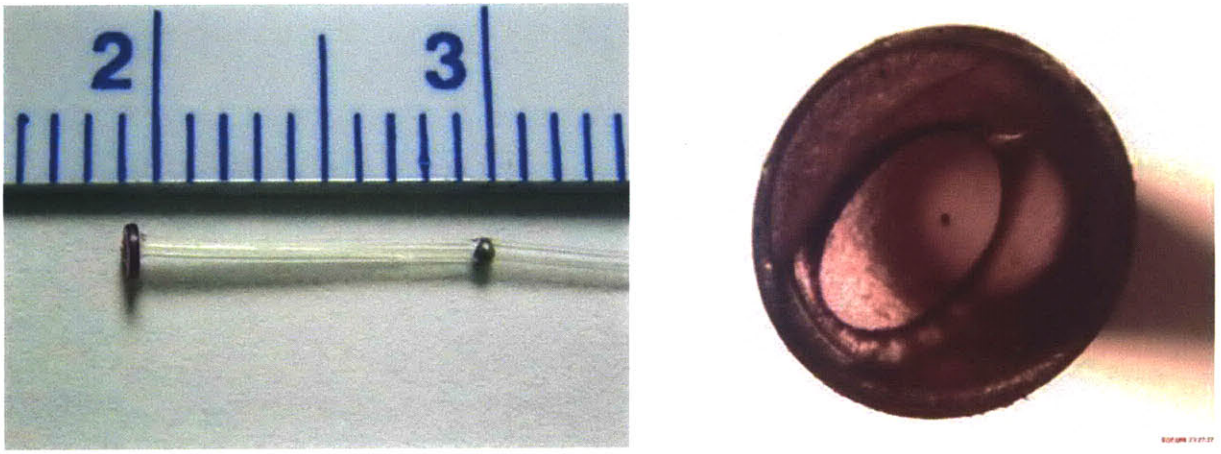

Figure 11. Device with ruby disc inserted (left), and the microscopic image of the orifice disc inserted side (right). The outer diameter of the orifice disc is 0.06" and the thickness is 0.01".

Excessive hydrostatic pressure buildup inside the silicone tube device can cause the inflation or swelling of the device. The swelling of the tube was observed for a device with 10 or 15 μm holes when *in vitro* CSC release experiments were performed. The device with smaller drug release hole, such as 10 or 15 μm orifice, requires sufficient pressure in order to push the liquid through a narrow orifice at the ruby disc. The position where the disc is inserted is most susceptible to the swelling in the tube since the position was stretched once the ruby orifice was inserted. Figure 12 shows the tube before swelling and after swelling when the ruby orifice with 10 μm diameter hole was submerged in water.

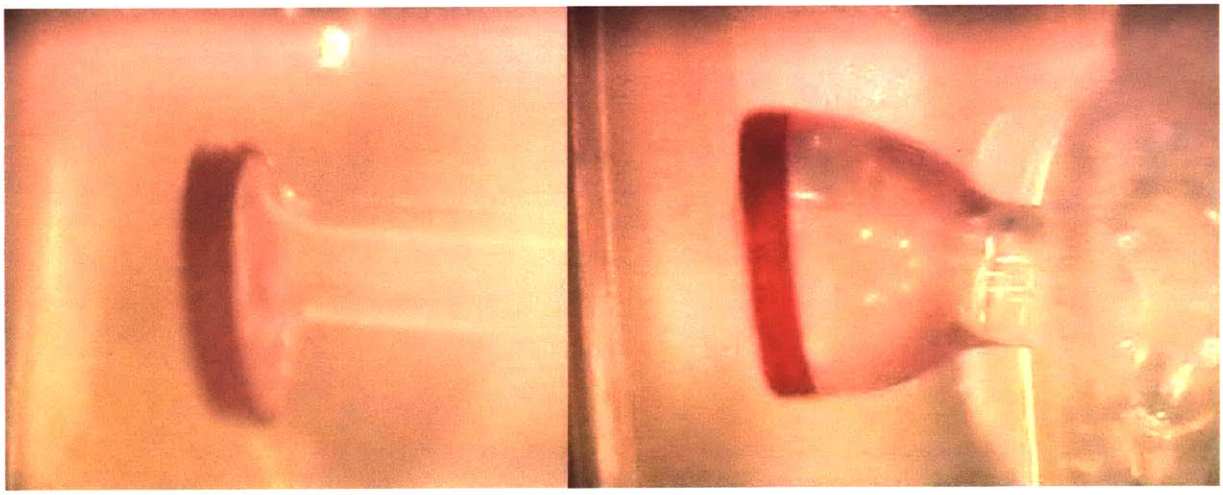

Figure 12. Device with the orifice disc inserted (10 μm diameter) when immersed in water (left). Inflated tube due to hydrostatic pressure build-up inside the device (right). The outer diameter of the orifice disc is 0.06" and the thickness is 0.01".

The size of the drug release orifice affected the drug release rate as shown in Figure 13. The excessive swelling of the tube may create sudden leakage of the drug around the inserted disc (15 μm orifice), or even lead to the expulsion of the orifice from the silicone tube (10 μm orifice). The CSC release experiment with 10 μm orifice was stopped when the disc orifice was detached from the tube. The drug release was retarded during the swelling of the tube because ingress of water through silicone tube wall is not balanced by the outflow through the orifice. Accumulated water ingress inside the tube is responsible for the swelling of the device as observed in Figure 12. The device with 150 μm orifice, in contrast, released CSC quickly such that most of the drug was released after 24 hours. The release profile with 50 μm orifice overall showed a first-order drug release rate.

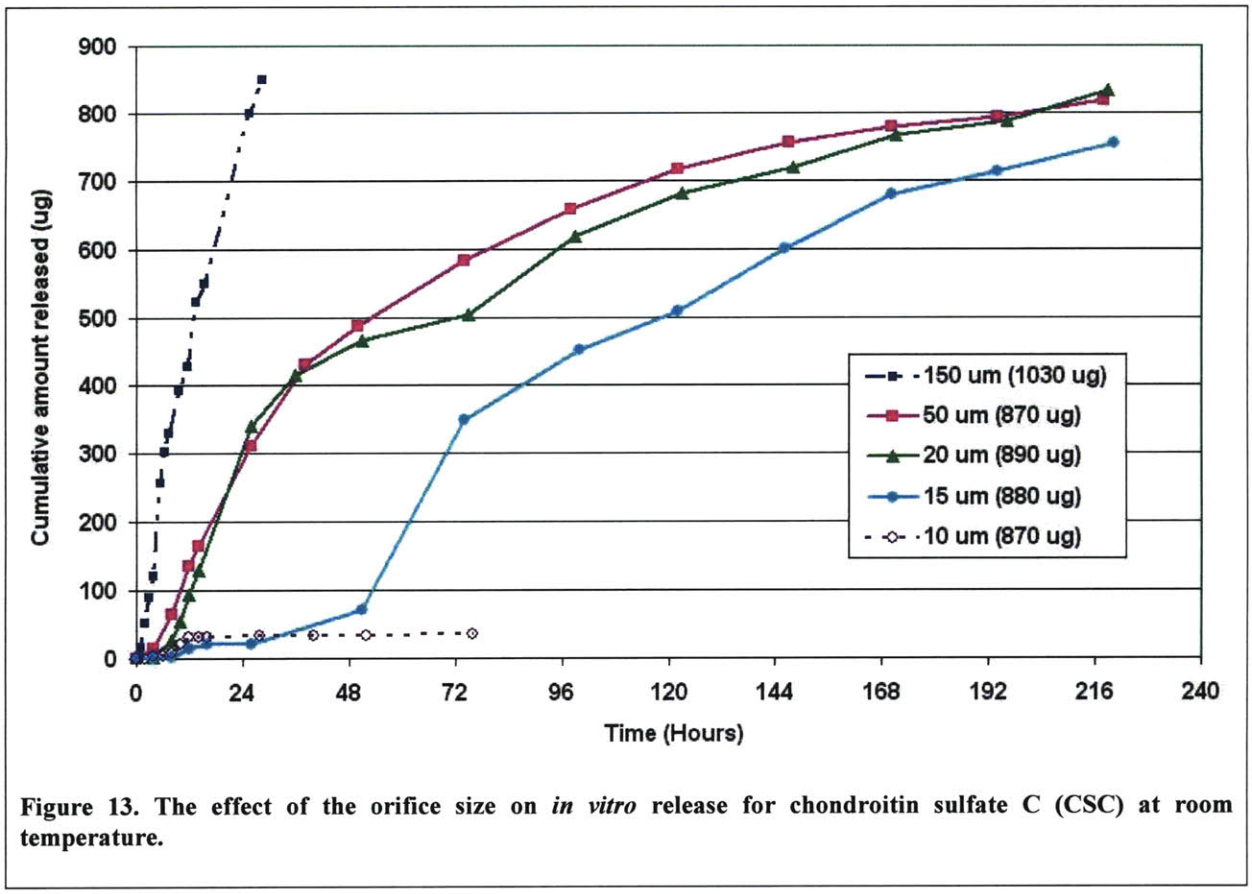

Figure 13. The effect of the orifice size on *in vitro* release for chondroitin sulfate C (CSC) at room temperature.

2.3.2 *In vitro* release study with lidocaine

High-performance liquid chromatographic (HPLC) was used to quantify lidocaine in the samples from *in vitro* lidocaine release study [33, 34]. The HPLC system was an Agilent Chem Station 1100 Series (Agilent Technologies, CA) equipped with an autosampler (G1313A), quaternary pump (G1311A), and diode array detector (G1315B) set at 214 nm. The column (μBondapak C18, 10 μm, 3.9 x 150 mm, WAT086684, Waters Corporation, MA) was maintained at 30 °C by a HPLC column heater (ThermaSphere TS-130, Phenomenex Inc., CA) and used with a mobile phase composed of 10% acetonitrole and 90% water buffered with

0.01M KH_2PO_4 adjusted to pH 2.1 with phosphoric acid. The flow rate was 1 mL/min, and the injection volume was 50 µL. Retention time was about 8 minutes.

Silicone tube devices with a laser drilled orifice, as shown in Figure 5 and Figure 6 , were used for *in vitro* lidocaine release study. 50 µm was chosen as the orifice diameter to obtain a first-order release profile based on the results from in vitro CSC release experiment. *In vitro* lidocaine release curves using four different types of devices are shown in Figure 14. Specifications for each type of device are shown in Table 1. Two different sizes (inner diameter x outer diameter) of silicone tubes were used, and both were purchased from Invotec International, Inc. There was no orifice with the control device, and it was observed that the microballs were pushed outward due to internal hydrostatic pressure buildup. Type 'III' device had a polyurethane sheath as shown in Figure 6 to reduce water permeation. Detailed discussion and interpretation about the *in vitro* release results are found in Chapter 6.

Table 1. Specifications for the devices used for *in vitro* lidocaine release study

Type	Payload	I.D. x O.D. (inches)	Tube wall thickness (inches)	Total tube length (cm)
I	2 mg	0.012 x 0.025	0.0065	2
II	1 mg	0.012 x 0.025	0.0065	1
III	2 mg	0.012 x 0.025	0.0065	2 (half covered with sheath)
IV	4 mg	0.020 x 0.037	0.0085	2
Control	4 mg	0.020 x 0.037	0.0085	2 (no orifice)

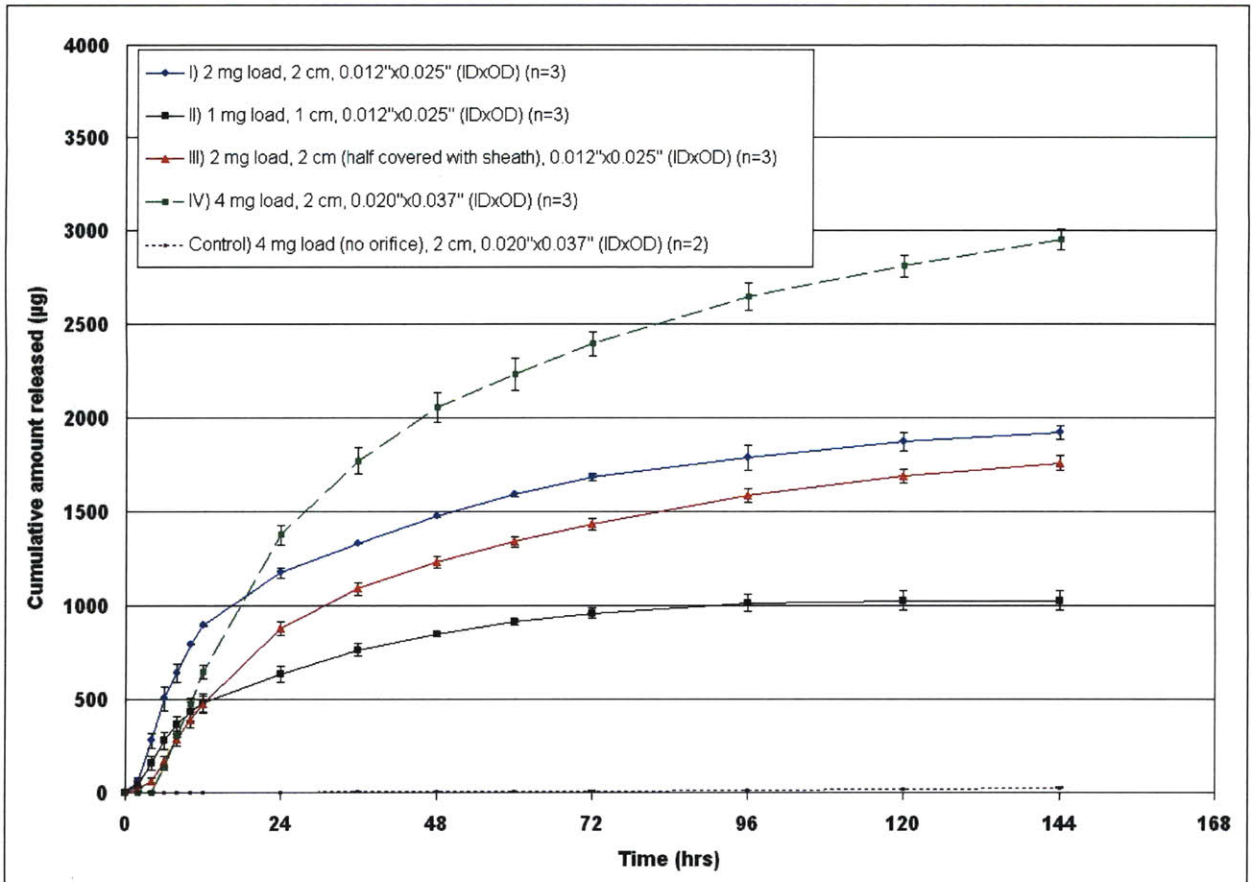

Figure 14. ***In vitro*** **lidocaine release curves at 37 °C with the device of silicone tube with a laser-drilled hole (50 µm diameter).**

2.4 Osmotic drug release

The mechanism of drug release from the device is that of the elementary osmotic pump (EOP). Felix Theeuwes described theoretical and experimental aspects of the EOP [21]. The EOP delivers drugs at a controlled rate through an orifice by water permeation through a semi-permeable membrane. Our device has a laser-drilled orifice on the silicone tube wall. The orifice was generated by an ultraviolet excimer laser micromachining system. The orifice can be considered as a circular channel with a length equal to the tube wall thickness (h). The radius of the orifice (R) varies depending on the amount of the ablated silicone material from the tube. A

straight channel shape is considered here for the simplicity of the analysis although there is some taper in the orifice between the outer and the inner surface of the tube. One example is that an entrance hole on the outer tube wall has a diameter of 55 μm and an exit hole on the inner wall has a diameter of 45 μm.

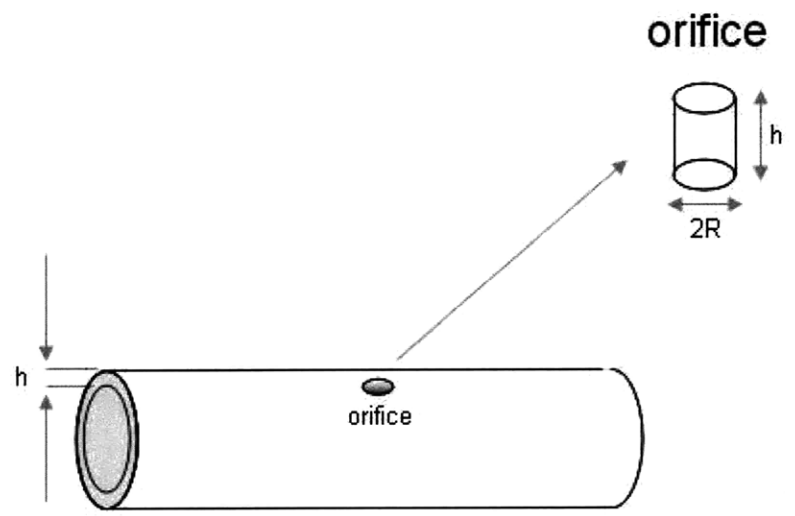

Figure 15. Laser drilled orifice on a silicone tube wall

Flow through a laser drilled orifice is considered here as circular Hagen-Poiseuille flow. Outward volume flow rate (Q_{out}) can be expressed as

$$Q_{out} = \int_0^R 2\pi urdr = \frac{\pi R^4}{8\mu}\left(-\frac{dp}{dx}\right) \approx \frac{\pi R^4}{8\mu}\frac{\Delta p}{h}$$

where u is the flow velocity along the orifice length and μ is the viscosity of the dispensed drug solution. Δp is hydrostatic pressure difference across the orifice channel. The solvent influx through the silicone tube wall is governed by the osmotic pressure difference ($\Delta\Pi$) and hydrostatic pressure difference (Δp) between inside and outside of the tube. Inward volume flow rate (Q_{in}) through the semi-permeable silicone tube wall can be expressed as

$$Q_{in} = \frac{A}{h} L_p(\sigma\Delta\Pi - \Delta p)$$

where A is the silicone tube surface area for solvent ingress; L_p and σ are the mechanical permeability and the reflection coefficient, respectively. It is assumed that the orifice area (πR^2) is sufficiently small compared with the overall silicone tube surface area (A). The osmotic pressure difference ($\Delta\Pi$) between the inside and outside of the tube can remain constant as long as there is solid undissolved drug in the device reservoir, and the concentration of the drug inside the tube is considered as the solubility of the drug. The inward volume flow rate is equal to outward volume flow rate when the silicone tube does not deform due to excessive hydrostatic pressure buildup, and so we get

$$Q_{out} = Q_{in}.$$

The hydrostatic pressure and osmotic pressure difference can be expressed as

$$\Delta p = \left(\frac{\sigma}{1 + \frac{\pi R^4}{8\mu A L_p}} \right) \Delta\Pi$$

and

$$Q = \left(\frac{AL_p\sigma}{1 + \frac{8\mu A L_p}{\pi R^4}} \right) \frac{\Delta\Pi}{h}.$$

The expression for the drug release rate (dm/dt) is described by

$$\frac{dm}{dt} = Q_{out} C = \frac{A}{h} L_p(\sigma\Delta\Pi - \Delta p)C$$

where C is the concentration of drug in the fluid dispensed through the orifice. The density inside the drug reservoir is initially that of the loaded drug, and solvent or water permeation occurs until the reservoir is completely filled with water.

The osmotic pressure difference ($\Delta\Pi$) can be much greater than the hydrostatic pressure difference (Δp) as the delivery orifice increases ($\Delta\Pi >> \Delta p$ or $R >> \left(8\mu AL_p / \pi\right)^{\frac{1}{4}}$). The expressions for the drug release rate, in this case, reduces to

$$\frac{dm}{dt} \approx \frac{A}{h} k\Delta\Pi C$$

where the constant k replaces $L_p\sigma$. Excessive hydrostatic pressure buildup inside the tube can deform elastomeric silicone tube. Swelling of the device was observed for the *in vitro* experiments with small ruby orifice. The increase of the device reservoir volume makes the assumption invalid that the inward volume flow rate is the same as the outward volume flow rate through the orifice. The outward volume flow rate, in this case, is smaller than the inward volume flow through the tube wall surface. One of the solutions to the problem of distension of the device is to increase the orifice size until the drug delivery by diffusion through the orifice is significant.

Our silicone tube device is an EOP with tubular geometry. A tubular osmotic pump with a length of 2L is shown in Figure 16. Tubular osmotic pump immersed in medium such as water or urine allows solvent or water permeation through the semi-permeable tube wall. Multiple orifices can be placed on the tube wall. Provided that the hole size of each orifice is within the range required for osmotic drug release where the drug diffusion through the orifice is minimized, multiple orifices will lower the pressure difference along the orifice channel. The outward and

inward volume flow rates for the device with multiple orifices with the condition of dominant osmotic pressure difference ($\Delta\Pi >> \Delta p$) can be expressed respectively as

$$Q_{out} = \frac{\pi R^4}{8\mu}\frac{\Delta p}{h}N$$

and

$$Q_{in} = \frac{A}{h}k\Delta\Pi$$

where N is the number of the orifices on the tube wall. The condition for the non-deformed device ($Q_{out} = Q_{in}$) gives

$$\Delta p = \frac{8\mu Ak}{N\pi R^4}\Delta\Pi$$

where the pressure difference across the orifice channel (Δp) is inversely proportional to the number of orifice (N).

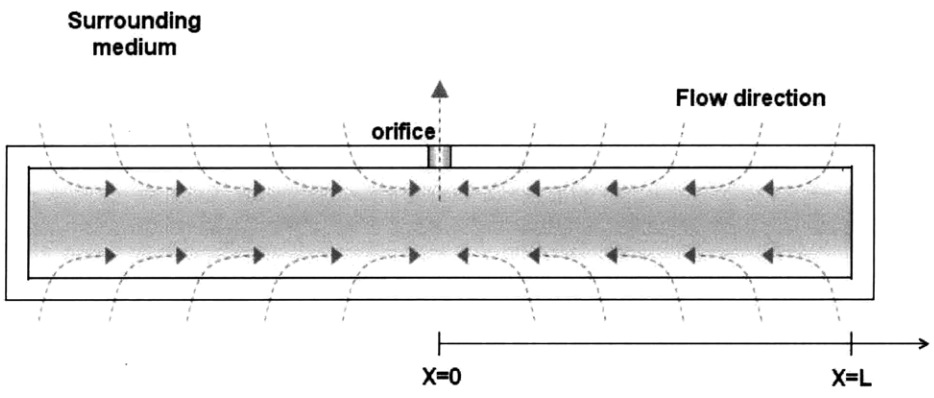

Figure 16. Tubular osmotic pump immersed in bath medium

Chapter 3 Retention feature of the intravesical drug delivery device

3.1 Concept

The preliminary *in vivo* test using the device made of silicone and suture materials revealed that a retention feature is important for the device to stay in the bladder without accidental expulsion or voiding over the designed treatment period. The detrusor muscle in the wall of the bladder contracts the bladder during urination. The contraction of the detrusor muscle combined with the hydrodynamic force during urination can expel the device before the completion of the treatment, which is undesirable. There is a possibility that the device may block the bladder neck or urethra during accidental voiding of the device. The implantable device for the bladder, therefore, should have a retention feature, which includes the proper design and material properties such as elastic modulus and elastic limit.

A closed loop or ring design is one of the simplest design options, but a ring-shaped device must undergo large deformation when it is implanted into the bladder cystoscopically. A cystoscope is a specialized telescope passing through the urethra to observe and manipulate inside the bladder. Cystoscopic implantation of the device requires the device to pass through the narrow working channel of the cystoscope. Most cystoscopes for adults are about 5 mm in diameter. The diameter of the working channel is about 2.4 mm or smaller. The ring-shaped device must be folded in half for cystoscopic insertion, and the two folded locations must go through large deformation. The device must then return to the ring shape after insertion into the bladder without collapsing into a linear shape to prevent accidental voiding of the device. The feasibility of a loop-shaped device depends on the availability of biocompatible materials with the proper elastic properties satisfying the conditions described above.

3.2 Analysis of the deformation of the elastic ring device

The analysis of the deformation of an elastic ring subject to two equal and opposite radial loads is a useful tool to find key design parameters and their relationships. The deformation of elastic circular rings was studied by R. Frisch-Fay when deformation is restricted in the initial plane of the ring [35]. Implicit solutions were obtained by the theory of non-linear deflections for three regimes depending on the magnitude of the radial loads. The relationship between force and deflection was numerically plotted (using MATLAB) in this section and the numerical codes are added in Appendix. Figure 17 shows the closed ring under two equal and opposite radial forces. Depending on the magnitude of the forces, the deformed shape can be in the regime of 1) the nodal elastica [36], 2) oval, or 3) peanut shape (Figure 17). The analytic method and approach for each regime varies because the associated geometry for analysis changes depending on the degree of deformation. The full analyses are lengthy and found in two papers by Frisch-Fay. Only key equations necessary for numerical analysis will be presented here. The following notation is used throughout this section:

$\bar{F}(p,\phi) = \int_0^{\phi} [d\varphi / \sqrt{1 - p^2 \sin^2 \varphi}]$: Legendre's incomplete elliptic integral of the first kind

$\bar{K}(p) = \int_0^{\pi/2} [d\varphi / \sqrt{1 - p^2 \sin^2 \varphi}]$: Legendre's complete elliptic integral of the first kind

$\bar{E}(p,\phi) = \int_0^{\phi} \sqrt{1 - p^2 \sin^2 \varphi} d\varphi$: Legendre's incomplete elliptic integral of the second kind

$\bar{E}(p) = \int_0^{\pi/2} \sqrt{1 - p^2 \sin^2 \varphi} d\varphi$: Legendre's complete elliptic integral of the second kind

F : Compression force
Δ : Vertical deflection of the ring
r : Radius of unloaded circular ring

3.2.1 Nodal elastica $(0 < \frac{Fr^2}{2EI} < 0.3148)$

This regime is when the analytical method of the nodal elastica, instead of the undulating elastica, is used [36]. This regime physically corresponds to a relatively small deformation of the ring. The range for this regime can be expressed as $0 < \frac{Fr^2}{2EI} < \frac{4}{\pi^2}\bar{F}^2(p=1,\frac{\pi}{4})$ where $\frac{4}{\pi^2}\bar{F}^2(p=1,\frac{\pi}{4}) = 0.3148$. The compression force and the corresponding deflection can be expressed respectively as

$$F = \frac{2EI}{r^2}\left[\frac{4}{\pi^2}p^2\bar{F}^2(p,\frac{\pi}{4})\right] \tag{3.1}$$

and

$$\Delta = r - \sqrt{\frac{2EI}{F}}\left[\frac{2}{p}\bar{E}\left(p,\frac{\pi}{4}\right) - \left(\frac{2}{p} - p\right)\bar{F}\left(p,\frac{\pi}{4}\right)\right] \tag{3.2}$$

where $0 < p < 1$. The force and the deflection is correlated by the parameter p.

3.2.2 Oval shape $(0.3148 < \frac{Fr^2}{2EI} < 1.3932)$

Oval shape of the ring is obtained when the initially circular ring is deformed by the compression lateral force until no point of inflection exists. The range where the ring becomes oval shape can be expressed as $\frac{4}{\pi^2}\bar{F}^2(p=1,\frac{\pi}{4}) < \frac{Fr^2}{2EI} < \frac{4}{\pi^2}\bar{K}^2(p=\frac{1}{\sqrt{2}})$ where

$\frac{4}{\pi^2}\bar{F}^2(p=1,\frac{\pi}{4})=0.3148$ and $\frac{4}{\pi^2}\bar{K}^2(p=\frac{1}{\sqrt{2}})=1.3932$. The expression for the compression force and the corresponding deflection is respectively,

$$F=\frac{2EI}{r^2}\left[\frac{4}{\pi^2}\bar{F}^2(p,\phi_B)\right] \tag{3.3}$$

and

$$\Delta=r-\sqrt{\frac{2EI}{F}}\left[2\bar{E}(p,\phi_B)-\bar{F}(p,\phi_B)\right] \tag{3.4}$$

where $\phi_B=\sin^{-1}(1/\sqrt{2}p)$ and $1/\sqrt{2}<p<1$.

3.2.3 Peanut shape ($1.3932<\frac{Fr^2}{2EI}$)

The ring assumes a peanut shape when the ring deforms further from the oval shape. The range for this regime is $\frac{4}{\pi^2}\bar{K}^2(p=\frac{1}{\sqrt{2}})<\frac{Fr^2}{2EI}$, where $\frac{4}{\pi^2}\bar{K}^2(p=\frac{1}{\sqrt{2}})=1.3932$. The expression for the compression force and the corresponding deflection can be written respectively as

$$F=\frac{8EI}{\pi^2r^2}\left[2\bar{K}(p)-\bar{F}(p,\phi_B)\right]^2 \tag{3.5}$$

and

$$\Delta=r-\sqrt{\frac{2EI}{F}}\left[4\bar{E}(p)-2\bar{K}(p)-2\bar{E}(p,\phi_B)+\bar{F}(p,\phi_B)\right] \tag{3.6}$$

where $\phi_B=\sin^{-1}(1/\sqrt{2}p)$ and $1/\sqrt{2}<p<1$.

3.2.4 Numerical plot for the deformation of elastic circular ring

The compression force (F) and the deflection (Δ) are correlated by parameters p and ϕ_B for each regime. The solution for each regime can be expressed using dimensionless force (Fr^2/EI) and deflection (Δ/r) (Table 2).

Table 2. Dimensionless force and deflection in three regiems

Regime	Dimensionless force (Fr^2/EI) and deflection (Δ/r)
Nodal elastica $0 < \frac{Fr^2}{EI} < 0.6297$	$\frac{Fr^2}{EI} = \frac{8}{\pi^2} p^2 \bar{F}^2(p, \frac{\pi}{4})$ $\frac{\Delta}{r} = 1 - \sqrt{\frac{2EI}{Fr^2}} \left[\frac{2}{p} \bar{E}\left(p, \frac{\pi}{4}\right) - \left(\frac{2}{p} - p\right) \bar{F}\left(p, \frac{\pi}{4}\right) \right]$ $(0 < p < 1)$
Oval shape $0.6297 < \frac{Fr^2}{EI} < 2.7864$	$\frac{Fr^2}{EI} = \frac{8}{\pi^2} \bar{F}^2(p, \phi_B)$ $\frac{\Delta}{r} = 1 - \sqrt{\frac{2EI}{Fr^2}} \left[2\bar{E}(p, \phi_B) - \bar{F}(p, \phi_B) \right]$ $(\phi_B = \sin^{-1}(1/\sqrt{2}p) \text{ and } 1/\sqrt{2} < p < 1)$
Peanut shape $2.7864 < \frac{Fr^2}{EI}$	$\frac{Fr^2}{EI} = \frac{8}{\pi^2} \left[2\bar{K}(p) - \bar{F}(p, \phi_B) \right]^2$ $\frac{\Delta}{r} = 1 - \sqrt{\frac{2EI}{Fr^2}} \left[4\bar{E}(p) - 2\bar{K}(p) - 2\bar{E}(p, \phi_B) + \bar{F}(p, \phi_B) \right]$ $(\phi_B = \sin^{-1}(1/\sqrt{2}p) \text{ and } 1/\sqrt{2} < p < 1)$

The three regimes are plotted altogether using MATLAB in Figure 17. The range of compressive displacement is set to less than a radius of the initial elastic ring. Dimensionless force (Fr^2 / EI) and deflection (Δ / r) represent vertical and horizontal axis, respectively. Figure 18 shows slope or dimensionless spring constant with respect to dimensionless compression.

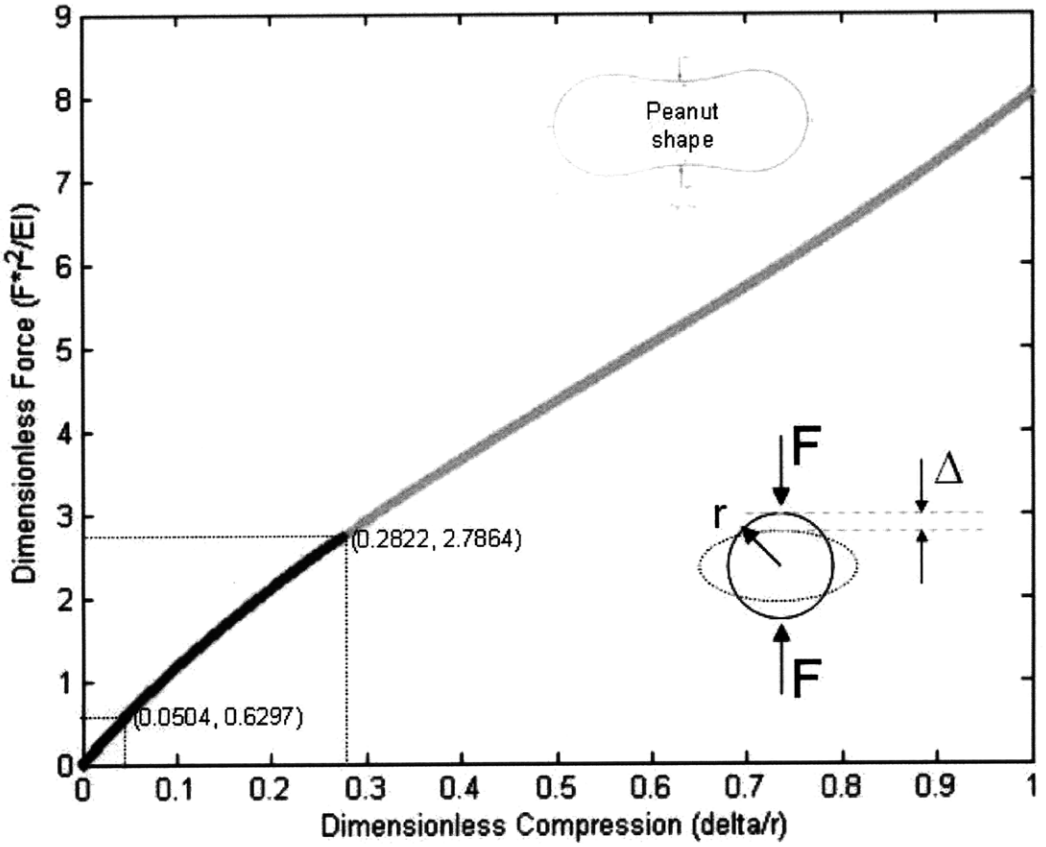

Figure 17. Elastic ring under compression (three different regimes are indicated). Relationship between compressive force and displacement

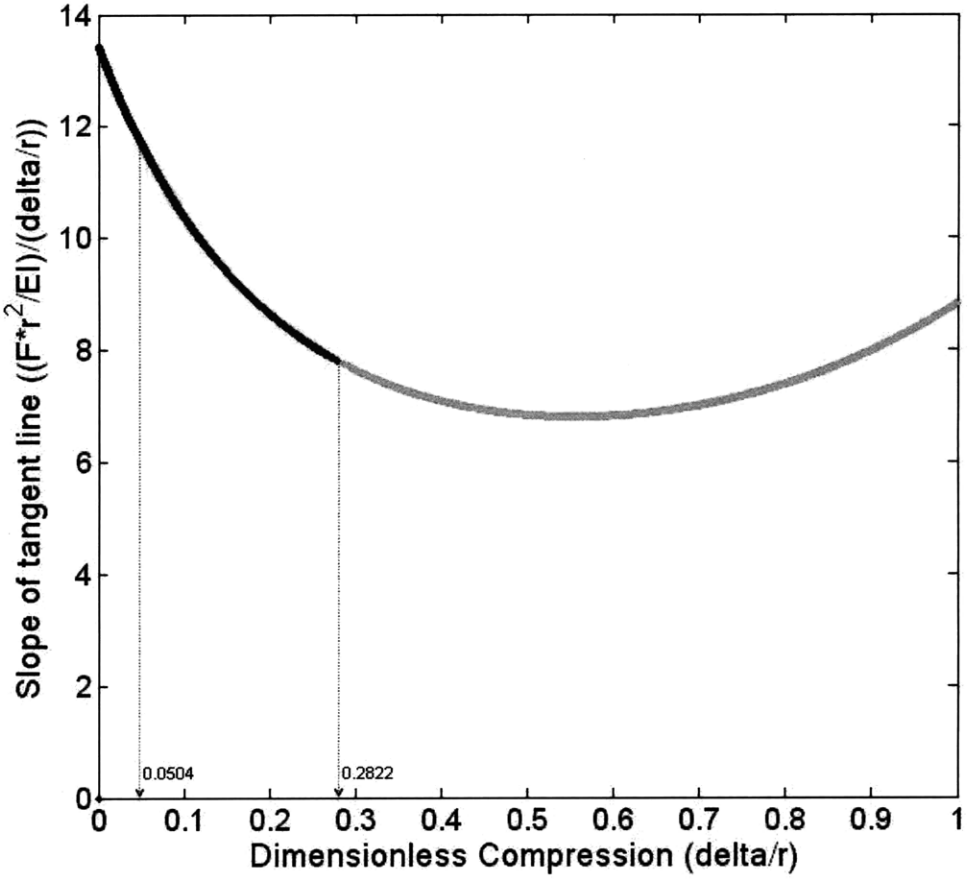

Figure 18. The relationship between dimensionless spring constant and compression.

3.3 Collapse-resistive design

The device should stay in the bladder over the treatment period without accidental voiding. The bladder is not a static environment for the device since the bladder contracts its volume and the urination causes a hydrodynamic force that may lead to the accidental expulsion of the device. Preliminary *in vivo* toleration test with rabbits shows that the device made of silicone tube and monofilament nylon suture was urinated out soon after the device implantation (Figure 7, Top right). The proper retention feature is, therefore, crucial for the device to reside in the bladder until the cystoscopic retrieval of the device. A unique structure with a shape is

similar to a pretzel was introduced to the device as a retention feature. The pretzel shape was chosen as its resistance to compression increases upon compression of the two sub-circles. The initial period of bladder contraction during urination causes a very small or negligible resistance force against the detrusor muscle because only the largest arch will be involved in the deformation. Further contraction of the detrusor muscle makes the two sub-circles overlap, and the total three arches will resist the compression. This feature prevents the collapse of the device structure to avoid accidental voiding. The device can immediately return to its original shape once the compression is removed due to the superelastic property of nitinol.

Mechanical compression testing of the pretzel-shaped spring was performed using an Instron 5542 with 10 kN load cell equipped with Merlin software. (Instron, MA). The spring was formed using the same superelastic nitinol wire that was used in the device. Video capturing of the compression event was recorded during the compression test. Figure 19 shows the experimental result showing the relationship between the compressive force and displacement. The initial spacing was 2.9 cm and the compression speed was 2 mm/min. There are three points (A,B,and C) indicated in the plot, and the corresponding instantaneous images are shown below the plot. Bilinear behavior was observed over the compression. A sudden slope increase was observed when the three arches overlapped. The slope or spring constant for the region A-B is about 0.0037 N/mm while that for the region B-C is about 0.057 N/mm. There is 15.4 times slope increase from the region A-B to B-C. The single arch contributed to the resistance to the compression from the point A to B. All three arches started to contribute to the resistance when the compression reached the point B. The pretzel spring returned to the original shape when the compressive load was removed after the compression reached the point C. The spring can return to the initial shape after large deformation because of the super elasticity of nitinol.

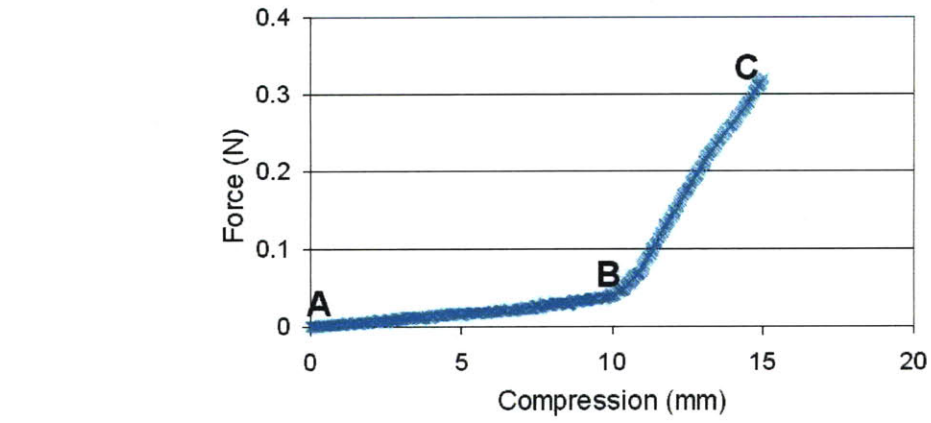

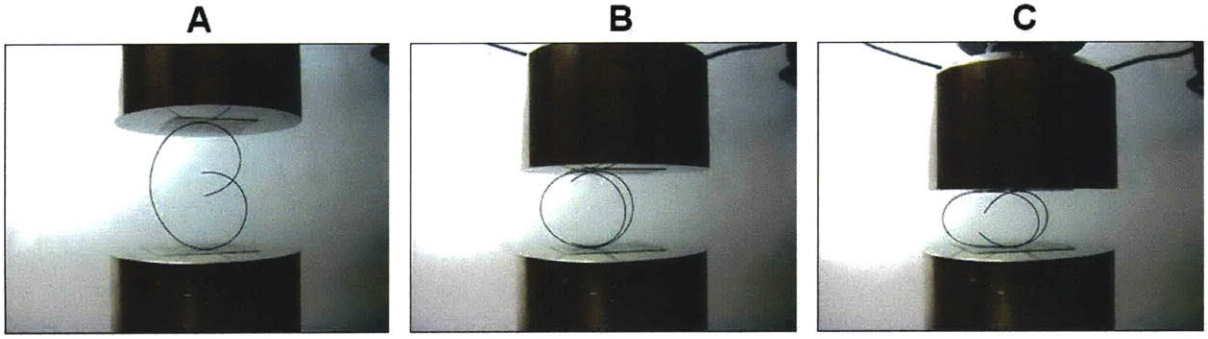

Figure 19. Compression test for a pretzel shape nitinol spring

The relationship between force and displacement for a small deflection can be obtained using Castigliano's second theorem [37]. Figure 20 shows a circular arc under compressive force F with its radius of r, its central angle of φ, and its flexural rigidity EI. Vertical displacement at the top free end is denoted as Δ and the bottom end is assumed to be fixed in place as in the compression test shown above. The strain energy U is expressed as

$$U = \frac{F^2 r^3}{2EI}\left(\varphi + \frac{\varphi}{2}\cos\varphi - \frac{3}{2}\sin\varphi\right) \tag{3.7}$$

The deflection is obtained from Castigliano's second theorem as:

$$\Delta = \frac{\partial U}{\partial F} = \frac{Fr^3}{EI}\left(\varphi + \frac{\varphi}{2}\cos\varphi - \frac{3}{2}\sin\varphi\right) \tag{3.8}$$

or in the dimensionless form:

$$\frac{Fr^2}{EI} = \frac{2}{(2\varphi + \varphi\cos\varphi - 3\sin\varphi)} \frac{\Delta}{r} \tag{3.9}$$

Eq. (3.9) for a semicircle ($\varphi = \pi$) is further reduced to:

$$\frac{Fr^2}{EI} = \frac{2}{\pi} \frac{\Delta}{r} \tag{3.10}$$

The spring constant ($dF / d\Delta$) is therefore

$$\frac{dF}{d\Delta} \approx \frac{2EI}{\pi r^3} = \frac{E}{32} \frac{d^4}{r^3} \tag{3.11}$$

where the moment of inertia (I) for the wire with a diameter d is substituted by $\pi d^4 / 64$.

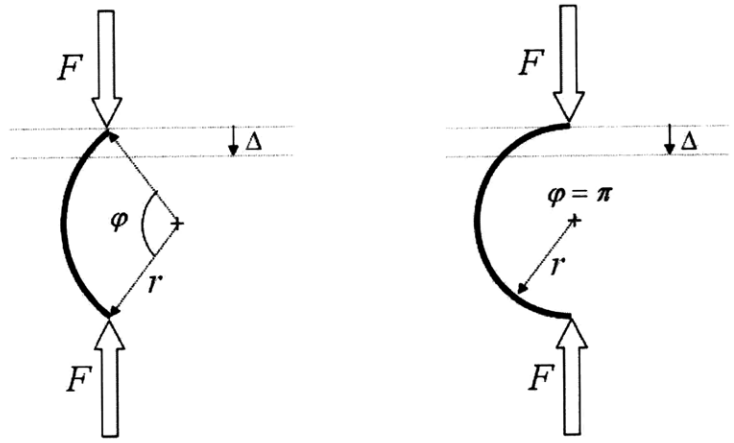

Figure 20. Compression of can circular arc (courtesy of Jongmin Shim)

The sudden slope increase in Figure 19 can be explained by Eq. (3.11). The ratio of the slope for the region B-C (three arches) to the initial slope for the region A-B (single arch) is

$$\frac{(dF / d\Delta)_{B\to C}}{(dF / d\Delta)_{A\to B}} \approx \frac{3/(1.7cm)^3}{1/(2.9cm)^3} = 14.9 \tag{3.12}$$

where 1.7 cm is the diameter when the three arcs start to overlap, and 2.9 cm is the initial diameter of the single arc. Compression test showed that about 15 times slope increase from the region A-B to region B-C, and Eq. (3.11) predicts the result well although simple linear elastic analysis is used. The superelasticity of nitinol is advantageous in extrapolating the result from the simple linear analysis for small deflection regime to predict the behavior for the large deflection regime.

3.4 Design approach for low modulus wires

Analysis for a elastic ring and an arc reveals a proportional equation for the spring constant (F/Δ) as

$$\frac{F}{\Delta} \sim \frac{EI}{r^3} \sim \frac{Ed^4}{r^3} \tag{3.13}$$

and the spring constant for the retentive body with multiple windings has the equation as

$$\frac{F}{\Delta} \sim n\frac{Ed^4}{r^3} \tag{3.14}$$

where n is the number of multiple windings. Nitinol was used for the retentive body, but an elastomer with low modulus can be used, still having a spring constant comparable to that of the nitinol retentive body. The elastomeric retentive body is especially useful when the device is made of completely biodegradable rubber such as poly(glycerol-sebacate) (PGS) [38]. According to Eq. (3.14) for a spring constant, the small Young's modulus E for low modulus elastomers can be compensated for by one or more of the following: decreasing the radius of an arc, increasing the wire diameter, and having multiple and/or overlapped circles or windings. Reducing the radius of an arc by a factor of two and increasing a wire diameter by a factor of two

can significantly increase a spring constant by a factor of 2^7 or 128. Examples of a spring constant are tabulated below for some low modulus elastomers. Relative magnitude of a spring constant for each material was evaluated with respect to nitinol device using Eq. (3.14). Parameters for each material were selected to show a spring constant comparable to the nitinol device. Other combinations of parameters can also used to obtain a desirable spring constant.

Table 3. Young's modulus and design parameters for nitinol and other low modulus materials.

Material / Parameter	Nitinol	Polyurethane	Silicone	PGS
Young's modulus (E)	30 GPa	25 MPa [39]	2.41 MPa	1.7 MPa
Diameter (d)	0.2286 mm	1 mm	1.2 mm	1.2 mm
Arc radius (r)	1.5 cm	1 cm	0.75 cm	0.76 cm
Number of coils (n)	1	1	2	3
Relative spring constant $\left(\frac{F/\Delta}{(F/\Delta)_{nitinol}}\right)$	1	1.03	0.96	0.99

Chapter 4 Topical absorption of lidocaine into the urothelium

4.1 One compartment model

The urinary bladder has several important functions: storage of an adequate volume of urine, facilitation of bladder emptying at appropriate time intervals, and protection of smooth muscle and nerve from exposure to urine. This last function is largely the role of the urothelium or transitional epithelium, the epithelial lining that covers the bladder wall and urinary tract such as the ureter and urethras. Urothelium has three layers: umbrella cell stratum, intermediate cell stratum and basal cell stratum. A layer of umbrella cells is closest to the bladder lumen and the glycosaminoglycan (GAG) layer covers the surface of the umbrella cells. It is widely believed that a defect in the GAG layer causes the symptoms of interstitial cystitis [15, 40, 41]. Lamina propria, located below a layer of basal cells, contains blood capillaries and nerves. Irritating urine constituents may leak through the urothelium, causing tissue inflammation and sensory nerve depolarization [42].

Absorption of drug into the bladder can be simplified by a one-compartment model to obtain the tissue concentration-time profiles. This model only considers the average drug concentration in the bladder tissue. Figure 21 shows the one-compartment model for the bladder. The average concentration of bladder tissue is denoted as $C(t)$, which is a time-dependent variable. The effective first-order rate constant for absorption of drug is referred to as k_a. The hybridized first-order rate constant describing absorption into the systemic circulation, degradation, and metabolism is represented by k_d. The concentration of drug solution in contact with bladder is denoted as $f(t)$. The exposure time of drug solution to the bladder is determined

by the residence time, t_r, of the instilled drug solution The equation for the bladder tissue concentration *C(t)* is given by:

$$\frac{dC}{dt} = k_a f(t) - k_d C, \quad C(0) = 0 \tag{4.1}$$

where $f(t) = \begin{cases} f_0 & (0 < t \le t_r) \\ 0 & (t > t_r) \end{cases}$ and f_0 is assumed to be constant. The analytical solution of Eq. (4.1) is obtained as:

$$C(t) = \begin{cases} \dfrac{k_a f_0}{k_d}(1 - e^{-k_d t}) & (0 < t \le t_r) \\ \dfrac{k_a f_0}{k_d}(e^{-k_d (t - t_r)} - e^{-k_d t}) & (t > t_r) \end{cases} \tag{4.2}$$

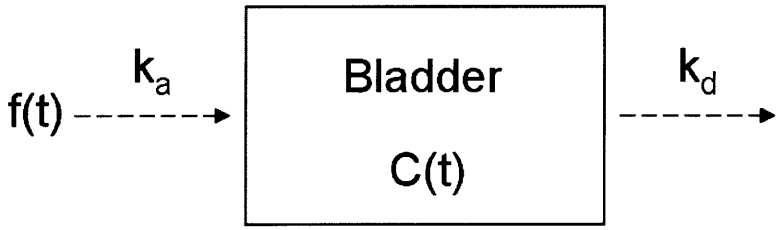

Figure 21. One-compartment model for transient bladder tissue concentration

The response of the bladder tissue concentration is different depending on the treatment type. Figure 22 shows two treatment types, A) intravesical instillation of drug solution, and B) the intravesical drug delivery device. The intravesical instillation features a short duration of drug exposure to the bladder determined by the drug retention time (t_r) and a high concentration of drug solution (f_0). The treatment of the intravesical device is characterized by extended drug exposure and relatively low drug concentration in the bladder. The results for the two treatments are quite different as illustrated in Figure 22. Based on Eq.(4.2), the treatment type A will show

a high peak of tissue concentration followed by its rapid drop after the voiding of the instilled solution. Bladder tissue concentration with the device will slowly reach the low magnitude plateau, but the low concentration will be sustained over an extended period of time.

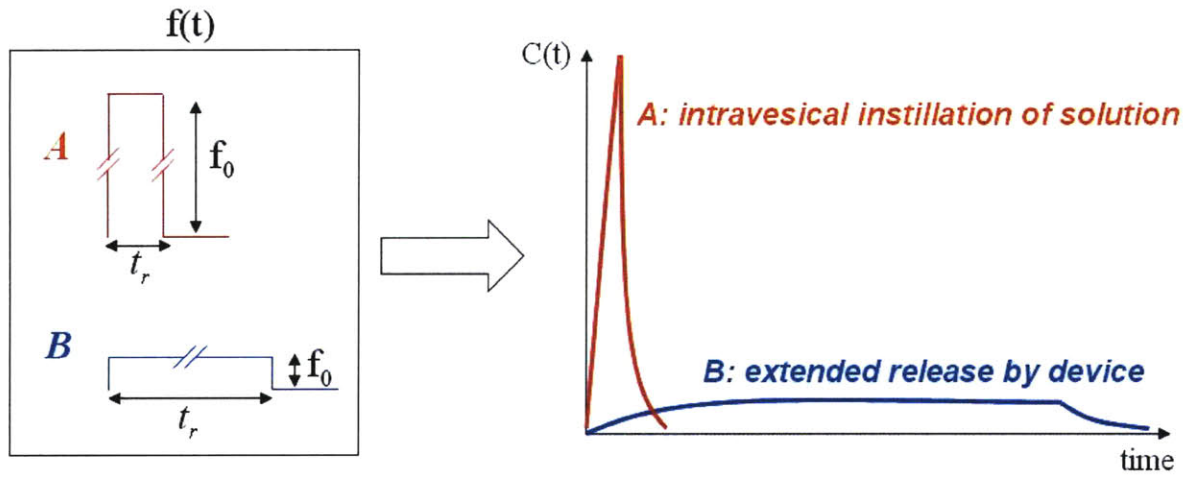

Figure 22. The response of the bladder tissue concentration depending on the treatment type

4.2 Drug distribution model for drug absorption in the bladder

4.2.1 Drug concentration in the urine

Intravesical instillation of cytotoxic agents into the bladder is a common treatment used for patients with superficial bladder cancer. There have been several attempts to find a mathematical model for drug absorption into the bladder during instillation treatment [43-47]. Mathematical models for the drug absorption during intravesical treatment can be used to develop intravesical drug delivery system. The drug concentration in urine during instillation treatment is time dependent due to urine production. The drug concentration can be found by solving the following equations as described in [48]:

$$\frac{dA}{dt} = -k_1 A \tag{4.3}$$

where $A = A(t) = V(t)C(t)$ and $V(t) = V_s + V_{res} + k_0 t$. $A(t)$, $C(t)$, and $V(t)$ are the amount and concentration of drug, and volume of the bladder contents at time t, respectively; the first-order absorption rate constant is denoted as k_1. The urine volume, $V(t)$, consists of the volume of instilled drug solution (V_S), residual urine volume (V_{res}), and the volume added by urine formation with the urine production rate (k_0). Solving Eq. (4.3) gives

$$C(t) = \frac{V(0)C(0)}{V(t)} \exp(-k_1 t) = \frac{Dose}{V(t)} \exp(-k_1 t) \tag{4.4}$$

This model assumes that the rate of drug decease in the bladder is proportional to the amount of drug present in the bladder [48]. An alternative model for the drug concentration present in urine can be developed by assuming that the drug absorption is proportional to the surface area of the bladder wall multiplied by the drug urine concentration. Introducing a spherical geometry of the bladder ($Area \propto volume^{2/3}$) and the first-order absorption rate constant (k_2), we get the differential equation as

$$\frac{dA}{dt} = -k_2 V^{2/3} C \tag{4.5}$$

where $A(t) = V(t)C(t)$ and $V(t) = V_s + V_{res} + k_0 t$. The solution to Eq. (4.5) is expressed as:

$$C(t) = \frac{V(0)C(0)}{V(t)} \exp\left(-\frac{3k_2}{2k_0}\left((V_s + V_{res} + k_0 t)^{2/3} - (V_s + V_{res})^{2/3}\right)\right) \tag{4.6}$$

4.2.2 *In vitro* drug distribution model in the bladder

The bladder wall can be considered as a thin diffusion barrier (the urothelium) covering the deeper capillary-perfused tissues of the lamina propria and muscle layers [46]. Systemic removal or capillary drainage in the capillary-perfused tissues can be neglected in the *in vitro* setting of drug absorption into the bladder. The urothelium thickness is about 200 μm for the human bladder while that for dog and rabbit bladder tissues is about 50 μm [44]. The simplest model for *in vitro* drug distribution in the bladder is to view the bladder as a semi-infinite medium at the following initial and boundary conditions:

$$C = C_0 = KC_u \quad at \quad x = 0,\ t > 0 \tag{4.7}$$

$$C = 0 \quad at \quad x > 0,\ t = 0 \tag{4.8}$$

where C and C_u are the tissue drug concentration in depth x at time t, and the luminal drug concentration in the bladder; K is the partition coefficient for the drug bladder tissue to the luminal solution. The luminal solution concentration can remain constant if the total amount of drug absorbed into the bladder is negligible compared with the total drug present in the luminal solution in the donor chamber of the diffusion cell. The drug tissue concentration for the semi-infinite model can be expressed using the complementary error function as

$$C = KC_u erfc\left(\frac{x}{2\sqrt{Dt}}\right) \tag{4.9}$$

where D is the drug diffusion coefficient in the bladder tissue. The total drug amount absorbed in the tissue through unit area of the bladder wall surface (M_t) is obtained as

$$M_t(t) = \int_0^t -D\frac{\partial C}{\partial x}\bigg|_{x=0} dt = 2C_0\sqrt{\frac{Dt}{\pi}} \tag{4.10}$$

where $C_0 = KC_u$.

Biphasic diffusion behavior in the bladder tissue is typically observed for drug tissue distribution [43]. The diffusion behavior in the urothelium is different from the rest of the deeper bladder wall. The decrease of drug tissue concentration in the urothelium is steeper than that in the tissues below the urothelium. The biphasic behavior introduces different drug diffusion coefficients for urothelium and the rest of the bladder tissue. Then, the drug distribution in the bladder wall can be viewed as diffusion in a semi-infinite composite medium with the surface layer (urothelium) having diffusion properties different from the deeper bladder tissue layers in Figure 23. The initial and boundary conditions are the same as Eq. (4.7) and Eq. (4.8) (zero initial concentration and constant surface concentration). The conditions at the interface is

$$C_1 = C_2 \quad at\ x = l \tag{4.11}$$

$$D_1 \frac{\partial C_1}{\partial x} = D_2 \frac{\partial C_2}{\partial x} \quad at\ x = l \tag{4.12}$$

where subscript 1 and 2 indicate the properties in the urothelium and in the deeper tissues, respectively, and l is the thickness of the urothelium. The solution for the semi-infinite composite medium is given by [49, 50]:

$$C_1(x,t) = C_0 \sum_{n=0}^{\infty} \alpha^n \left\{ erfc\left(\frac{(2n)l + x}{2\sqrt{D_1 t}} \right) - \alpha erfc\left(\frac{(2n+2)l - x}{2\sqrt{D_1 t}} \right) \right\} \quad \text{for } 0 < x \le l \tag{4.13}$$

$$C_2(x,t) = \frac{2kC_0}{k+1} \sum_{n=0}^{\infty} \alpha^n erfc\left(\frac{(2n+1)l + k(x-l)}{2\sqrt{D_1 t}} \right) \quad \text{for } x \ge l \tag{4.14}$$

where $k = \sqrt{D_1 / D_2}$ and $\alpha = (1-k)/(1+k)$. The total amount of drug absorbed through unit area of the bladder surface at $x=0$ during time t is M_t, give by

$$M_t(t) = 2C_0\sqrt{\frac{D_1 t}{\pi}}\left\{1+2\sum_{n=1}^{\infty}\alpha^n \exp(-n^2 l^2 / D_1 t)\right\} - 4lC_0\sum_{n=1}^{\infty} n\alpha^n erfc\left(\frac{nl}{\sqrt{D_1 t}}\right) \tag{4.15}$$

and for sufficiently large times, we have an approximate expression for M_t as

$$M_{t\to\infty} \approx 2C_0\sqrt{\frac{D_1 t}{\pi}}\left(\frac{1+\alpha}{1-\alpha}\right) - \frac{4\alpha}{(1-\alpha)^2} \tag{4.16}$$

where $k = \sqrt{D_1 / D_2}$ and $\alpha = (1-k)/(1+k)$. We can see from Eq. (4.10) and (4.16) that M_t is proportional to $t^{1/2}$.

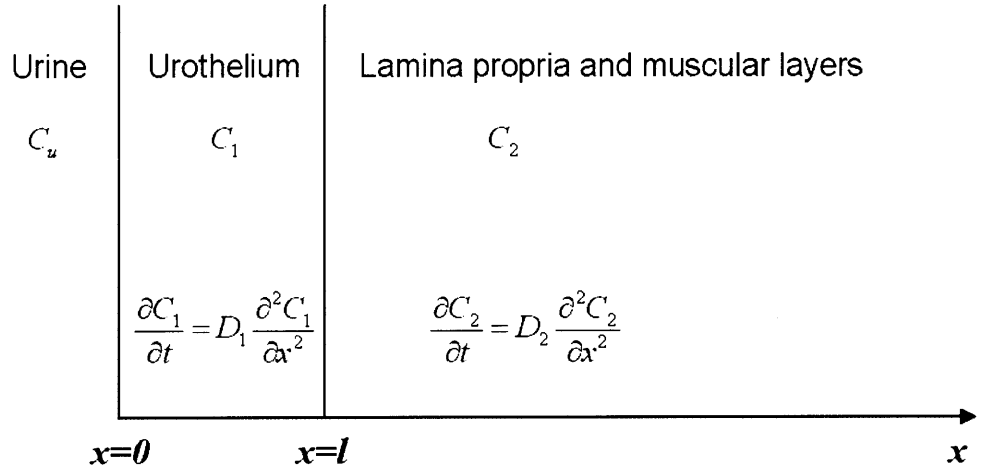

Figure 23. Semi-infinite composite model for the drug diffusion in the bladder *in vitro*

4.2.3 *In vivo* drug distribution model in the bladder

In vivo drug absorption in the bladder is different from *in vitro* absorption because systemic drug absorption occurs in the lamina propria and muscular layers where capillaries are

perfused and drug can be removed via the blood [46, 51]. Systemic drug absorption in the lamina propria and muscular layers can be considered by introducing microscopic permeability coefficient (p) and surface area of the capillaries (a) as in Figure 24. The steady solution ($\partial C / \partial t = 0$) can be achieved as follows:

$$C_1 = C_0 - \frac{(C_0 - C_l)}{l} x \quad \text{for } 0 < x \le l \tag{4.17}$$

$$C_2 = C_b + (C_l - C_b) \exp\left(-\sqrt{\frac{pa}{D_2}} (x - l) \right) \quad \text{for } x \ge l \tag{4.18}$$

where $C_0 = KC_u$; C_l is the concentration at the interface between the urothelium and the submucosa (lamina propria); C_b is the plasma drug concentration in blood vessels. The drug tissue concentration in the urothelium declines linearly with increasing depth. There is an exponential decrease of the drug tissue concentration in the lamina propria and muscular layers due to the removal of drug by capillaries. The biphasic behavior for drug tissue concentration-depth profiles is caused by the existence of capillaries perfused in the tissues. The concentration difference between the tissue and the perfusing blood determines the amount of systemic drug removal as in Figure 24. There is a limitation to obtain an analytical solution for *in vivo* drug distribution model. Numerical simulation for kinetic model of drug distribution after intravesical instillation was studied by Grabnar *et al* [46]. The model parameters used in their study were obtained under *in vitro* conditions, and so the numerical simulation has a limitation of precisely depicting *in vivo* conditions [45]. However, despite its limitations, the urine and tissue pharmacokinetic models can not only offer an insight into the relationship between treatment conditions and parameters but also can provide the basis to design future intravesical drug delivery system.

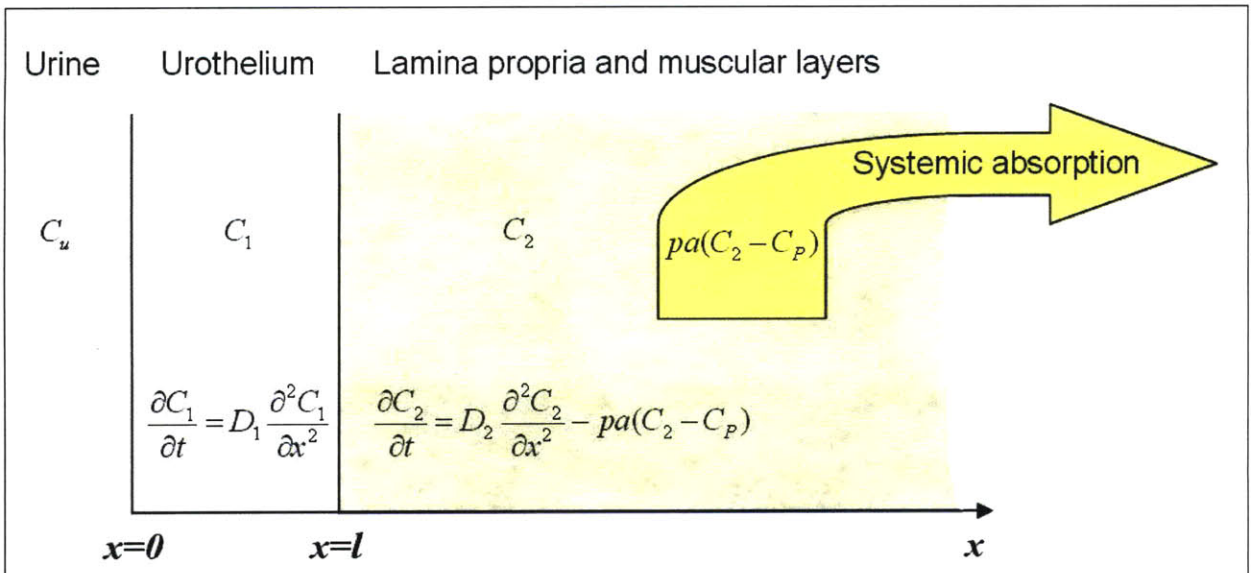

Figure 24. Semi-infinite composite model for the drug diffusion in the bladder *in vivo*

4.3 *In vitro* lidocaine absorption study with rat bladder

Lidocaine absorption *in vitro* into urothelium was investigated with rat bladders (Pel-Freez Biologicals). The effect of urine pH and absorption time were also studied. A lidocaine solution was made with artificial urine (Surine Negative, Dyna-Tek Industries, Inc.), radiolabeled lidocaine hydrochloride [carbonyl-^{14}C] (50-60 mCi/mmol, M.W.=270.9, American Radiolabeled Chemicals, Inc.), and lidocaine hydrochloride monohydrate (Sigma-Aldrich Co.). A 1% solution has the radioactivity of 0.06 μCi/mL, and a 10^{-5}% solution has the radioactivity of 0.02 μCi/mL. Radiolabeled lidocaine solution was made with ethanol and the concentration is 0.1 μCi/μL. 20 mL 1% lidocaine solution having the radioactivity of 0.06 μCi/mL was made with 200 mg of non-radioactive lidocaine, 12 μL of radioactive lidocaine solution. 20 mL 10^{-5}% lidocaine solution having the radioactivity of 0.02 μCi/mL was made as follows. First, 10 μg/mL solution was made with 50 μg (100 μL) of radioactive lidocaine and 5 mL of artificial

urine. Then, 1mL from the previous 10 μg/mL solution was added to 9 mL of artificial urine (1 μg/mL solution). Finally, 0.1 μg/mL (10^{-5}%) solution was obtained by adding 2 mL of the 1 μg/mL solution to 18 mL of artificial urine. The pH of synthetic urine was adjusted with HCl 1.0N solution (Sigma-Aldrich Co.) or 8.4% Sodium bicarbonate (Sigma-Aldrich Co.) to obtain solution pH ranging from 4.0 to 8.5. Lidocaine hydrochloride did not dissolve at pH levels higher than 8.5.

Rat bladders were inverted to expose the urothelium (inner lining of the bladder) and the inverted neck was closed by suture (Ethilon, 4-0, Ethicon, Inc.) to avoid having the lidocaine solution come in contact with the outer lining of the bladders. Inverting the bladder was done by tweezers and a plastic cotton applicator. First, the opening of rat bladder (Pel-Freez Biologicals, Sprague-Dawley rats, 56002-2, 7-8 weeks old, mixed gender) is stretched out by tweezers. Then, the bladder portion opposite to the opening is pushed by plastic cotton tipped applicator so that the bladder can be inverted. The bladder tissue over applicator is further stretched out to make sure that the bladder is completely inverted. Once inverted, a knot is made with suture as close to the bladder opening as possible. The applicator is withdrawn from the bladder once the first suture knot is made. The first knot is further tighten up after the withdrawal of the applicator, and two extra knots are made to ensure that drug solution does not leak into the bladder when it is immersed in the solution. Figure 25 shows the procedure of inverting the rat bladder. A leak test was performed with trypan blue saline solution (Sigma-Aldrich Co.). Bladders were placed in the solution at 37 °C for one hour and were taken out of the solution. The bladders were rinsed in saline and water to eliminate dye from the urothelium surface, and then the bladders were inverted again so that the outer layer of the bladder could be checked for leaks. No dye penetration through the knotted part of the bladder was observed by microscopic examination.

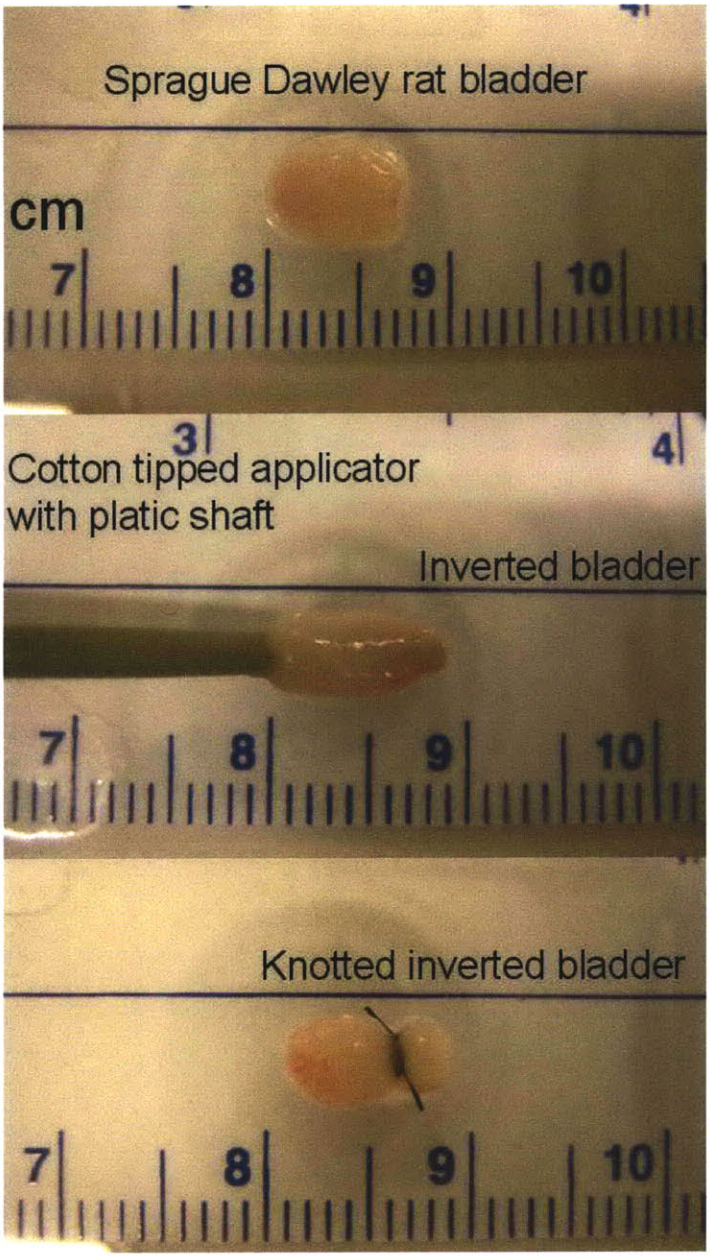

Figure 25. Procedure of inverting the rat bladder: (top) Sprague Dawley rat bladder, about 1 cm in length. (Middle) Inverted bladder on a cotton tipped applicator. (Bottom) The inverted bladder knotted by suture.

Each inverted bladder was placed in each lidocaine solution (1 mL of lidocaine solution in 7 mL vial) having different concentration and pH. Bladders were immersed completely in the solution to make sure the whole inner bladder surface was in contact with the lidocaine solution. Each vial was capped to avoid evaporation and placed in an incubator at 37 °C. Incubation time

was 10 min, 1 hour, 1 day, 3 days or 5 days, and the bladder was removed from the solution after the designated incubation time. Each bladder, after taken from a vial, was rinsed three times in phosphate buffered saline (PBS) to remove excess lidocaine solution surrounding the bladder. Tweezers were also rinsed in PBS to avoid possible contamination. Each bladder was cut off below the suture, and then it was weighed. Each prepared bladder sample weighed about 100 mg.

Lidocaine tissue concentration was detected by liquid scintillation counting (LSC) method. The method of whole tissue solubilization was adopted for the extraction of lidocaine from the bladder tissue, and the detailed procedures can be found in the reference. Weighed tissue samples were placed in 20 mL glass scintillation vial. 1 mL of tissue solubilizer (Solvable^{TM}, PerkinElmer, Inc.) was added to the vial, and it was placed in an oven at 50-60 °C for about 3 hours until tissue was completely dissolved. Once the vials had been removed from the oven and the tissue had been dissolved, the amount of radioactivity in each vial was quantified by liquid scintillation counter (Packard Tri-Carb 2200CA, PerkinElmer, Waltham, MA). Raw data (disintegrations per minute, DPM) from the liquid scintillation counter were converted to nanocuries (nCi) by using the conversion factor of 2,200 dpm = 1 nCi. 10 mL of the LSC cocktail (Hionic-Fluor, PerkinElmer) was poured into each vial. The sample vials were placed in rack inside the scintillation counter for at least an hour before counting for temperature and light adaptation. The radioactivity in each sample was detected using the proper protocol for ^{14}C in the scintillation counter, and the data was analyzed after running the tissue samples. The total radioactivity counted in each vial was divided by the tissue mass to normalize the amount of lidocaine absorbed in the bladder tissue.

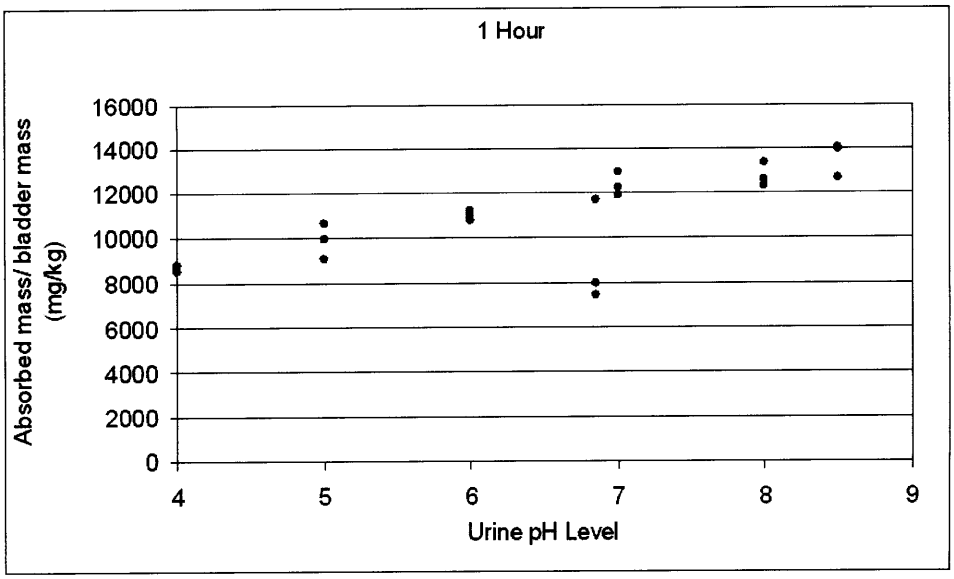

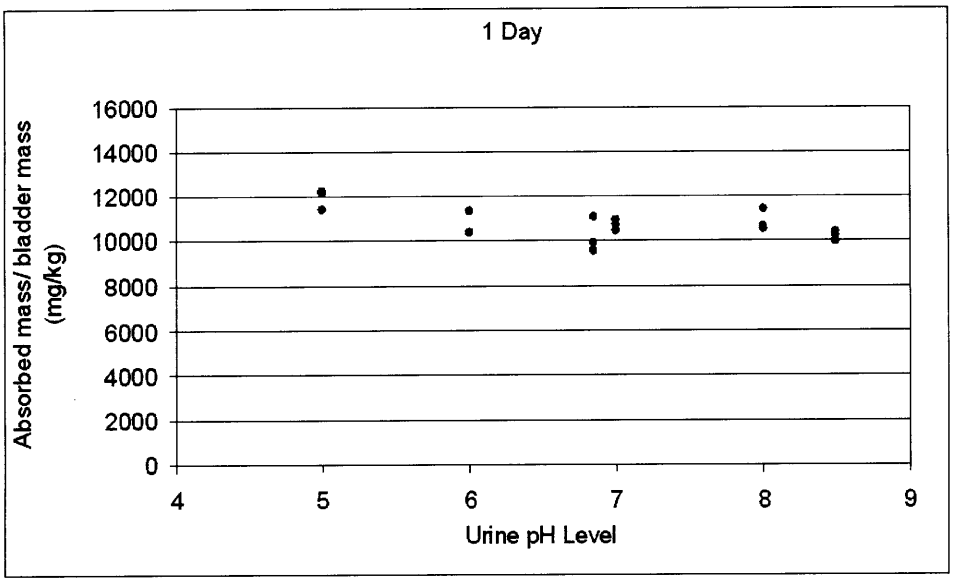

Figure 26. The effect of pH on the absorption of lidocaine in rat bladder for 1 hour and 1 day. The bladder samples were placed in 1% lidocaine solution (0.06 μCi/mL).

Figure 26 shows the effect of pH on the absorption of lidocaine into the bladder tissue. The lidocaine concentration of the tested solutions was all 1% (10 mg/mL), and tested pH were 4.0, 5.0, 6.0, 6.85, 7.0, 8.0 and 8.5. The lidocaine absorption to the bladder is shown to be slightly affected by the pH of lidocaine solution after an hour. There is, however, no significant

effect of pH on lidocaine absorption after one day. The plateau tissue concentration (or absorbed lidocaine mass per bladder tissue mass) is about 10000 mg/kg or 1%, which is the lidocaine concentration of the vial where the bladder was immersed. This result implies that the topical absorption of lidocaine from the bladder for a long term period can be independent of the pH of the lidocaine solution. This result also indicates no need to buffer the lidocaine solution *in situ* in the bladder for a long term application to increase the topical lidocaine absorption from urothelium.

Figure 27 shows the effect of the concentration and pH of lidocaine solution on the lidocaine absorption into the bladder tissue over the time (n=3 for each pH and each time point). Error bars indicate the standard deviation for three samples. Lidocaine tissue concentration increases quickly (within about ten minutes) and reach plateau for both 10^{-5}% and 1% lidocaine solutions. The plateau lidocaine tissue concentration for 10^{-5}% lidocaine urine solution is in the order of 0.1 mg/kg or 10^{-5}% while that for 1% lidocaine urine solution is in the order of 10000 mg/kg or 1%. This result means that the partition coefficient for lidocaine tissue to lidocaine solution is about unity for *in vitro* lidocaine absorption into urothelium. Higher lidocaine concentration shows higher lidocaine absorption into urothelium. Future studies will include obtaining tissue concentration-depth profiles for the *in vivo* setting using a cryomicrotome technique at multiple time points to establish the *in vivo* lidocaine distribution model in the bladder.

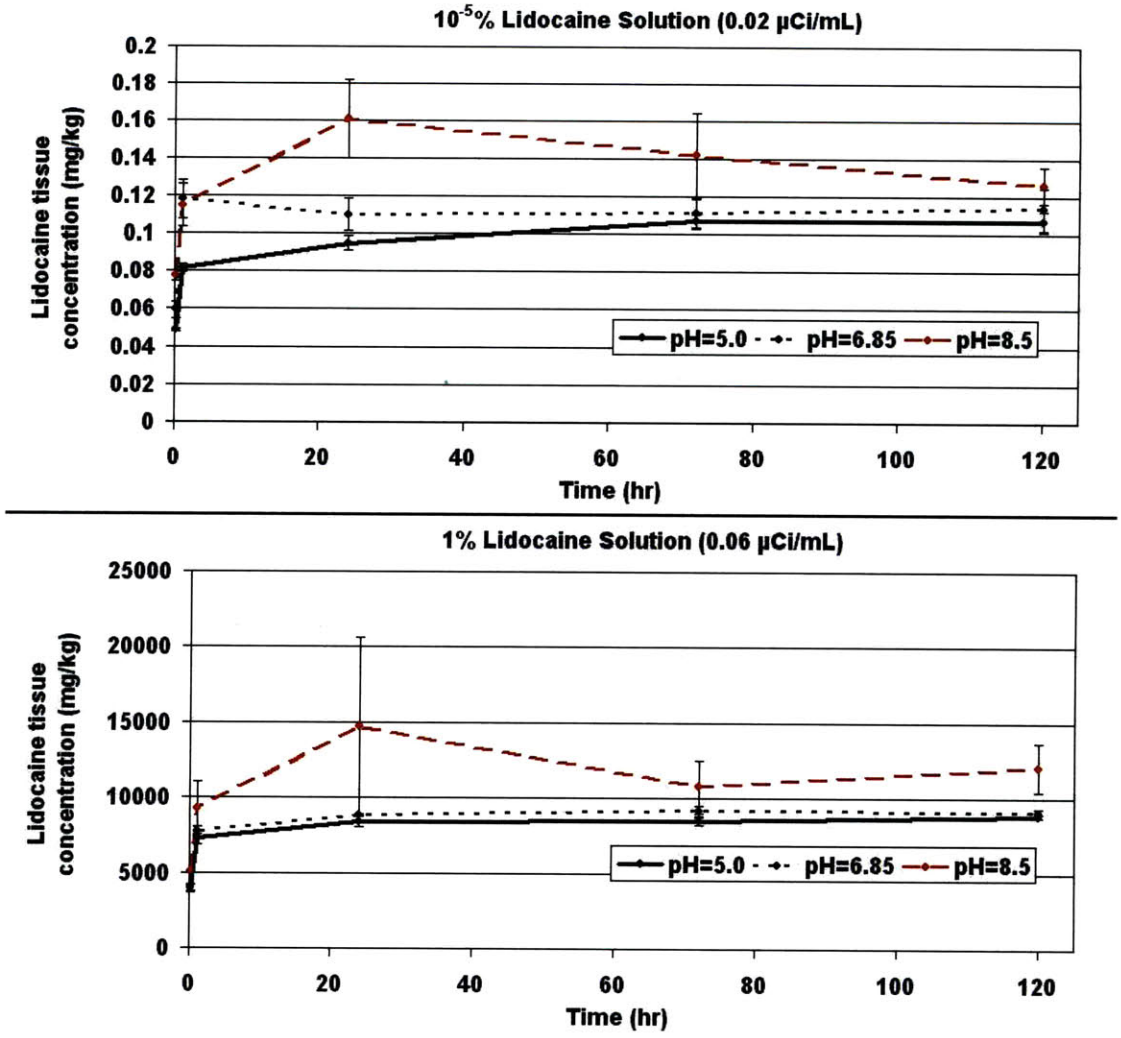

Figure 27. Lidocaine tissue concentration-time profiles for 10^{-5}% and 1% lidocaine solutions (n=3 for each pH and each time point. Error bars indicate the standard deviation of three samples).

Chapter 5 *In vivo* lidocaine exposure studies in a rabbit model

In vivo drug exposure studies with intravesical lidocaine have been performed to investigate the absorption of lidocaine by the bladder. Two types of *in vivo* experiments were performed with a rabbit model. One was to instill lidocaine solution directly into the bladder and the other was to implant the lidocaine delivery device into the bladder. The solution instillation was performed to emulate conventional intravesical solution instillation treatments while the device implantation was done to investigate treatment with the intravesical drug delivery device.

5.1 Intravesical instillation of lidocaine solution

Intravesical instillation of lidocaine solutions is used to treat patients with interstitial cystitis/painful bladder syndrome (IC/PBS) [14, 15, 52-56]. A pharmacokinetic study of intravesical lidocaine therapy shows that pain experienced by IC/PBS patients is relieved because the sensory neurons within the submucosal plexus are blocked [14]. Pain relief is related to the lidocaine concentration within the bladder wall. Intravesical instillation of a lidocaine solution was conducted with a rabbit model, and tissue and plasma concentrations of lidocaine were measured.

The study was conducted with male New Zealand White rabbits weighing 2.5-2.9 kg (Covance Inc.). The rabbits had no restrictions on food and water. The rabbits were cared for in compliance with protocols approved by the Massachusetts Institute of Technology Committee on Animal Care, in conformity with the NIH guidelines for the care and use of laboratory animals (NIH publication #85–23, revised 1985). Intramuscular injection of ketamine (35 mg/kg) and xylazine (5 mg/kg) was used to anesthetize the rabbits, and the rabbits were kept under

anesthesia during the experiment. Sterile ocular lubricant (Puralube Ointment, Fougera, Inc. NY) was applied to relieve dryness of the eyes during anesthesia. The animals under adequate depth of anesthesia were positioned supinely. Blood samples were drawn from the marginal ear vein with a 24-gauge catheter. A 10-Fr pediatric Foley catheter (Rusch, Teleflex Medical, IL) was inserted into the urethra, and 3 mL distilled water was used for ballooning within the bladder. Lubricant (Surgilube, Fougera, Inc. NY) was applied on the surface of the catheter to facilitate the insertion of the catheter through the urethra. The bladder was emptied by collecting urine through the inserted catheter. 10 mL of lidocaine aqueous solution made with sterile water and lidocaine hydrochloride was instilled by a syringe attached to the end of the Foley catheter. The dose was 2 mg/kg or 5 mg/kg, which was based on the clinical studies [14, 15]. Blood samples were collected before and after the intravesical instillation at multiple time points through the catheter in the ear vein. The bladder was emptied after 1 hour or 2 hours, which is the solution dwell time in the bladder. Then, the Foley catheter and the ear vein catheter were removed from the rabbits. The rabbits were placed into the cage after recovering from the anesthesia. The rabbits were taken out of the cage afterwards at about 10 hours and 24 hours for collecting blood samples from the marginal ear vein using a 23-gauage butterfly needle (Surflo Winged Infusion Set, Terumo Medical Corporation). Then, the animals were euthanized at 24 hours by pentobarbital overdose and the bladders were extracted for the tissue collection. Methods to detect lidocaine in blood and bladder tissue as well as sample preparation methods are described in the section 5.3.

5.2 Implantation of intravesical drug delivery device

The study was conducted with male New Zealand White rabbits weighing 2.5-3.2 kg (Covance Inc.). The rabbits had no restrictions on food and water. The rabbits were cared for in compliance with protocols approved by the Massachusetts Institute of Technology Committee on Animal Care, in conformity with the NIH guidelines for the care and use of laboratory animals (NIH publication #85–23, revised 1985). A modified urethral catheter (10 Fr, feeding tube and urethral catheter, Kendall, Sovereign, Tyco Healthcare) was made by cutting the rounded closed-tip end of the catheter and flame polishing the cut surface to make it smooth. The device was stretched and pushed gently into the smoothened end into the catheter until the device was fully loaded into the catheter. Ethylene oxide (EtO) gas was used to sterilize the device-loaded catheter as well as the push rod. Intramuscular injection of ketamine (35 mg/kg) and xylazine (5 mg/kg) was used to anesthetize the rabbits and they were kept under anesthesia during the experiment. Sterile ocular lubricant (Puralube Ointment, Fougera, Inc. NY) was applied to relieve dryness of the eyes during anesthesia. The animals under adequate depth of anesthesia were positioned supinely, and the catheter loaded with the device was inserted into the bladder through the urethra of the animal. Lubricant (Surgilube, Fougera, Inc. NY) was applied on the surface of the catheter to facilitate the insertion of the catheter through the urethra. The tip of the push rod was also lubricated to reduce the surface friction between the inner surface of the catheter and the push rod. Urine could be collected at this point through the inserted catheter once the catheter tip was placed in the bladder. Abdominal pressure was applied to stimulate voiding of the urine from the bladder. The device was deployed from the catheter into the bladder by the push rod. The catheter was pulled out after the device implantation. The sequence of the device implantation is shown in Figure 28. The entire procedure was performed aseptically. An x-ray was taken to confirm the implantation location. Blood samples were

collected from the marginal ear vein or artery of the animals at multiple time points before and after the device implantation. The marginal ear vein is normally used for smaller volume of blood samples while artery is for larger volume samples. Several techniques were employed to allow for serial blood sampling. Hematoma and bruising were minimized, especially when blood was drawn from the ear artery. Blood sampling was also performed distally to proximally along the blood vessel (from the tip of the ear and toward the base of the ear), alternating ears instead of using the same vein consecutively. The animals were secured in a restrainer to avoid inadvertent movement during blood sampling.

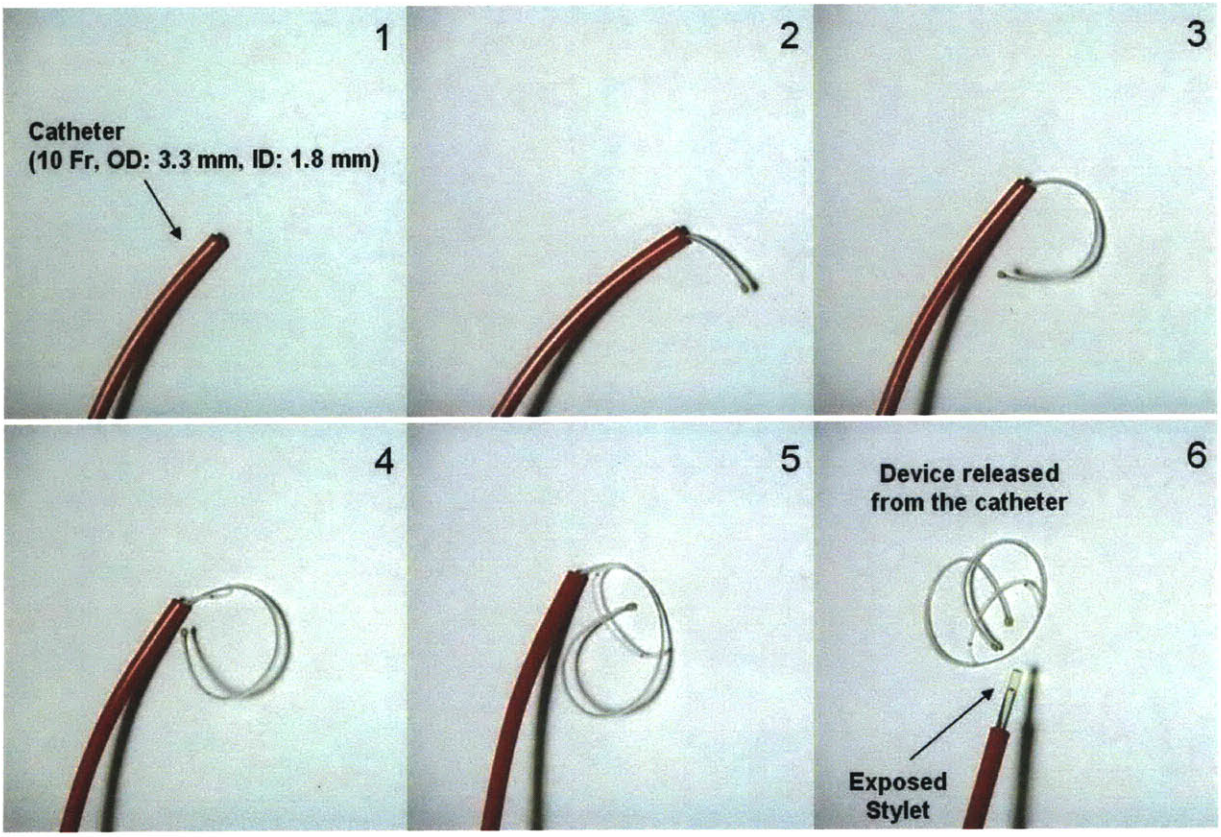

Figure 28. The device implantation sequence by the catheter-stylet system

X-ray images were taken at multiple time points (immediately after implantation, 2 days after, and 9 days after device implantation) with one rabbit (Figure 29). X-rays were taken both

in the right lateral recumbent position and supine position. Multiple x-ray images taken at different times revealed that the device can move freely within the bladder rather than staying in one position. The platinum parts embedded at the end of the two arms are shown more clearly due to its enhanced radioopacity compared with nitinol. The device was well tolerated by rabbits during the period of *in vivo* study without any health problem. The animals were euthanized at multiple pre-determined end points by pentobarbital overdose and the bladders were extracted for the tissue collection.

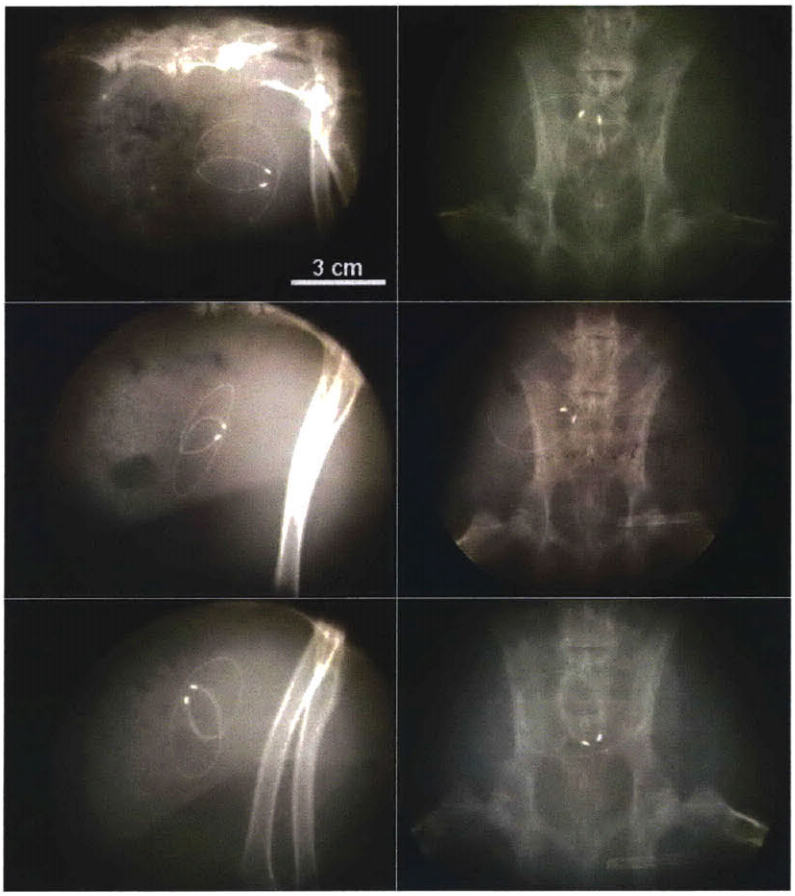

Figure 29. Radiographs of implanted devices. (Top row) Immediately after implantation, (Middle row) 2 days after implantation, (Bottom row) 9 days after implantation. Left column is when the animal was in the right lateral recumbent position and right column is when the animal was in the supine position.

5.3 Measurement of the lidocaine concentration in blood and bladder

5.3.1 Blood samples

Blood samples from the animals were collected from marginal ear vein or artery in blood collection tubes (BD Vacutainer, Lithium Heparin #367884, Becton, Dickinson and Company). Collected blood sample was centrifuged at 10000 RPM for 10 minutes at room temperature (Centrifuge 5415C, Eppendorf) and supernatant or plasma was used in an Enzyme-Linked ImmunoSorbent Assay (ELISA). Lidocaine ELISA kits (#106719-I, Neogen Corporation, KY) were used as suggested by the manufacturer to detect lidocaine in plasma. The ELISA kit operates based on competitive binding between the lidocaine or its metabolite in the sample and the lidocaine-enzyme conjugate to a limited number of antibody binding sites (anti-lidocaine antibodies). The lidocaine hapten and horseradish peroxidase (HRP) were linked to form a covalently-linked lidocaine-enzyme conjugate [57-59]. The optical densities of each sample were measured using a micro-plate reader (SpectraMax plus384, Molecular Devices) at a wavelength of 650 nm. Standard dilutions of plasma for a standard curve were prepared by centrifugation of blood spiked with lidocaine. The concentrations for standard dilutions were 0, 0.5, 1, 2, 4, and 8 ng/mL. Representative typical standard curves are shown in Figure 30. Dilutions of 1/10, 1/100, and 1/1000 were performed to bring sample concentration within the assay range. Dilutions of samples were performed with phosphate buffered saline solution with bovine serum and a preservative (EIA buffer, Neogen Corporation, KY).

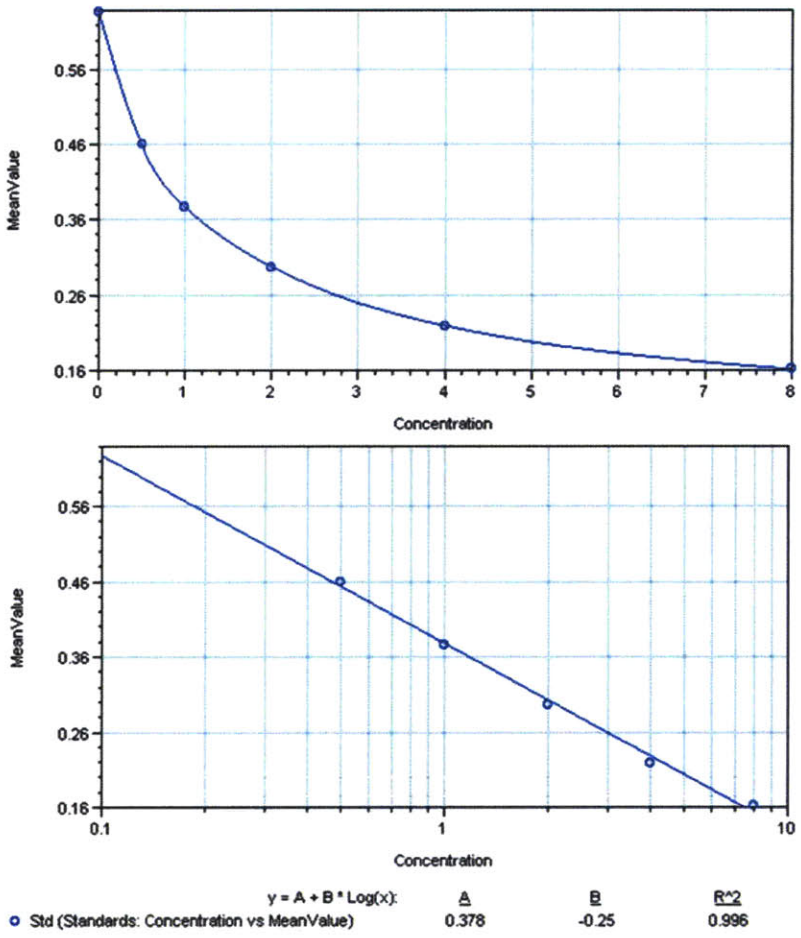

Figure 30. Representative typical standard curve for standard dilutions of plasma (0, 0.5, 1, 2, 4, and 8 ng/mL). Cubic spline curve (top) and semi-log graph (bottom).

5.3.2 Bladder tissue samples

Bladders were collected from the animals after multiple time points, 1, 2, 3, and 6 days. The bladder from each animal was cut into 100-200 mg segments after removing as much fat and connective tissue from the bladder as possible. Each piece of bladder tissue segment was weighed, and a tissue homogenization process was followed. The bead beater (Mini-Beadbeater-1, BioSpec Products, OK) was used to homogenize the tissue. The bead beater vigorously agitates a sealed vial containing tissue, extraction solution and hundreds of minute beads. A

weighed tissue segment was placed into a 2 mL conical bottom vial with o-ring seal cap (BioSpec Products, OK) containing zirconia beads with 1 mm diameter (BioSpec Products, OK) and 1 mL of EIA buffer (Neogen Corporation, KY). Heating of the homogenate during bead beating was minimized by starting with pre-chilled vials in ice water as well as by alternating one minute bead beating and one minute cooling (cooling between bead beating). Bead beating was repeated several times until the beads and tissue flowed freely inside the vials. The number of bead beating depends on the mass of tissue segment; as a larger tissue mass requires more bead beating. The homogenate after the completion of homogenization process was transferred to a 1.5 mL microcentrifuge vial after the beads settled to the bottom of the 2 mL conical bottom vial. Then, the homogenate was centrifuged at 10000 RPM for 10 minutes at room temperature (Centrifuge 5415C, Eppendorf), and the lidocaine concentration in the supernatant was quantified by ELISA as described above. Standard dilutions for a standard curve were made using a control rabbit bladder (Pel-Freez Biologicals). The rabbit bladder was cut into 100-200 mg sections, and known amounts of lidocaine was spiked into the vial containing the beads and EIA buffer. The homogenization process for standard dilutions was the same as that of tissue samples. The concentrations for standard dilutions were 0, 0.5, 1, 2, 4, and 8 ng/mL. Sample dilutions of 1/10, 1/100, and 1/1000 were performed with EIA buffer (Neogen Corporation, KY) to bring sample concentration within the assay range.

5.4 Biodistribution of lidocaine

Lidocaine concentration in plasma and bladder tissue after either intravesical instillation treatment or device treatment was measured to investigate the biodistribution after each treatment. Lidocaine plasma concentrations over time for the instillation treatment (dotted lines)

and the device treatment (solid lines) are shown in Figure 31. The weight of each animal is also shown (Figure 31, inset). The device containing 2 mg is denoted as '3 day device' while the one with 4 mg as '6 day device'. Specifications and *in vitro* release curves for 3 day and 6 day devices are shown in Chapter 2.

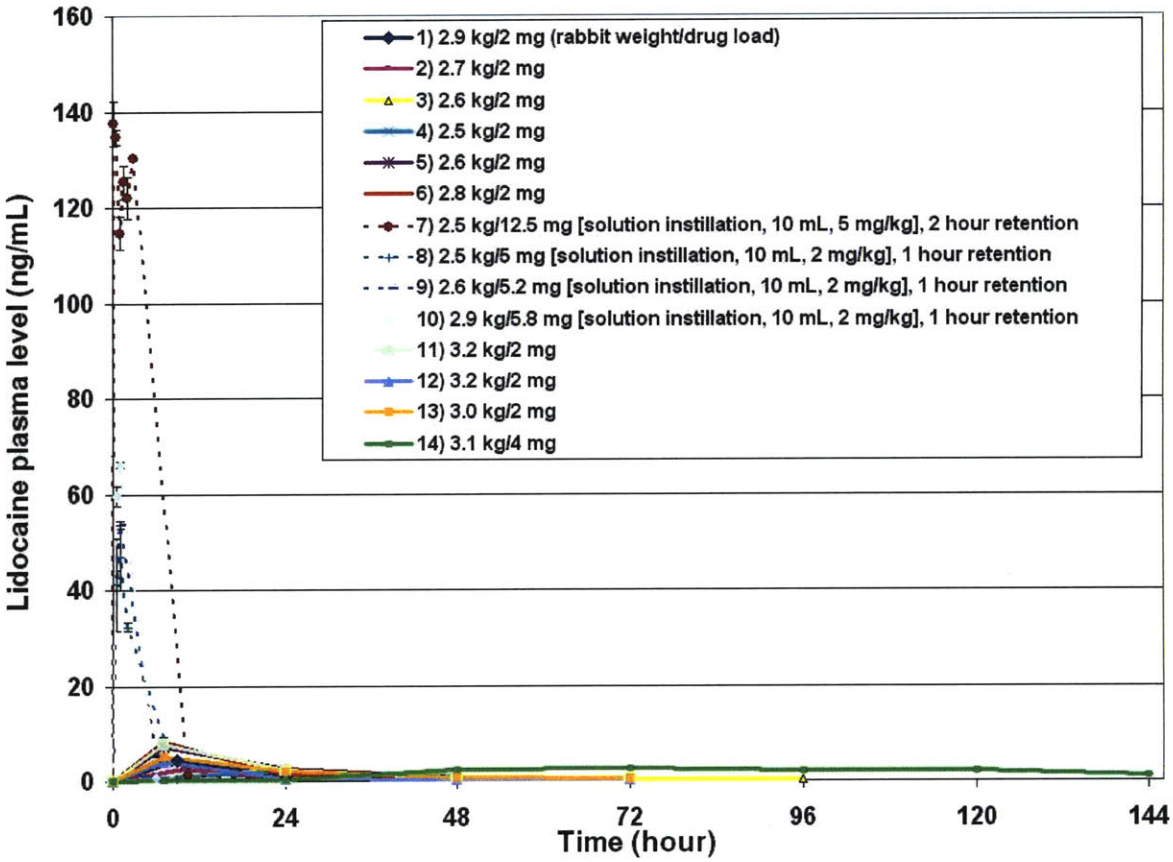

Figure 31. *In vivo* results for lidocaine plasma concentration. Lidocaine plasma concentration for the instillation treatment (dotted lines) and the device treatment (solid lines). Errors bars represent the standard deviation for the duplicate samples for ELISA assay.

Intravesical instillation of lidocaine solution resulted in an initial surge in the plasma after, but lidocaine was not detected in plasma after 24 hours. The plasma concentration for the instillation treatment is characterized by the sudden increase and then rapid drop of lidocaine plasma concentration. The peak plasma concentration from the instillation of lidocaine solution

with the dose of 5 mg/kg and two hour retention time exceeds 100 ng/mL, which is within a factor of ten of the known toxicity limit of lidocaine [11, 21-24]. The high initial peak concentration may, however, be necessary to extend the relief between repeated instillations in the intravesical solution therapy approach. Figure 31 was redrawn in Figure 32 with modified vertical scale in order to show the results of the device treatment.

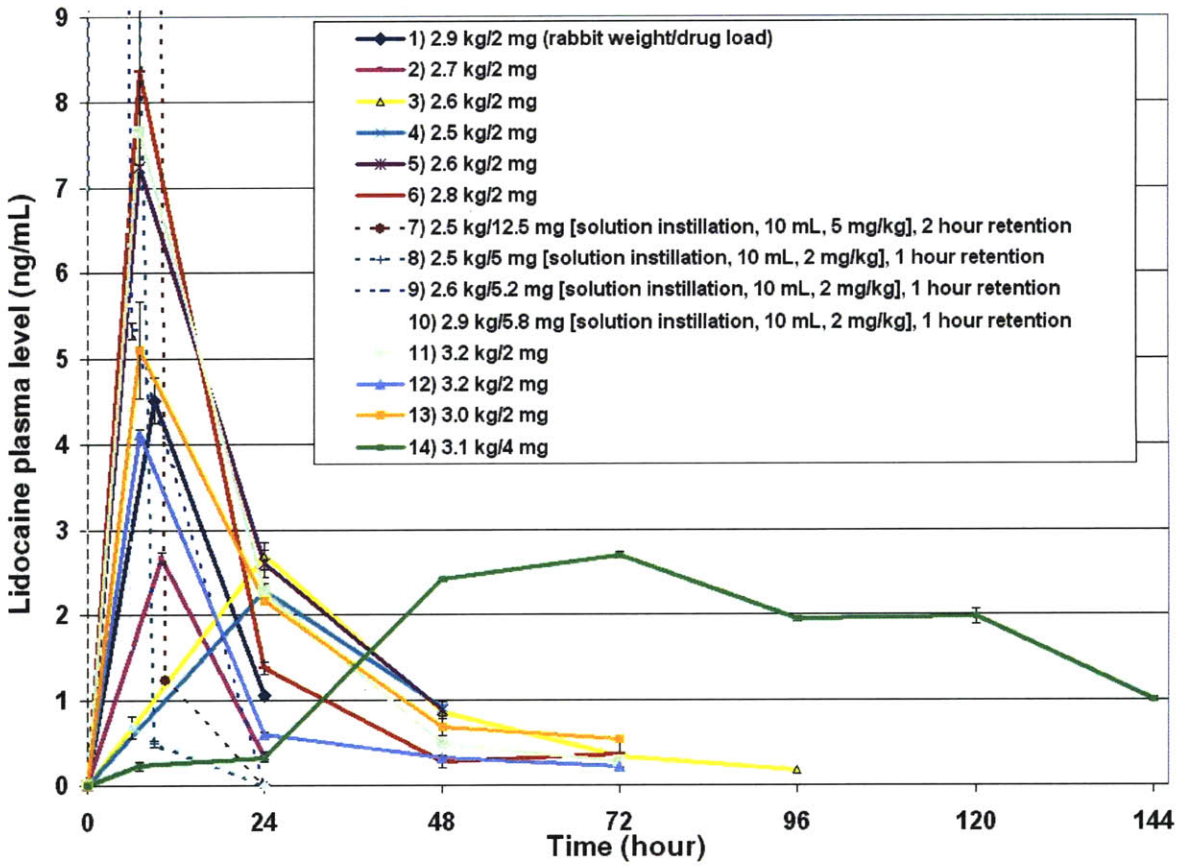

Figure 32. *In vivo* results for lidocaine plasma concentration. The scale of the vertical is modified from Error! Reference source not found. **to better show the results from the device treatment. Errors bars represent the standard deviation for the duplicate samples for ELISA assay.**

The device treatment shows much lower but extended plasma lidocaine level than that of the instillation treatment. The *in vitro* release experiments with 3 day device in Chapter 2 showed that the drug release rate from the device slows down after 12 hours, and this fact is

reflected in the *in vivo* exposure result. The pilot *in vivo* exposure study with 6 day device is also shown in Figure 32 labeled with the number 14. Compared with the 3 day device, the 6 day device has a doubled payload as well as a more extended release profile. There was an initial lag time observed for the *in vitro* release profile for the 6 day device (Figure 14, device 'IV'). The thicker wall of the silicone tube for the 6 day device is hydrated during the initial lag time before lidocaine starts to release from the device. The *in vitro* time lag was reflected in the *in vivo* exposure result in Figure 32. The depot delivery method by the device may avoid the high peak plasma concentration yet provide higher drug exposure for a long-term application.

The bladder tissue concentration of lidocaine is a more direct index to determine the efficacy of treatment than the plasma concentration since the target site for the intravesical treatment is the bladder tissue. Figure 33 shows the lidocaine concentration in the bladder tissue over time. The animals implanted with the 3 day device were sacrificed for bladder extraction at one, two, and three days after device implantation. The tissue concentration decreases over time. The tissue concentration from the 6 day device shows that the lidocaine level at day 6 is comparable to the level after 24 hours for the 3 day device. The tissue concentrations at 24 hours after intravesical instillation of lidocaine solutions were also measured by the same method, but lidocaine was not detected or below the detection limit (about 0.5 ng/mL) of the current lidocaine ELISA kit. It should be noted that the lidocaine tissue concentration is in the order of microgram per gram of tissue. Tissue homogenate samples were diluted by 1:1000 to bring sample concentration within the ELISA assay range. The rabbits, unlike humans, were under general anesthesia for cystoscopic implantation of the device. The reduced fluid intake of individual animal while recovering from anesthesia affects the drug release from the device, which is related to the drug plasma level as well as drug tissue level. Some clinical treatments

recommend fluid restriction after intravesical instillation to achieve the highest exposure possible and reduce wash-out, but this would ideally not be necessary.

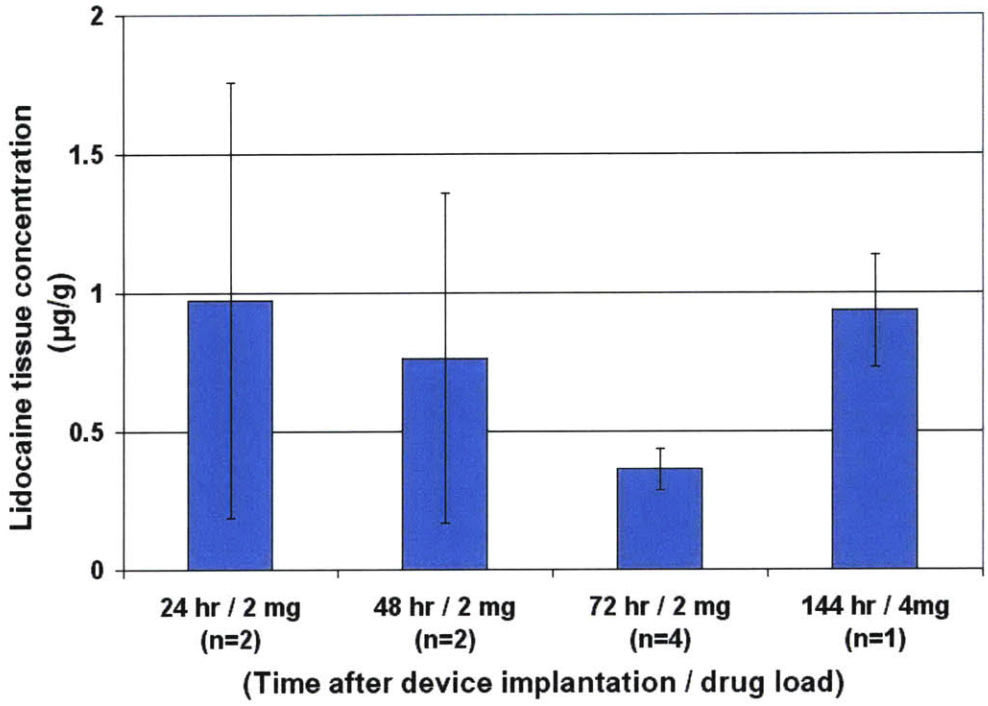

Figure 33. Lidocaine tissue concentration (µg/g). Device residence time and drug payload are indicated. Errors bars represent the standard deviation for the samples from multiple animals or from multiple positions in the bladder.

Lidocaine plasma and tissue concentration for each animal are simultaneously shown in Figure 34 to represent the correlation between them. The *in vivo* results at 24 hours after the intravesical instillation treatment are also shown in Figure 34, but they are all negligible compared with the results from the device treatment. Horizontal error bars indicates the standard deviation for the tissue samples from multiple positions in the bladder, and vertical error bars indicate the standard deviation for the duplicate plasma samples for the assay. There is a general trend that higher plasma concentrations are associated with higher tissue concentrations. The tissue concentration is approximately thousand times as high as that for the plasma concentration.

Therefore, our depot delivery approach by the device treatment may provide higher drug exposure to the bladder tissue while avoiding the high peak plasma concentration.

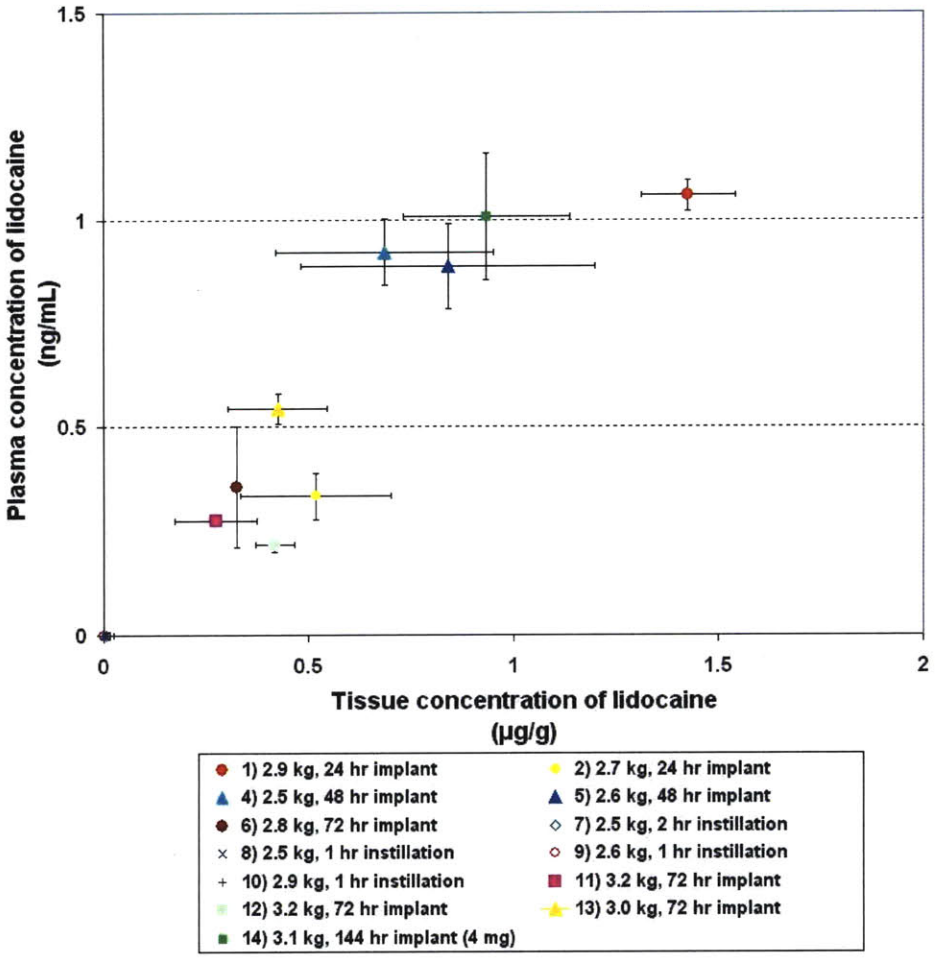

Figure 34. Correlation between lidocaine plasma concentration and tissue concentration. Errors bars represent the standard deviation for the tissue samples from multiple positions in the bladder or for the duplicate plasma samples for ELISA.

Lidocaine urine concentration was also measured for two animals that were treated with the 3 day device and 6 day device individually. Lidocaine ELISA kits (#106719-I, Neogen Corporation, KY) were used to detect lidocaine in urine. Rabbit urine was collected from the bladder after the animal was sacrificed. Collected urine sample was centrifuged at 10000 RPM for 10 minutes at room temperature (Centrifuge 5415C, Eppendorf), and then the supernatant

was used for the assay. Standard dilutions of urine for a standard curve were made with artificial urine (Surine Negative, Dyna-Tek Industries, Inc.) spiked with lidocaine. The concentrations for standard dilutions were 0, 0.5, 1, 2, 4, and 8 ng/mL. Dilutions of 1:10, 1:100, and 1:1000 were performed to bring sample concentration within the assay range. Lidocaine urine and tissue concentration are shown in Figure 35. The bladder tissue and urine samples were collected from each animal after 3 days with the 3 day device (Figure 35, left) or after 6 days with the 6 day device (Figure 35, right). The order of magnitude of urine concentration is comparable to that of tissue concentration, which was previously shown in Figure 27 for *in vitro* lidocaine absorption studies with lidocaine urine solutions of 10^{-5}% (0.1 µg/mL) and 1% (0.01 g/mL).

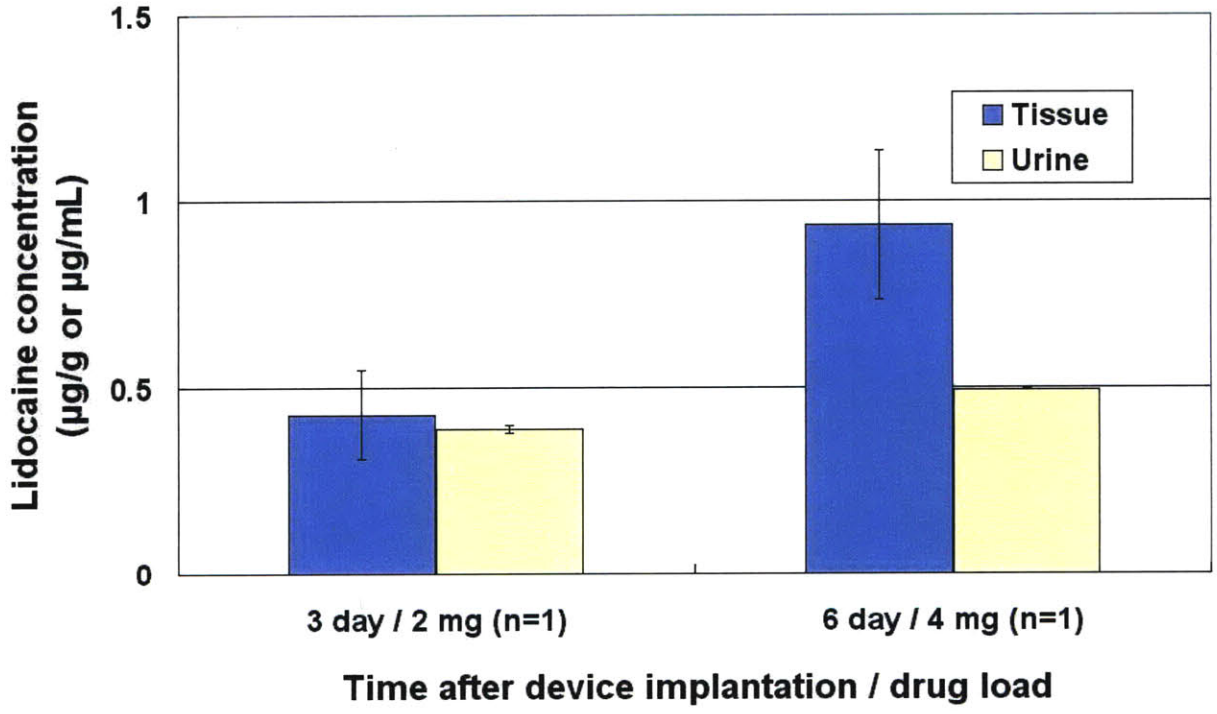

Figure 35. Lidocaine concentration of tissue and urine. Device implantation time and drug loading are indicated. Errors bars represent the standard deviation for the tissue samples from multiple positions in the bladder or for the duplicate plasma samples for ELISA.

5.5 Implantation in the seminal vesicle

A pilot *in vivo* experiment was conducted to explore the situation when the device is implanted in a location other than the bladder, such as the seminal vesicle for men. Figure 36 shows the genital organs of a male New Zealand White rabbit, and the seminal vesicle is located at the position from 2.5 cm to 3.5 cm in Figure 36. The seminal vesicle has sac-like structure originating from the base of the bladder [60, 61]. Figure 37 shows porcine genitourinary organs, which is similar to those of a rabbit. The device made of silicone tube and monofilament nylon suture (Ethilon, monofilament nylon, size 1, 4.0 metric, Ethicon, inc.) was implanted to the lumen of the seminal vesicle of a rabbit. The drug release unit in the device was the same as that for the 3 day device, and the drug load was 2 mg as in the 3 day device. Lidocaine plasma concentration over the time is shown in Figure 38. The peak concentration appeared at 48 hours after device implantation, which is delayed compared with the result of the previous experiment for the 3 day device in the bladder. The water-scarce environment in the seminal vesicle compared with the bladder may have caused the longer induction time when water permeates through the silicone device and dissolve the solid cast lidocaine in the drug reservoir to initiate drug release.

Figure 36. Genital organs of a male New Zealand White rabbit. The bladder is shown in the left and the penile urethra in the right.

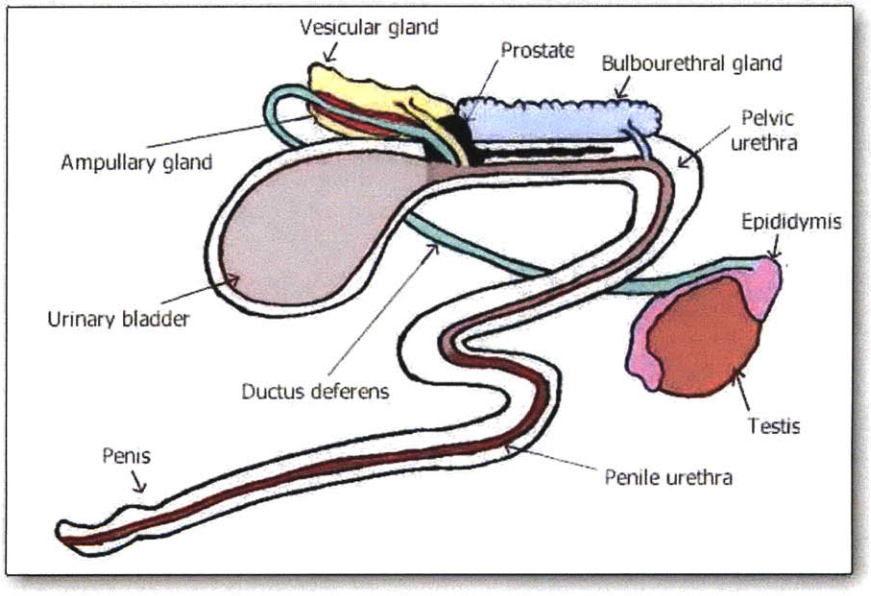

Figure 37. Porcine male reproductive system (Diagram reproduced here with permission from Dr. Charlotte L. Ownby, College of Veterinary Medicine, OKlahoma State University, Stillwater, OK)

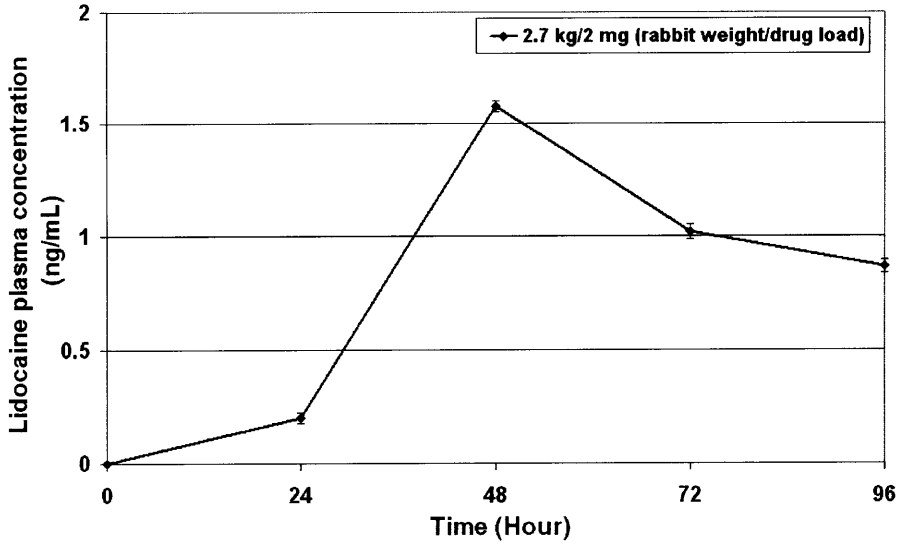

Figure 38. Lidocaine plasma concentration with the device implanted in the seminal vesicle. The device shape was that of the one at top right in Figure 7.

5.6 Encrustation and low calcium diet

Rabbits are unusual in that the plasma calcium concentration reflects the dietary calcium level. Figure 39 shows that the plasma calcium concentration increases in proportion to the dietary calcium level [62, 63]. Rabbits lack the homeostatic control of their serum calcium level while many other animal species homeostatically maintain the serum calcium level at a nearly constant level by the interactions the parathyroid hormone (PTH), vitamin D, and calcitonin [62, 64]. Another unusual concept of calcium metabolism in rabbits is that the urine is the main route of excretion of excess calcium while the bile is the major route of calcium excretion in other animals [65-68]. Rabbits excrete about 45-60% of their ingested calcium in the urine while other mammals excrete only less than 2% of ingested calcium in their urine [62, 63]. Rabbit urine appears cloudy, creamy, or turbid in general. Figure 40 shows rabbit urine in a tube placed vertically so that excess calcium carbonate crystals settled to the bottom of the tube.

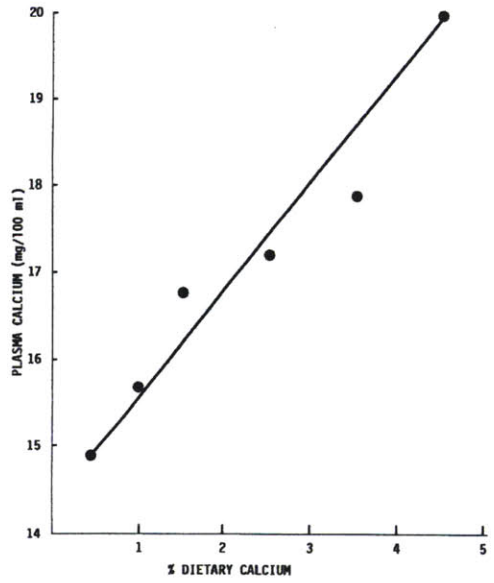

Figure 39. The effect of the dietary calcium level on the plasma calcium level. The range for calcium excretion for the rabbit is about 45-60% while other mammals excrete less than 2% of ingested calcium in the urine [63].

Figure 40. Rabbit urine in 15 mL centrifuge tube. Urine was placed vertically, not centrifuged, and precipitated calcium carbonate is shown as sediment.

Considering the excessive calcium present in the rabbit urine, it is not surprising that encrustation can be found on devices even after a short dwelling time in the bladder. Studies on

the encrustation on urinary tract biomaterials suggested that formation of encrustation depends on catheter materials and the urine composition [69-73]. The placebo device without drug reservoir was implanted to the bladder and retrieved at nine weeks after implantation. The outer surface of the device was silicone. The long-term device toleration study with a rabbit clearly shows the severe encrustation on the device in Figure 41. Encrustation could be observed in x-ray radiographs before retrieval of the device from the bladder. More encrustation was observed on both arms at the device compared to other locations of the device. This may reflect the fact that once implanted, each arm has less chance of being directly in contact with the bladder wall and experiences less deformation during the residence of the device in the bladder compared to other locations of the device.

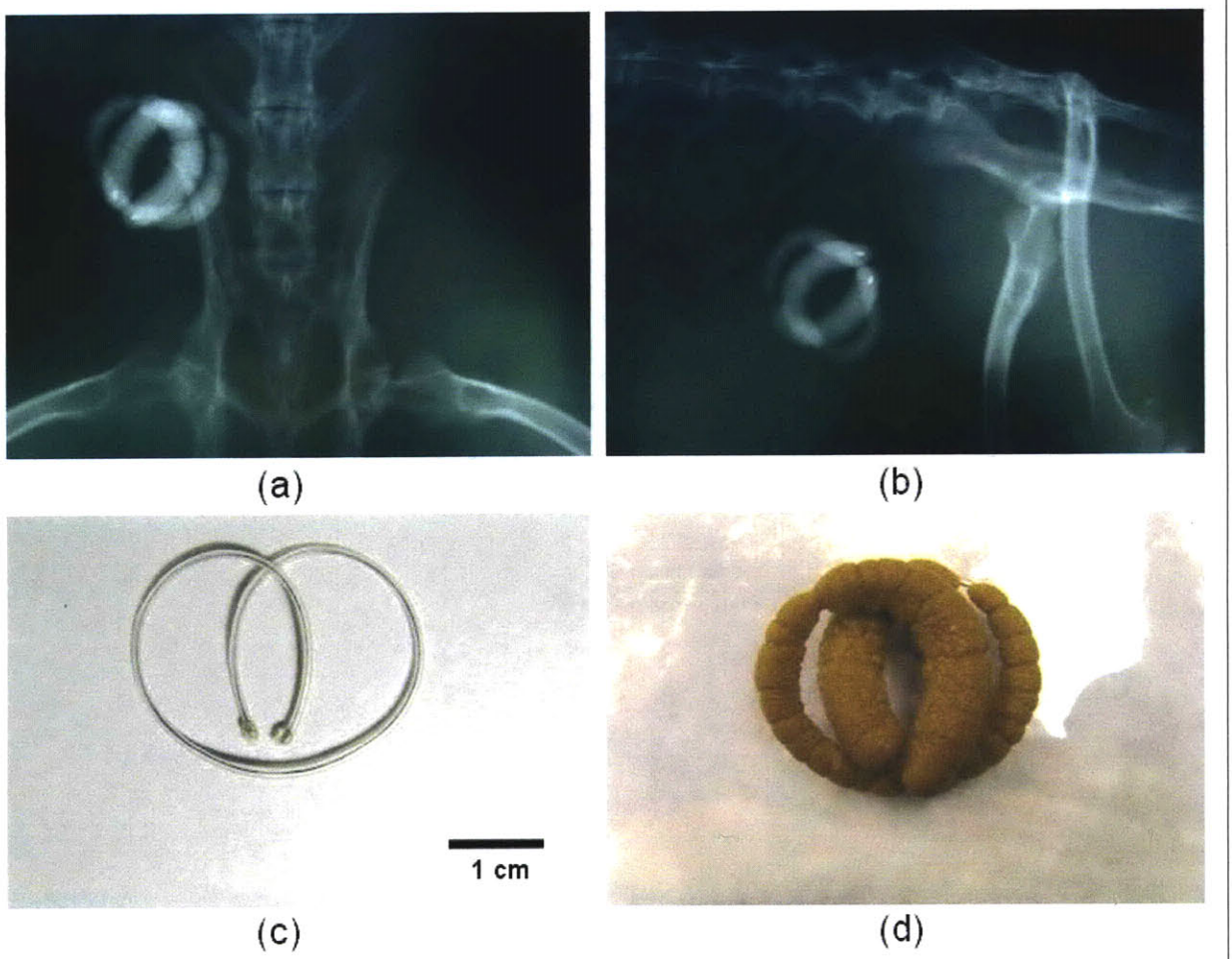

Figure 41. Encrusted placebo device without drug release reservoir. The device was implanted in the bladder for 9 weeks. Radiographs (a) in the supine position and (b) in the right lateral recumbent position. (c) The device before implantation. (d) The retrieved device from the bladder at 9 weeks after implantation. The calcium encrustation on the device can be seen in Radiographs.

Encrustation on the device can be reduced by surface treatment such as coating with heparin, pentosanpolysulfate (PPS, a semisynthetic polysaccharide chemically similar to heparin), or oxalate-degrading enzymes from *Oxalobacter formigenes* [73-76]. Surface treatment with heparin-like polysaccharides for our silicone device should be investigated further. Another method to reduce encrustation for the rabbit model is to adopt a low calcium diet since the urine calcium excretion is in proportional to the dietary calcium intake for rabbits as described earlier. A rabbit's blood and urine calcium concentrations directly reflect dietary calcium intake.

Reduced calcium in rabbit diet leads to lowered serum calcium levels, and subsequently the amount of calcium excreted in the urine will decrease. The chemical composition for control rabbit diet (Laboratory Rabbit Diet HF, 5326, PMI Nutrition International) is shown in Appendix 2, where the calcium is 0.95% and phosphorus is 0.51%. Customized low calcium diet (Modified Labdiet 5321 w/ reduced calcium, 5S4T, PMI Nutrition International) was formulated by TestDiet®, and the chemical composition is shown in Appendix 3, where the calcium is 0.51% and phosphorus is 0.44%. Each composition was carefully controlled to provide the animals with necessary nutritional ingredients. The low calcium diet contains 46% less calcium than the control diet. Each diet has a pellet form with similar size of about 4-5 mm diameter and 10 mm height (Figure 42).

Figure 42. Rabbit diet pellets. (Left) control rabbit diet (LabDiet®). (Right) low calcium diet (TestDiet®).

Control diet and low calcium diet were used to feed the rabbits during *in vivo* experiments with the device. Rabbits were fed with the control diet more than two weeks before starting the low calcium diet. Rabbits did not show any reluctance to the low calcium diet.

There were two different feed durations for the low calcium diet, which were two and four weeks. Figure 43 shows the devices from three rabbits after three days. Rabbits were fed with the control diet, the low calcium diet for two weeks, or the low calcium diet for four weeks before and during the device implantation. The device from the rabbit with the control diet was fully covered with calcium encrustation. The encrustation on the device from the rabbits with the low calcium diet was less than the one from the control diet rabbit. There appears to be an optimum duration for the low calcium diet as the 4 week low calcium diet device exhibited more encrustation than the 2 week low calcium diet device, but still less than the control diet. These results illustrate the utility of the low calcium diet for the rabbit model to reduce the encrustation on the device implanted in the bladder. The device with anti-encrustation coating using heparin-like polysaccharides combined with a low calcium diet will increase the utility of a rabbit model for the long-term study of the intravesical drug delivery device.

Figure 43. The device with encrustation after 3 day implantation in the rabbit bladder: (left) the device from the rabbit with the control diet, (middle) the device from the rabbit with low calcium diet for 2 weeks, (right) the device from the rabbit with low calcium diet for 4 weeks.

5.7 Lidocaine toxicity

Adverse toxic reactions should be considered when lidocaine is used as a local anesthetic agent although the frequency of toxic reactions is extremely low [77]. Systemic toxicity involves the central nervous system (CNS) and cardiovascular system, and local toxicity includes localized nerve damage and localized neural and skeletal muscle irritation. Figure 44 shows the signs and symptoms of systemic toxicity with respect to lidocaine plasma concentration. High lidocaine plasma concentration should be avoided to prevent possible systemic toxicity when lidocaine is used as a local anesthetic agent. *In vivo* exposure studies with the intravesical device showed that low lidocaine level in plasma can be achieved while maintaining lidocaine level in bladder tissue a thousand-fold high in the section 5.4. Therefore, there is low risk of systemic toxicity with the device treatment. Studies on local toxicity using an isolated rabbit vagus nerve and intact rabbit sciatic nerve reported that there were no signs of neurotoxicity with lidocaine [78, 79]. Studies on the long-term application of lidocaine patch suggests that extended application of the patch does not cause sensory loss at the application site [80-83]. No signs of systemic or local toxicity were observed in the studies conducted.

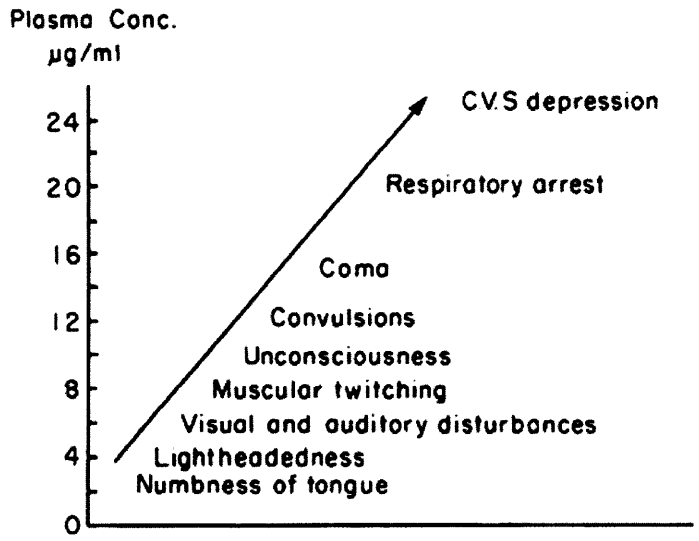

Figure 44. Relationship of signs and symptoms of local anesthetic-induced central nervous system (CNS) toxicity to plasma concentrations of lidocaine [77].

Chapter 6 Design scheme for tubular drug release device

6.1 Basic equations for tubular osmotic pump

The drug delivery device has a tubular osmotic pump made of silicone. Other biocompatible polymer tubes such as polyurethane can be used depending on its permeability to water (and drug) and mechanical properties. Design equations for the tubular osmotic pump are important to obtain the desired drug payload and release rate. Tube thickness is related to mechanical integrity and water permeability. Tube inner diameter and tube wall thickness determine the drug payload and outer diameter of the tube. Tube length affects both drug payload as well as the macro size or loop diameter of the tubular osmotic pump. Osmotic surface area where water can permeate through the tube is affected by tube outer diameter and tube length. All these parameters influences the overall performance of the osmotic pump depends on them.

The inner side of the tube contains drug and the drug contained tubular osmotic pump is our system of consideration for drug mass transfer to the outside medium. Each parameter is defined below.

C: instantaneous drug concentration in the device reservoir

ρ: drug density

S: drug solubility

d: tube inner diameter

h: tube wall thickness

D: diameter of macro loop made of tube

L: tube total length, $L=\pi D$

L_n: tube length without permeation blocking sheath

Ls: tube length with permeation blocking sheath, $L_s=L-L_n$

V: volume of drug reservoir, $V = \frac{\pi d^2 L}{4}$

m: instantaneous drug amount remaining in the device reservoir, $m = CV = C\frac{\pi d^2}{4}L$

m_p: total drug payload, $m_p = \rho V = \rho\frac{\pi d^2}{4}L$

$\Delta\Pi$: osmotic pressure difference between the inside and outside of the tube

$\Delta\Pi_S$: osmotic pressure difference at saturation between the inside and outside of the tube

k: permeability coefficient for solvent transport

A: osmotic surface area for water permeation, $A=\pi(d+h)L_n$

t_z : duration of zero order release

$\frac{dm}{dt}$: the rate of drug mass change in the reservoir, $\frac{dm}{dt} = -kA\frac{\Delta\Pi}{h}C$

$\dot{m}_z$: zero order release rate, $\dot{m}_z = -\left.\frac{dm}{dt}\right|_{zero} = kA\frac{\Delta\Pi_S}{h}S$

m_z : amount released during zero order release, $m_z = \dot{m}_z \cdot t_z$

The notation of 'dm/dt' is defined differently from the definition in section 2.4. Here, it is defined as the rate of drug mass loss in the device reservoir since 'm' indicates the instantaneous drug amount remaining in the device reservoir. The minus sign in the expression 'dm/dt' reflects the fact that the device will lose its drug by osmotic release once the device is immersed in water or urine. When the osmotic pressure of the surrounding medium is small enough compared to the osmotic pressure of the formulation inside the drug reservoir, van't Hoff's law can be used to obtain:

$$\frac{\Delta\Pi_C}{\Delta\Pi_S} = \frac{C}{S} \tag{6.1}$$

where the proportional relationship between the osmotic pressure and concentration is used.

The drug release rate from the device remains constant at the initial time period when the concentration inside the drug reservoir is the solubility of drug loaded. The amount of drug released during this initial 'zero-order release period' can be expressed as

$$m_z = \left(1 - \frac{S}{\rho}\right) m_p \tag{6.2}$$

The drug release rate decreases after the zero-order release period as the drug concentration inside the reservoir becomes reduced. The rate of drug mass change (dm/dt) in the reservoir can still be expressed in terms of zero order release rate ($\dot{m}_z$):

$$\frac{dm}{dt} = -kA\frac{\Delta\Pi}{h}C = \left(-kA\frac{\Delta\Pi_S}{h}S\right)\frac{C}{S}\frac{\Delta\Pi}{\Delta\Pi_S}$$

$$= -\dot{m}_z\frac{C^2}{S^2} \tag{6.3}$$

The expressions for the amount of drug remaining in the reservoir (m) and the rate of drug mass change (dm/dt) are different for two time periods, the zero order release period and the non-zero order release period. The expressions for the zero-order release period ($0 \le t \le t_z$) are:

$$m = m_p - \dot{m}_z t \tag{6.4}$$

$$\frac{dm}{dt} = -\dot{m}_z \tag{6.5}$$

Integrating Eq. (6.3) is used to find the expressions for the non-zero order release period ($t \ge t_z$). Drug concentration (C) and drug mass (m) are time-dependent variables and are related by

$$m = CV \tag{6.6}$$

Integrating Eq. (6.3) from t_z to t after combining Eq. (6.6) with Eq. (6.3), we get

$$\int_{SV}^{m} m^{-2} dm = \int_{t_z} -\frac{\dot{m}_z}{(SV)^2} dt \tag{6.7}$$

Drug mass remaining inside the reservoir at time t ($\geq t_z$) can be expressed as

$$m = \frac{S}{\rho} m_p \left[1 + \frac{\rho}{S} \frac{\dot{m}_z}{m_p} (t - t_z) \right]^{-1} \tag{6.8}$$

and

$$\frac{dm}{dt} = -\dot{m}_z \left[1 + \frac{\rho}{S} \frac{\dot{m}_z}{m_p} (t - t_z) \right]^{-2} \tag{6.9}$$

where

$$t_z = \left(1 - \frac{S}{\rho} \right) \frac{m_p}{\dot{m}_z} \tag{6.10}$$

The drug mass in the device reservoir beyond t_z can be expressed as

$$m = \alpha m_p \ (\alpha \leq 1) \tag{6.11}$$

where α is the ratio parameter indicating remaining drug mass compared to the initial loading (for example, if α is 0.05, then 5% of the total payload remains in the device or 95% of the total loading is released out). Substituting Eq. (6.11) into Eq. (6.8) gives the time t as

$$t = t_z + \frac{m_p}{\dot{m}_z} \left(-\frac{S}{\rho} + \frac{1}{\alpha} \frac{S^2}{\rho^2} \right) = \frac{m_p}{\dot{m}_z} \left(1 - 2\frac{S}{\rho} + \frac{1}{\alpha} \frac{S^2}{\rho^2} \right) \tag{6.12}$$

where t_z is replaced by Eq. (6.10). We can see from Eq. (6.12) that $\frac{m_p}{\dot{m}_z}$ is the factor determining the delivery time scale. This result implies that total payload and initial zero order release rate decides the overall behavior of drug release profile over time.

Examples of the application of Eq. (6.12) are presented here. Figure 45 shows *in vitro* lidocaine release profiles using three different devices made of silicone. Drug payload (m_p) and zero-order drug release rate ($\dot{m}_z$) are different for each device. The relative values of two variables are shown in Table 4 with respect to the values for the device 'A'. The device 'A' has a length of 2 cm and the device 'B' has half the length of the device 'A'. Therefore, both drug payload and zero order release rate for device 'B' are half the values of the device 'A'. This results in the same delivery time scale for 'A' and 'B'. We can see from Figure 45 that overall *in vitro* release profiles with respect to time are similar for 'A' and 'B'. The device 'C' has the same length as the device 'A'. Half the length of the device 'C' is, however, covered with polyurethane sheath to minimize the water permeation so that the zero order release rate for 'C' can be half the value for 'A'. Therefore, the delivery time scale of 'C' is as twice as that of 'A'. Figure 45 shows that the drug release for the device 'C' is twice as slow as that for 'A'.

Table 4. Three different types of device

Variable / Device	Drug payload (m_p)	Zero order release rate ($\dot{m}_z$)	Delivery time scale ($m_p / \dot{m}_z$)
A	1	1	1
B	1/2	1/2	1
C	1	1/2	2

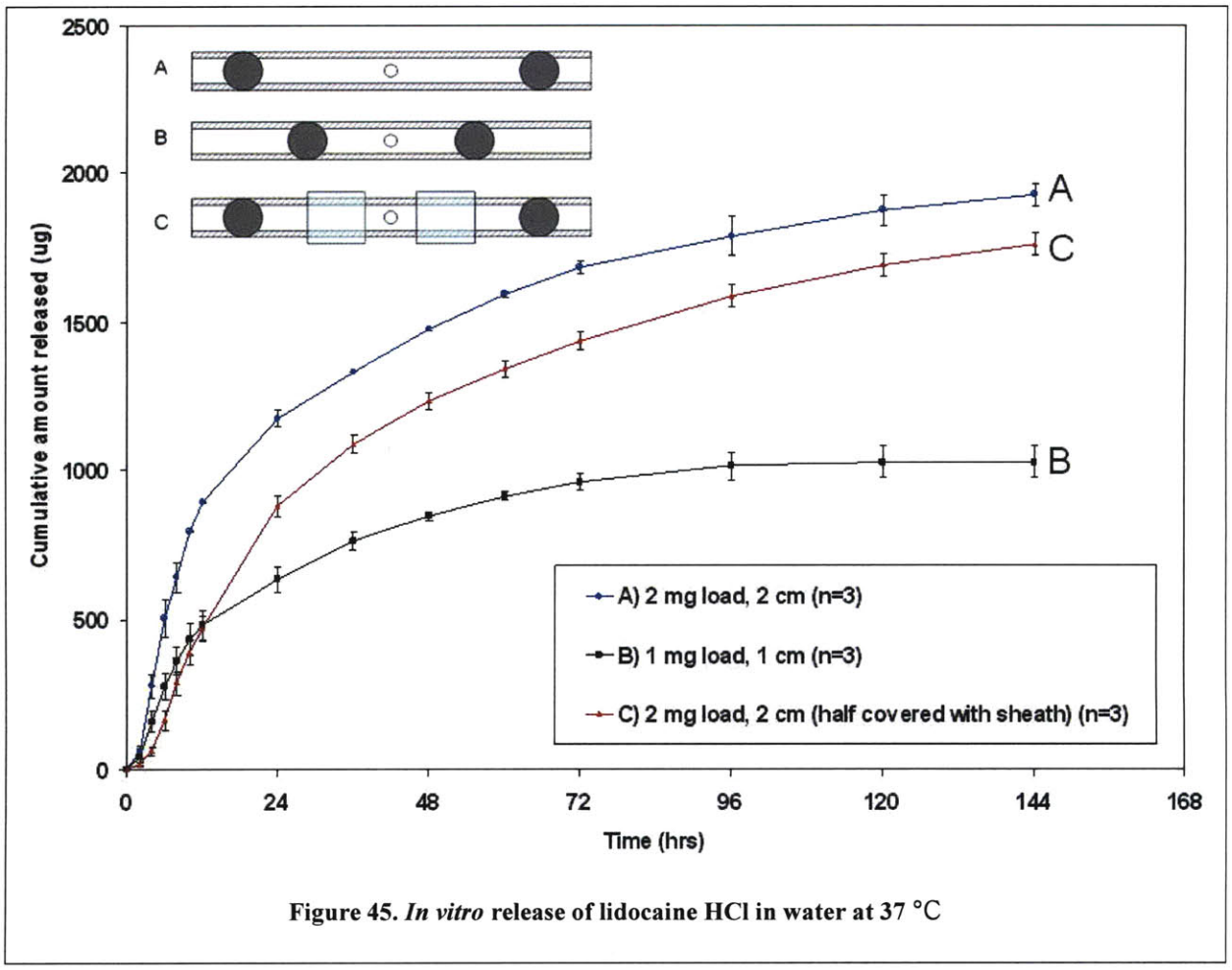

Figure 45. ***In vitro*** **release of lidocaine HCl in water at 37 °C**

6.2 Design of tubular osmotic pump

Modification of design parameters is required to obtain a desirable drug delivery rate and payload. *In vitro* release data for one device can be used to find design parameters necessary to achieve a given drug delivery rate and payload. This section will describe the design method by presenting several examples. *In vitro* release data is compared to *in vivo* exposure data for the device 'A' in Figure 32, and the design parameters for this device will be referred to as the 'base condition' in this section. The parameters for the base condition are specified as:

Base condition

- Tube inner diameter: d_o=0.3048 mm

- Tube wall thickness: h_o=0.1651 mm
- Tube length: L_o=2 cm
- Payload: $m_{p,o}$=2 mg
- Treatment duration: about 3 days

Starting from the information on the base condition, our goal is to obtain design parameters or dimensional information for the device with the desired delivery rate and payload. Two variables, 'a' and 'b,' are defined as the multiplication factor for the target zero order delivery rate and that for the target payload, respectively. The definitions yield the desired target condition as follows:

Target condition

- Zero order delivery rate ($\dot{m}_z$): 'a' times increase compared with the base condition
- Drug payload (m_p): 'b' times increase compared with the base condition

It is assumed here that drug and tube material remain the same for both the base condition and the target condition. The parameters for the target condition have no subscripts here. The zero-order delivery rate condition gives

$$\frac{d+h}{h} L_n = \left(\frac{d_o + h_o}{h_o} L_o \right) a \tag{6.13}$$

and the drug payload condition gives

$$d^2 L = \left(d_o{}^2 L_o \right) b \tag{6.14}$$

Tube wall thickness can vary, but here it is fixed for simplicity:

$$h = h_0 \tag{6.15}$$

A thin tube wall will deteriorate the mechanical integrity of the polymer tube while a thick tube wall may cause undesirable longer induction time for initial drug release from the device. The

reasonable range of the tube wall thickness is determined by mechanical properties and water permeation property of the polymer tube material.

6.2.1 Device made of polymer tube

A silicone tube with a thin wall can act as a water permeable membrane when drug is loaded inside the tube. The case where the device consists of water permeable tube without a polymer sheath will be considered. Silicone tube or other polymer tube can have sheath or coating that is made of polymers with very low permeability to water to minimize water permeation. This case will be treated in the section 6.2.2. The device 'A' and 'B' in Figure 45 show such a case. Water can permeate into the drug reservoir through the entire length of the tube, and so

$$L = L_n \tag{6.16}$$

Quadratic equation for the inner diameter can be obtained from Eq. (6.13) and Eq. (6.14) as

$$d^2 - \frac{(b/a)d_o^2}{d_o + h_o} d - \frac{(b/a)d_o^2}{d_o + h_o} h_o = 0 \tag{6.17}$$

where one solution is positive and the other is negative. The positive solution is designated as d_1, and we get the solution for the tube length as

$$L_1 = \frac{d_0^2 L_0 b}{d_1^2} = \frac{d_0 + h_0}{d_1 + h_0} L_0 a \tag{6.18}$$

Two examples are shown below. We can obtain the tube inner diameter and tube length once the multiplication factors for the delivery rate and the drug payload are chosen. Introduction of a different polymer tube or drug into the drug delivery device will require another *in vitro* release study to obtain the base condition for that specific combination of polymer and drug.

Table 5. Specifications for two examples of devices for human application

Multiplication factor / Design parameter	For delivery rate (a): 10 For payload (b): 50	For delivery rate (a): 20 For payload (b): 200
Tube inner diameter (d_1)	1.1326 mm	2.1303 mm
Tube length (L_1)	7.2418 cm	8.1885 cm
Macro loop diameter (D_1)	2.3051 cm	2.6065 cm
Drug payload (m_p)	100 mg	400 mg
Treatment period	15 days	30 days

6.2.2 Device with sheath for minimizing water permeation

A sheath made of polyurethane can be used to cover some portion of the tube in order to minimize the water permeation through the polymer tube wall as in Figure 45. Special coating such as parylene can also be used to reduce water permeation. The length covered with sheath is denoted as L_S. The previous section corresponds to the case where $L_S = 0$. This situation is often met since diameter of working channel in cystoscope is usually less than 2.4 mm. Eq. (6.13) and Eq. (6.14) show that the tube length (L) increases faster than the sheath covered length (L_n) as the tube inner diameter (d) deceases ($L \propto 1/d^2$ and $L_n \propto 1/(d+h)$). The length of the portion covered with sheath is

$$L_S = L - L_n \tag{6.19}$$

Using Eq. (6.13), (6.14), and (6.19), the length covered with sheath is expressed as

$$L_s = \pi D - \frac{(d_o + h_o) L_o a}{d_o \sqrt{(L_o b)/(\pi D)} + h_o} \tag{6.20}$$

or using Eq. (6.18), we get

$$\frac{L_s}{L_1} = \frac{D}{D_1} - \frac{d_1 + h_o}{d + h_o} \tag{6.21}$$

where subscript 1 indicates the case of no sheath used. The portion of the tube length covered with sheath can be expressed in terms of the tube inner diameter (d) as

$$\frac{L_S}{L} = 1 - \frac{a(d_o + h_o)}{b d_o^2} \left(\frac{d^2}{d + h_o} \right) \tag{6.22}$$

or in terms of the loop diameter (D) as

$$\frac{L_S}{L} = 1 - \frac{(d_o + h_o) L_o a}{d_o \sqrt{\pi b L_o D} + \pi h_o D} \tag{6.23}$$

Two examples in the previous section are reconsidered here. The maximum value for the macro loop diameter under consideration is limited to 5 cm. The adult human bladder capacity is about 500 cm^3, and the corresponding diameter with the assumption of sphere shape bladder is about 10 cm $\left(V = \pi D^3 / 6\right)$. The device with a loop diameter of 5 cm will be only half the size of the maximum linear length in the bladder, approximately. The multiplication factors for the delivery rate (a) and the payload (b), respectively, are shown in Figure 46 and Figure 47. They show the dependency of required sheath length (L_S) and sheath covered portion (L_S / L) on loop diameter (D) and tube inner diameter (d) to achieve given delivery rate and payload. The circle in each plot shows the case without sheath and the corresponding values are in Table 5. Square indicates the case where the loop diameter is 5 cm in each plot. The payload for each example is 100 mg and 400 mg, respectively. The sheath covered portion is less than 40% for

both cases. The tube inner diameter range for 100 mg payload case is smaller than that for 400 mg payload case.

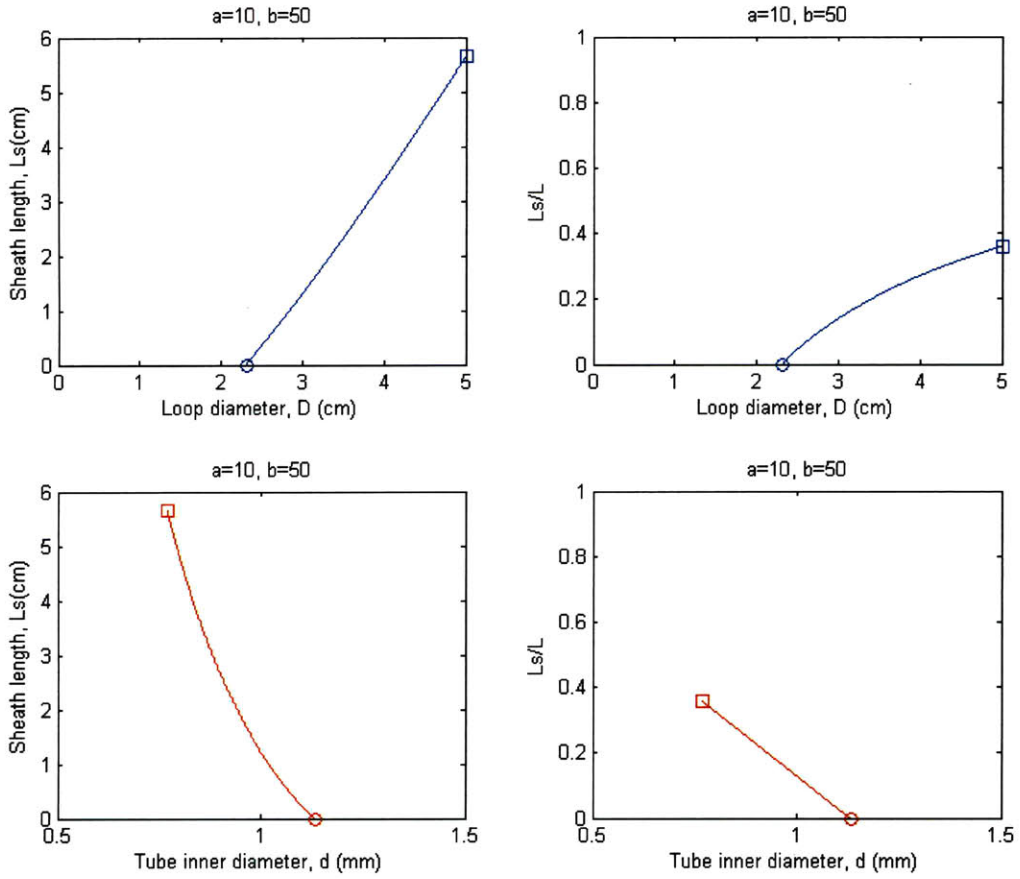

Figure 46. Dependency of sheath length and sheath covered portion on loop diameter and tube inner diameter for a=10 and b=50 (payload: 100 mg)

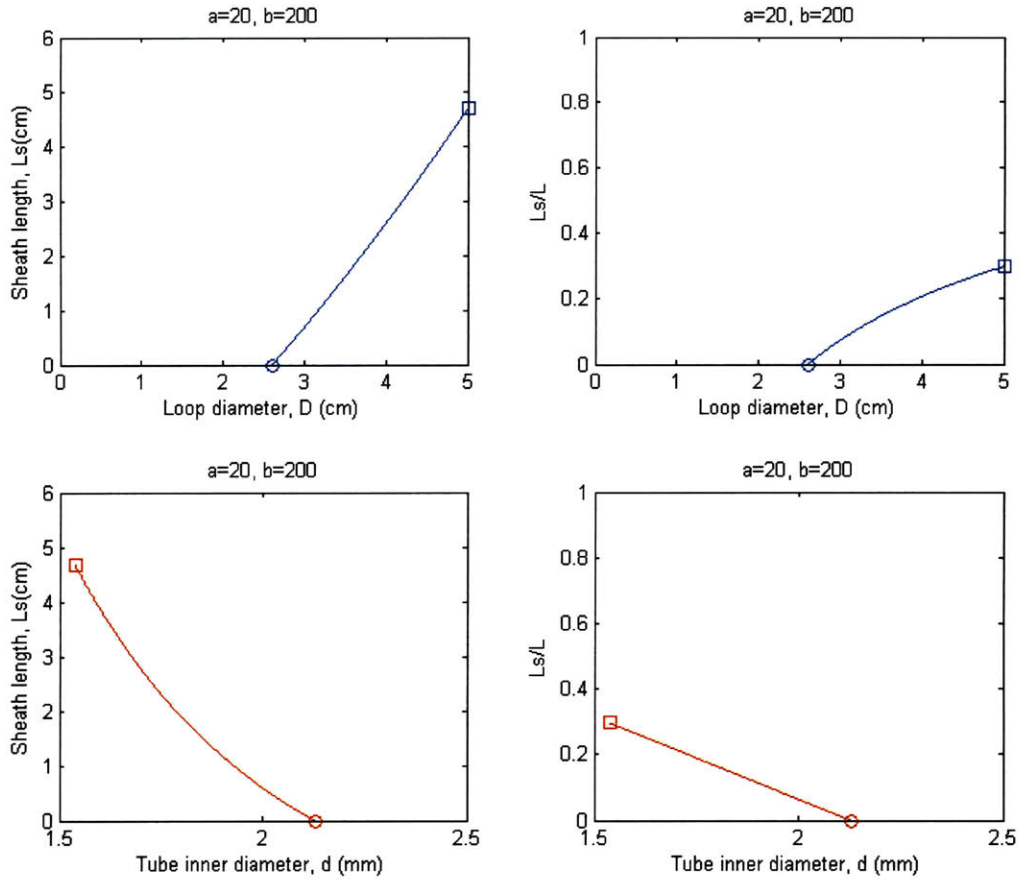

Figure 47. Dependency of sheath length and sheath covered portion on loop diameter and tube inner diameter for a=20 and b=200 (payload: 400 mg)

Chapter 7 Conclusions and future work

7.1 Summary

This thesis covers the design and testing of a drug delivery device that is non-surgically implantable in the bladder. A device with a retentive feature resistant to the contraction of the bladder was implemented and tested *in vitro* and *in vivo* with a rabbit model. Analysis on deformation of elastic ring and semi-circle was performed to find design parameters affecting the elastic property of the device and to enable the fabrication of the device with low modulus elastomers. A cylindrical solid form of chondroitin sulfate C (CSC) and lidocaine with a diameter of approximately 300 μm was formulated to maximize the payload. *In vitro* drug release experiments with CSC and lidocaine were performed to establish design equations for modulating an osmotic drug release rate by changing device parameters such as the dimension and permeability of semi-permeable membrane. Intravesical drug absorption models were investigated to understand the role of the urothelium as a drug diffusion barrier and its effect on the overall drug absorption into the bladder. An *in vitro* lidocaine absorption study with rat bladders showed that the effect of pH on the lidocaine absorption into the urothelium is insignificant after one day. *In vivo* tests using lidocaine, a local anesthetic used for IC/PBS treatment, showed that a sustained and local treatment to the bladder can be achieved with the device. The lidocaine bladder tissue concentration was found to be a thousand-fold higher than the lidocaine plasma concentration at three and six days in a rabbit model. The combination of low systemic and high local tissue concentrations with the device is ideal for intravesical treatments with therapeutic agents such as lidocaine for IC/PBS, oxybutynin for OAB, and chemotherapeutic agents for superficial bladder cancer. Finally, the design strategy for a sustained two to four week intravesical drug delivery device for humans was suggested.

7.2 Future directions

Future studies should investigate the intravesical drug delivery device for long-term applications and additional therapeutic agents. Other animal models may avoid the calcification problem observed with a rabbit model. Possible species (with available Foley catheter size) include a dog (6-12 Fr)[84], a cat (3.5-5 Fr)[84], a pig (8-10 Fr)[85], and a sheep (8-14 Fr)[86] compared with a rabbit (8-12 Fr)[87]. A device for long-term applications may require a larger payload of drug, which necessitates a larger size catheter for device implantation. Histological examination with a device for long-term use can be performed to investigate the safety and tolerability of the device. An intravesical device made of biodegradable materials can be pursued to remove the need for a retrieval procedure. Future studies may use the device for other therapeutic agents that are currently used intravesically. Some exemplary drugs include oxybutynin for OAB and mitomycin C and thiotepa for intravesical chemotherapy to reduce the rate of bladder tumor recurrence.

References

[1] NIH, "Treatments for Urinary Incontinence in Women NIH Publication No. 03-5104 Published June 2003. (Online)."

[2] NIH, "Interstitial Cystitis/Painful Bladder Syndrome. NIH Publication No. 05-3220. Published June 2005. (Online)."

[3] R. R. Dmochowski, "Treatment of the overactive bladder: where we stand in 2003," *Rev Urol*, vol. 5 Suppl 8, pp. S11-7, 2003.

[4] I. Milsom, P. Abrams, L. Cardozo, R. G. Roberts, J. Thuroff, and A. J. Wein, "How widespread are the symptoms of an overactive bladder and how are they managed? A population-based prevalence study," *BJU Int*, vol. 87, pp. 760-6, 2001.

[5] P. A. Norton, L. D. MacDonald, P. M. Sedgwick, and S. L. Stanton, "Distress and delay associated with urinary incontinence, frequency, and urgency in women," *Bmj*, vol. 297, pp. 1187-9, 1988.

[6] J. G. Ouslander, "Management of overactive bladder," *N Engl J Med*, vol. 350, pp. 786-99, 2004.

[7] S. K. Keay, Z. Szekely, T. P. Conrads, T. D. Veenstra, J. J. Barchi, Jr., C. O. Zhang, K. R. Koch, and C. J. Michejda, "An antiproliferative factor from interstitial cystitis patients is a frizzled 8 protein-related sialoglycopeptide," *Proc Natl Acad Sci U S A*, vol. 101, pp. 11803-8, 2004.

[8] S. K. Keay, C. O. Zhang, J. Shoenfelt, D. R. Erickson, K. Whitmore, J. W. Warren, R. Marvel, and T. Chai, "Sensitivity and specificity of antiproliferative factor, heparin-binding epidermal growth factor-like growth factor, and epidermal growth factor as urine markers for interstitial cystitis," *Urology*, vol. 57, pp. 9-14, 2001.

[9] L. Dong, A. Yum, J. Nguyen, and P. Wong, "Enhanced ileal absorption of a hydrophilic macromolecule, pentosan polysulfate sodium (PPS)," *J Biomater Sci Polym Ed*, vol. 15, pp. 671-82, 2004.

[10] G. R. Sant, K. J. Propert, P. M. Hanno, D. Burks, D. Culkin, A. C. Diokno, C. Hardy, J. R. Landis, R. Mayer, R. Madigan, E. M. Messing, K. Peters, T. C. Theoharides, J. Warren, A. J. Wein, W. Steers, J. W. Kusek, and L. M. Nyberg, "A pilot clinical trial of oral pentosan polysulfate and oral hydroxyzine in patients with interstitial cystitis," *J Urol*, vol. 170, pp. 810-5, 2003.

[11] S. K. Gupta and G. Sathyan, "Pharmacokinetics of an oral once-a-day controlled-release oxybutynin formulation compared with immediate-release oxybutynin," *J Clin Pharmacol*, vol. 39, pp. 289-96, 1999.

[12] G. Sathyan, M. B. Chancellor, and S. K. Gupta, "Effect of OROS controlled-release delivery on the pharmacokinetics and pharmacodynamics of oxybutynin chloride," *Br J Clin Pharmacol*, vol. 52, pp. 409-17, 2001.

[13] P. Dull, "Transdermal oxybutynin (oxytrol) for urinary incontinence," *Am Fam Physician*, vol. 70, pp. 2351-2, 2004.

[14] R. Henry, L. Patterson, N. Avery, R. Tanzola, D. Tod, D. Hunter, J. C. Nickel, and A. Morales, "Absorption of alkalized intravesical lidocaine in normal and inflamed bladders: a simple method for improving bladder anesthesia," *J Urol*, vol. 165, pp. 1900-3, 2001.

[15] C. L. Parsons, "Successful downregulation of bladder sensory nerves with combination of heparin and alkalinized lidocaine in patients with interstitial cystitis," *Urology*, vol. 65, pp. 45-8, 2005.

[16] A. Jemal, R. Siegel, E. Ward, Y. Hao, J. Xu, T. Murray, and M. J. Thun, "Cancer statistics, 2008," *CA Cancer J Clin*, vol. 58, pp. 71-96, 2008.
[17] G. Dalbagni, "The management of superficial bladder cancer," *Nat Clin Pract Urol*, vol. 4, pp. 254-60, 2007.
[18] P. U. Malmstrom, "Intravesical therapy of superficial bladder cancer," *Crit Rev Oncol Hematol*, vol. 47, pp. 109-26, 2003.
[19] M. C. Walker, J. R. Masters, C. N. Parris, P. J. Hepburn, and P. J. English, "Intravesical chemotherapy: in vitro studies on the relationship between dose and cytotoxicity," *Urol Res*, vol. 14, pp. 137-40, 1986.
[20] J. L. Au, R. A. Badalament, M. G. Wientjes, D. C. Young, J. A. Warner, P. L. Venema, D. L. Pollifrone, J. D. Harbrecht, J. L. Chin, S. P. Lerner, and B. J. Miles, "Methods to improve efficacy of intravesical mitomycin C: results of a randomized phase III trial," *J Natl Cancer Inst*, vol. 93, pp. 597-604, 2001.
[21] F. Theeuwes, "Elementary osmotic pump," *J Pharm Sci*, vol. 64, pp. 1987-91, 1975.
[22] G. Steinhoff, B. Ittah, and S. Rowan, "The efficacy of chondroitin sulfate 0.2% in treating interstitial cystitis," *Can J Urol*, vol. 9, pp. 1454-8, 2002.
[23] J. C. Nickel, B. Egerdie, J. Downey, R. Singh, A. Skehan, L. Carr, and K. Irvine-Bird, "A real-life multicentre clinical practice study to evaluate the efficacy and safety of intravesical chondroitin sulphate for the treatment of interstitial cystitis," *BJU Int*, 2008.
[24] J. Nordling and A. van Ophoven, "Intravesical glycosaminoglycan replenishment with chondroitin sulphate in chronic forms of cystitis. A multi-national, multi-centre, prospective observational clinical trial," *Arzneimittelforschung*, vol. 58, pp. 328-35, 2008.
[25] D. Porru, M. Cervigni, L. Nasta, F. Natale, R. Lo Voi, C. Tinelli, B. Gardella, A. Anghileri, A. Spinillo, and B. Rovereto, "Results of endovesical hyaluronic acid/chondroitin sulfate in the treatment of Interstitial Cystitis/Painful Bladder Syndrome," *Rev Recent Clin Trials*, vol. 3, pp. 126-9, 2008.
[26] M. Cervigni, F. Natale, L. Nasta, A. Padoa, R. L. Voi, and D. Porru, "A combined intravesical therapy with hyaluronic acid and chondroitin for refractory painful bladder syndrome/interstitial cystitis," *Int Urogynecol J Pelvic Floor Dysfunct*, vol. 19, pp. 943-7, 2008.
[27] G. C. Randall and P. S. Doyle, "Permeation-driven flow in poly(dimethylsiloxane) microfluidic devices," *Proc Natl Acad Sci U S A*, vol. 102, pp. 10813-8, 2005.
[28] E. B. Verneuil, A.; Silberzan, P, "Permeation-induced flows: Consequences for silicone-based microfluidics," *Europhysics Letters*, vol. 68, pp. 412-418, 2004.
[29] K. Alfons and S. Engstrom, "Drug compatibility with the sponge phases formed in monoolein, water, and propylene glycol or poly(ethylene glycol)," *J Pharm Sci*, vol. 87, pp. 1527-30, 1998.
[30] Y. Cui and S. G. Frank, "Isothermal crystallization kinetics of lidocaine in supersaturated lidocaine/polyacrylate pressure sensitive adhesive systems," *J Pharm Sci*, vol. 94, pp. 2039-48, 2005.
[31] H. Mitsuhashi, Y. Tsukada, K. Ono, S. Yano, and T. Naruse, "Urine glycosaminoglycans and heparan sulfate excretions in adult patients with glomerular diseases," *Clin Nephrol*, vol. 39, pp. 231-8, 1993.
[32] D. C. Grant, S. D. Forrester, D. L. Panciera, and J. B. Meldrum, "Measurement of urinary glycosaminoglycans in dogs," *Am J Vet Res*, vol. 67, pp. 51-5, 2006.

[33] P. Le Guevello, P. Le Corre, F. Chevanne, and R. Le Verge, "High-performance liquid chromatographic determination of bupivacaine in plasma samples for biopharmaceutical studies and application to seven other local anaesthetics," *J Chromatogr*, vol. 622, pp. 284-90, 1993.
[34] G. Lunn and N. R. Schmuff, *HPLC methods for pharmaceutical analysis*. New York: Wiley, 1997.
[35] R. Frisch-Fay, "The deformation of elastic circular rings," *Aust. J. Appl. Sci.*, vol. 11, pp. 329-340, 1960.
[36] R. Frisch-Fay, "On large deflections," *Aust. J. Appl. Sci.*, vol. 10, pp. 418-32, 1959.
[37] J. M. Gere and S. Timoshenko, *Mechanics of materials*, 3rd ed. Boston: PWS-KENT Pub. Co., 1990.
[38] Y. Wang, G. A. Ameer, B. J. Sheppard, and R. Langer, "A tough biodegradable elastomer," *Nat Biotechnol*, vol. 20, pp. 602-6, 2002.
[39] G. M. Bernacca, B. O'Connor, D. F. Williams, and D. J. Wheatley, "Hydrodynamic function of polyurethane prosthetic heart valves: influences of Young's modulus and leaflet thickness," *Biomaterials*, vol. 23, pp. 45-50, 2002.
[40] P. M. Hanno, J. R. Landis, Y. Matthews-Cook, J. Kusek, and L. Nyberg, Jr., "The diagnosis of interstitial cystitis revisited: lessons learned from the National Institutes of Health Interstitial Cystitis Database study," *J Urol*, vol. 161, pp. 553-7, 1999.
[41] C. A. Jones and L. Nyberg, "Epidemiology of interstitial cystitis," *Urology*, vol. 49, pp. 2-9, 1997.
[42] J. F. Metts, "Interstitial cystitis: urgency and frequency syndrome," *Am Fam Physician*, vol. 64, pp. 1199-206, 2001.
[43] M. G. Wientjes, R. A. Badalament, and J. L. Au, "Use of pharmacologic data and computer simulations to design an efficacy trial of intravesical mitomycin C therapy for superficial bladder cancer," *Cancer Chemother and Pharmacol*, vol. 32, pp. 255-262, 1993.
[44] M. G. Wientjes, R. A. Badalament, R. C. Wang, F. Hassan, and J. L. Au, "Penetration of mitomycin C in human bladder," *Cancer Res*, vol. 53, pp. 3314-20, 1993.
[45] Z. Shen, T. Shen, M. G. Wientjes, M. A. O'Donnell, and J. L. Au, "Intravesical treatments of bladder cancer: review," *Pharm Res*, vol. 25, pp. 1500-10, 2008.
[46] I. Grabnar, M. Bogataj, A. Belic, V. Logar, R. Karba, and A. Mrhar, "Kinetic model of drug distribution in the urinary bladder wall following intravesical instillation," *Int J Pharm*, vol. 322, pp. 52-9, 2006.
[47] J. L. Au, S. H. Jang, and M. G. Wientjes, "Clinical aspects of drug delivery to tumors," *J Control Release*, vol. 78, pp. 81-95, 2002.
[48] J. T. Dalton, M. G. Wientjes, R. A. Badalament, J. R. Drago, and J. L. Au, "Pharmacokinetics of intravesical mitomycin C in superficial bladder cancer patients," *Cancer Res*, vol. 51, pp. 5144-52, 1991.
[49] H. S. Carslaw and J. C. Jaeger, *Conduction of heat in solids*, 2d ed. Oxford,: Clarendon Press, 1959.
[50] J. Crank, *The mathematics of diffusion*, 2d ed. Oxford, [Eng]: Clarendon Press, 1979.
[51] M. G. Wientjes, J. T. Dalton, R. A. Badalament, J. R. Drago, and J. L. Au, "Bladder wall penetration of intravesical mitomycin C in dogs," *Cancer Res*, vol. 51, pp. 4347-54, 1991.
[52] S. P. Petrou, "Dyspareunia response in patients with interstitial cystitis treated with intravesical lidocaine, bicarbonate, and heparin," *Int Braz J Urol*, vol. 34, pp. 247-8, 2008.

[53] B. K. Welk and J. M. Teichman, "Dyspareunia response in patients with interstitial cystitis treated with intravesical lidocaine, bicarbonate, and heparin," *Urology*, vol. 71, pp. 67-70, 2008.
[54] X. Giannakopoulos and P. Champilomatos, "Chronic interstitial cystitis. Successful treatment with intravesical idocaine," *Arch Ital Urol Nefrol Androl*, vol. 64, pp. 337-9, 1992.
[55] B. Asklin and J. Cassuto, "Intravesical lidocaine in severe interstitial cystitis. Case report," *Scand J Urol Nephrol*, vol. 23, pp. 311-2, 1989.
[56] T. Gurpinar, H. Y. Wong, and D. P. Griffith, "Electromotive administration of intravesical lidocaine in patients with interstitial cystitis," *J Endourol*, vol. 10, pp. 443-7, 1996.
[57] A. Voller, D. E. Bidwell, and A. Bartlett, "Enzyme immunoassays in diagnostic medicine. Theory and practice.," *Bull World Health Organ.*, vol. 53, pp. 55-65, 1976.
[58] L. Dirikolu, A. F. Lehner, W. Karpiesiuk, J. D. Harkins, W. E. Woods, W. G. Carter, J. Boyles, M. Fisher, and T. Tobin, "Identification of lidocaine and its metabolites in post-administration equine urine by ELISA and MS/MS," *J Vet Pharmacol Ther*, vol. 23, pp. 215-22, 2000.
[59] J. D. Harkins, G. D. Mundy, W. E. Woods, A. Lehner, W. Karpiesiuk, W. A. Rees, L. Dirikolu, S. Bass, W. G. Carter, J. Boyles, and T. Tobin, "Lidocaine in the horse: its pharmacological effects and their relationship to analytical findings," *J Vet Pharmacol Ther*, vol. 21, pp. 462-76, 1998.
[60] P. Popesko, Rajtova, V.,Horak, J., *Colour Atlas of Anatomy of Small Laboratory Animals*, vol. 1, 1d ed: Saunders Ltd, 2003.
[61] S. C. Gad, *Animal Models in Toxicology*, 2 ed: Informa HealthCare, 2006.
[62] R. E. Chapin and S. E. Smith, "Calcium requirement of growing rabbits," *J Anim Sci*, vol. 26, pp. 67-71, 1967.
[63] P. R. Cheeke and T. J. Cunha, *Rabbit feeding and nutrition*: Academic Press, 1987.
[64] R. E. Chapin and S. E. Smith, "The calcium tolerance of growing and reproducing rabbits," *Cornell Vet*, vol. 57, pp. 480-91, 1967.
[65] P. Besancon and F. Lebas, "True digestive utilization and calcium retention in the growing rabbit receiving a calcium and phosphorus rich diet," *Ann. Zootech.*, vol. 18, pp. 437-443, 1969.
[66] P. R. Cheeke and J. W. Amberg, "Comparative calcium excretion by rats and rabbits," *J Anim Sci*, vol. 37, pp. 450-4, 1973.
[67] A. Kennedy, "The urinary excretion of calcium by normal rabbits," *J. Comp. Pathol.*, vol. 75, pp. 69-74, 1965.
[68] N.R.C., "Nutrient Requirements of Rabbits," in *Natl. Acad. Sci.*, 2 ed. Washington, D. C., 1977, pp. 437-443.
[69] D. T. Beiko, B. E. Knudsen, J. D. Watterson, P. A. Cadieux, G. Reid, and J. D. Denstedt, "Urinary tract biomaterials," *J Urol*, vol. 171, pp. 2438-44, 2004.
[70] H. Fuse, M. Ohkawa, T. Nakashima, and S. Tokunaga, "Crystal adherence to urinary catheter materials in rats," *J Urol*, vol. 151, pp. 1703-6, 1994.
[71] D. Pantazopoulos, P. Karagiannakos, F. Sofras, A. Kostakopoulos, C. Deliveliotis, and C. Dimopoulos, "Effect of drugs on crystal adhesion to injured urothelium," *Urology*, vol. 36, pp. 255-9, 1990.

[72] M. M. Tunney, P. F. Keane, D. S. Jones, and S. P. Gorman, "Comparative assessment of ureteral stent biomaterial encrustation," *Biomaterials*, vol. 17, pp. 1541-6, 1996.
[73] P. Zupkas, C. L. Parsons, C. Percival, and M. Monga, "Pentosanpolysulfate coating of silicone reduces encrustation," *J Endourol*, vol. 14, pp. 483-8, 2000.
[74] F. Cauda, V. Cauda, C. Fiori, B. Onida, and E. Garrone, "Heparin coating on ureteral Double J stents prevents encrustations: an in vivo case study," *J Endourol*, vol. 22, pp. 465-72, 2008.
[75] C. R. Riedl, M. Witkowski, E. Plas, and H. Pflueger, "Heparin coating reduces encrustation of ureteral stents: a preliminary report," *Int J Antimicrob Agents*, vol. 19, pp. 507-10, 2002.
[76] J. D. Watterson, P. A. Cadieux, D. T. Beiko, A. J. Cook, J. P. Burton, R. R. Harbottle, C. Lee, E. Rowe, H. Sidhu, G. Reid, and J. D. Denstedt, "Oxalate-degrading enzymes from Oxalobacter formigenes: a novel device coating to reduce urinary tract biomaterial-related encrustation," *J Endourol*, vol. 17, pp. 269-74, 2003.
[77] M. J. Cousins and P. O. Bridenbaugh, *Neural Blockade in Clinical Anesthesia and Management of Pain*, 3 ed: Lippincott Williams & Wilkins, 1998.
[78] J. E. Prentiss, "Cardiac arrest following caudal anesthesia," *Anesthesiology*, vol. 50, pp. 51-3, 1979.
[79] J. E. Barsa, M. Batra, B. R. Fink, and S. M. Sumi, "Prolonged neural blockade following regional analgesia with 2-chloroprocaine," *Anesth Analg*, vol. 61, pp. 961, 1982.
[80] A. R. Gammaitoni, N. A. Alvarez, and B. S. Galer, "Safety and tolerability of the lidocaine patch 5%, a targeted peripheral analgesic: a review of the literature," *J Clin Pharmacol*, vol. 43, pp. 111-7, 2003.
[81] A. R. Gammaitoni, N. A. Alvarez, and B. S. Galer, "Pharmacokinetics and safety of continuously applied lidocaine patches 5%," *Am J Health Syst Pharm*, vol. 59, pp. 2215-20, 2002.
[82] A. R. Gammaitoni and M. W. Davis, "Pharmacokinetics and tolerability of lidocaine patch 5% with extended dosing," *Ann Pharmacother*, vol. 36, pp. 236-40, 2002.
[83] A. M. Comer and H. M. Lamb, "Lidocaine patch 5%," *Drugs*, vol. 59, pp. 245-9; discussion 250-1, 2000.
[84] D. K. Macintire, D. K. J., S. C. Haskins, and W. D. Saxon, *Manual of Small Animal Emergency and Critical Care Medicine*: Blackwell Publishing, 2004.
[85] O. G. Ananiadou, G. E. Drossos, K. N. Bibou, G. M. Palatianos, and E. O. Johnson, "Acute regional neuronal injury following hypothermic circulatory arrest in a porcine model," *Interact Cardiovasc Thorac Surg*, vol. 4, pp. 597-601, 2005.
[86] W. Berman, Jr. and J. Musselman, "The relationship of age to the metabolism and protein binding of digoxin in sheep," *J Pharmacol Exp Ther*, vol. 208, pp. 263-6, 1979.
[87] L. V. Evans, *Biofilms: Recent Advances in Their Study and Control*: CRC Press, 2000.

Appendix

Appendix 1. MATLAB code for the deformation of elastic circular ring

```
% R. Frisch-Fay, The deformation of elastic circular rings. Australian J of
Applied Science, 11, 1960, pp. 329-340.

close all
clear all

%F(phi,m) = int(1/sqrt(1-m*sin(t)^2), t=0..phi);
%E(phi,m) = int(sqrt(1-m*sin(t)^2), t=0..phi);
%[K_complete,E_complete] = elliptic12(pi/2, p.^2);
%[F,E] = elliptic12(angle, p.^2);

%1) Nodal Elastica
% 0 < P < 0.3148EI/r^2
clear all
SIZE=5000;
i=0;

m=linspace(10^-10,1,SIZE);

[F,E] = elliptic12(pi/4, m);
p=m.^(1/2);


NF1=(8/pi^2)*m.*F.^2;
ND1=1-sqrt(2*NF1.^-1).*(2*E.*p.^(-1)-F.*(2*p.^-1-p));

for i=2:SIZE-1
   slopey1(i)=(NF1(i+1)-NF1(i))/(ND1(i+1)-ND1(i));
   slopex1(i)=(ND1(i+1)+ND1(i))/2;
end

NF1(1)=0;
ND1(1)=0;

%if p=1, ND1=0.0504 and NF1=0.6297

% ================================================================= %
% 2) Oval shape
% 0.3148EI/r^2 < P < 1.3932EI/r^2

p=linspace(1/sqrt(2),1,SIZE);
Ob=(asin( (p.^-1)*(1/sqrt(2)) ));

[F,E] = elliptic12(Ob, p.^2);

NF2=8/pi^2*F.^2;
ND2=1-sqrt(2*NF2.^-1).*(2*E-F);

for i=1:SIZE-1
```

```
   slopey2(i)=(NF2(i+1)-NF2(i))/(ND2(i+1)-ND2(i));
   slopex2(i)=(ND2(i+1)+ND2(i))/2;
end
plot(slopex2,slopey2)


%if p=1/sqrt(2), ND2=0.2822, and NF2=2.7864

% ================================================================= %

% 3) Peanut shape
% 1.39EI/r^2 < P
SIZE=5000;
p=linspace(1/sqrt(2),1,SIZE);
Ob=(asin( (p.^-1)*(1/sqrt(2)) ));

[F,E] = elliptic12(Ob, p.^2);
[Kc3,Ec3] = elliptic12(pi/2, p.^2);


NF3=8/pi^2*(2*Kc3-F).^2;
ND3=1-sqrt(2*NF3.^-1).*(4*Ec3-2*Kc3-2*E+F);


for i=1:SIZE
    if ND3(i)>1
        break
    end
end

max3=i-1;   % Compression only when ND3<1;

NF3=NF3(1:max3);
ND3=ND3(1:max3);

for i=1:max3-1
   slopey3(i)=(NF3(i+1)-NF3(i))/(ND3(i+1)-ND3(i));
   slopex3(i)=(ND3(i+1)+ND3(i))/2;
end

%if p=1/sqrt(2), ND3=0.2822, and NF3=2.7864


% ================================================================= %
figure(1)
plot(ND1,NF1,'b.',ND2,NF2,'r.',ND3,NF3,'g.');
xlabel('Dimensionless Compression (delta/r)')
ylabel('Dimensionless Force (F*r^2/EI)')

% ================================================================= %

figure(2)
plot(slopex1,slopey1,'b.',slopex2,slopey2,'r.',slopex3,slopey3,'g.');
```

```
xlabel('Dimensionless Compression (delta/r)')
ylabel('Slope of tangent line ((F*r^2/EI)/(delta/r))')

% Axes: Helvetica Font 14
% Label: Microsoft Sans Serif Font 16



function [F,E,Z] = elliptic12(u,m,tol)
% ELLIPTIC12 evaluates the value of the Incomplete Elliptic Integrals
% of the First, Second Kind and Jacobi's Zeta Function.
%
%   [F,E,Z] = ELLIPTIC12(U,M,TOL) where U is a phase in radians, 0<M<1 is
%   the module and TOL is the tolerance (optional). Default value for
%   the tolerance is eps = 2.220e-16.
%
%   ELLIPTIC12 uses the method of the Arithmetic-Geometric Mean
%   and Descending Landen Transformation described in [1] Ch. 17.6,
%   to determine the value of the Incomplete Elliptic Integrals
%   of the First, Second Kind and Jacobi's Zeta Function [1], [2].
%
%       F(phi,m) = int(1/sqrt(1-m*sin(t)^2), t=0..phi);
%       E(phi,m) = int(sqrt(1-m*sin(t)^2), t=0..phi);
%       Z(phi,m) = E(u,m) - E(m)/K(m)*F(phi,m).
%
%   Tables generating code ([1], pp. 613-621):
%       [phi,alpha] = meshgrid(0:5:90, 0:2:90);                  % modulus
and phase in degrees
%       [F,E,Z] = elliptic12(pi/180*phi, sin(pi/180*alpha).^2);  % values of
integrals
%
%   See also ELLIPKE, ELLIPJ, ELLIPTIC3, THETA, AGM.
%
%   References:
%   [1] M. Abramowitz and I.A. Stegun, "Handbook of Mathematical Functions",
%       Dover Publications", 1965, Ch. 17.1 - 17.6 (by L.M. Milne-Thomson).
%   [2] D. F. Lawden, "Elliptic Functions and Applications"
%       Springer-Verlag, vol. 80, 1989

%   For support, please reply to
%       moiseev[at]sissa.it, moiseev.igor[at]gmail.com
%       Moiseev Igor,
%       34106, SISSA, via Beirut n. 2-4,  Trieste, Italy
%
%   The code is optimized for ordered inputs produced by the functions
%   meshgrid, ndgrid. To obtain maximum performace (up to 30%) for singleton,
%   1-dimensional and random arrays remark call of the function unique(.)
%   and edit further code.

if nargin<3, tol = eps; end
if nargin<2, error('Not enough input arguments.'); end

if ~isreal(u) || ~isreal(m)
    error('Input arguments must be real.')
end
```

```
if length(m)==1, m = m(ones(size(u))); end
if length(u)==1, u = u(ones(size(m))); end
if ~isequal(size(m),size(u)), error('U and M must be the same size.'); end

F = zeros(size(u));
E = F;
Z = E;
m = m(:).';    % make a row vector
u = u(:).';

if any(m < 0) || any(m > 1), error('M must be in the range 0 <= M <= 1.');
end

I = uint32( find(m ~= 1 & m ~= 0) );
if ~isempty(I)
    [mu,J,K] = unique(m(I));   % extracts unique values from m
    K = uint32(K);
    mumax = length(mu);
    signU = sign(u(I));

    % pre-allocate space and augment if needed
    chunk = 7;
    a = zeros(chunk,mumax);
    c = a;
    b = a;
    a(1,:) = ones(1,mumax);
    c(1,:) = sqrt(mu);
    b(1,:) = sqrt(1-mu);
    n = uint32( zeros(1,mumax) );
    i = 1;
    while any(abs(c(i,:)) > tol)   % Arithmetic-Geometric Mean of A, B and C
        i = i + 1;
        if i > size(a,1)
          a = [a; zeros(2,mumax)];
          b = [b; zeros(2,mumax)];
          c = [c; zeros(2,mumax)];
        end
        a(i,:) = 0.5 * (a(i-1,:) + b(i-1,:));
        b(i,:) = sqrt(a(i-1,:) .* b(i-1,:));
        c(i,:) = 0.5 * (a(i-1,:) - b(i-1,:));
        in = uint32( find((abs(c(i,:)) <= tol) & (abs(c(i-1,:)) > tol)) );
        if ~isempty(in)
          [mi,ni] = size(in);
          n(in) = ones(mi,ni)*(i-1);
        end
    end

    mmax = length(I);
    mn = double(max(n));
    phin = zeros(1,mmax);     C  = zeros(1,mmax);
    Cp = C;  e  = uint32(C);  phin(:) = signU.*u(I);
    i = 0;   c2 = c.^2;
    while i < mn                  % Descending Landen Transformation
        i = i + 1;
        in = uint32(find(n(K) > i));
        if ~isempty(in)
```

```
            phin(in) = atan(b(i,K(in))./a(i,K(in)).*tan(phin(in))) + ...
                pi.*ceil(phin(in)/pi - 0.5) + phin(in);
            e(in) = 2.^(i-1) ;
            C(in) = C(in)  + double(e(in(1)))*c2(i,K(in));
            Cp(in)= Cp(in) + c(i+1,K(in)).*sin(phin(in));
        end
    end

  Ff = phin ./ (a(mn,K).*double(e)*2);
 F(I) = Ff.*signU;              % Incomplete Ell. Int. of the First Kind
 Z(I) = Cp.*signU;              % Jacobi Zeta Function
 E(I) = (Cp + (1 - 1/2*C) .* Ff).*signU;
                                % Incomplete Ell. Int. of the Second Kind
end

% Special cases: m ={0,1}
m0 = find(m == 0);
if ~isempty(m0), F(m0) = u(m0); E(m0) = u(m0); Z(m0) = 0; end

m1 = find(m == 1);
um1 = abs(u(m1));
if ~isempty(m1),
    N = floor( (um1+pi/2)/pi );
    M = find(um1 < pi/2);

    F(m1(M)) = log(tan(pi/4 + u(m1(M))/2));
    F(m1(um1 >= pi/2)) = Inf.*sign(u(m1(um1 >= pi/2)));

    E(m1) = ((-1).^N .* sin(um1) + 2*N).*sign(u(m1));

    Z(m1) = (-1).^N .* sin(u(m1));
end
```

Appendix 2. Control rabbit diet

Laboratory Rabbit Diet HF 5326*

DESCRIPTION

Laboratory Rabbit Diet HF (High Fiber) is a complete rabbit diet formulated for use where research animals are held under maintenance conditions during the investigation period and free-choice feeding is desired. Not intended for use when reproduction, lactation and growth are major goals. Refer to the Shelf Life section at the end of this book for product longevity information and storage suggestions.

Features and Benefits

- High fiber content allows free-choice feeding without excessive weight gains
- Nutritionally complete diet

Product Forms Available

- Pellet, 4 mm (5/32") diameter x 10 mm (3/8") length
- Meal (ground pellets), special order

GUARANTEED ANALYSIS

Crude protein not less than	14.0%
Crude fat not less than	1.5%
Crude fiber not more than	25.0%
Ash not more than	10.0%
Added minerals not more than	1.5%

INGREDIENTS

Dehydrated alfalfa meal, ground soybean hulls, wheat middlings, cane molasses, dehulled soybean meal, ground corn, dicalcium phosphate, monocalcium phosphate, salt, porcine animal fat preserved with BHA, calcium carbonate, DL-methionine, choline chloride, magnesium oxide, vitamin A acetate, folic acid, cholecalciferol, pyridoxine hydrochloride, dl-alpha tocopheryl acetate, calcium pantothenate, nicotinic acid, riboflavin, cyanocobalamin, manganous oxide, zinc oxide, cobalt carbonate, ferrous carbonate, copper sulfate, zinc sulfate, calcium iodate, sodium selenite.

FEEDING DIRECTIONS

Laboratory Rabbit Diet HF should be fed free-choice to maintain animals. If animals become obese it may be necessary to restrict the level of feed intake. Levels of feed intake of 150–200 grams per day, depending on body size and condition have been used to maintain body weight. Plenty of clean, fresh water should be available to the animals at all times.

CHEMICAL COMPOSITION[1]

Nutrients[2]	
Protein, %	**14.8**
Arginine, %	0.70
Cystine, %	0.18
Glycine, %	0.54
Histidine, %	0.38
Isoleucine, %	0.75
Leucine, %	0.99
Lysine, %	0.76
Methionine, %	0.33
Phenylalanine, %	0.77
Tyrosine, %	0.57
Threonine, %	0.53
Tryptophan, %	0.20
Valine, %	0.84
Serine, %	0.77
Aspartic Acid, %	1.73
Glutamic Acid, %	2.89
Alanine, %	0.70
Proline, %	1.16
Taurine, %	<0.01
Fat (ether extract), %	**2.3**
Fat (acid hydrolysis), %	**3.5**
Cholesterol, ppm	<10
Linoleic Acid, %	0.84
Linolenic Acid, %	0.24
Arachidonic Acid, %	<0.01
Omega-3 Fatty Acids, %	0.24
Total Saturated Fatty Acids, %	0.60
Total Monounsaturated Fatty Acids, %	0.52
Fiber (Crude), %	**22.5**
Neutral Detergent Fiber[3], %	41.8
Acid Detergent Fiber[4], %	27.3
Nitrogen-Free Extract (by difference), %	**42.8**
Starch, %	9.4
Glucose, %	0.27
Fructose, %	0.92
Sucrose, %	3.10
Lactose, %	0.00
Total Digestible Nutrients, %	**63.2**
Gross Energy, kcal/gm	**2.95**
Physiological Fuel Value[5], kcal/gm	**2.51**
Metabolizable Energy, kcal/gm	**2.01**

Minerals	
Ash, %	**6.8**
Calcium, %	0.95
Phosphorus, %	0.51
Phosphorus (non-phytate), %	0.33
Potassium, %	1.85
Magnesium, %	0.30
Sulfur, %	0.23
Sodium, %	0.25
Chlorine, %	0.62
Fluorine, ppm	14
Iron, ppm	400
Zinc, ppm	120
Manganese, ppm	130
Copper, ppm	20
Cobalt, ppm	1.7
Iodine, ppm	1.6
Chromium, ppm	1.4
Selenium, ppm	0.48

Vitamins	
Carotene, ppm	18
Vitamin K (as menadione), ppm	3.4
Thiamin Hydrochloride, ppm	5.3
Riboflavin, ppm	6.5
Niacin, ppm	52
Pantothenic Acid, ppm	19
Choline Chloride, ppm	1600
Folic Acid, ppm	7.4
Pyridoxine, ppm	4.5
Biotin, ppm	0.30
B_{12}, mcg/kg	7.0
Vitamin A, IU/gm	20
Vitamin D_3 (added), IU/gm	1.1
Vitamin E, IU/kg	48
Ascorbic Acid, mg/gm	—

Calories provided by:	
Protein, %	23.541
Fat (ether extract), %	8.302
Carbohydrates, %	68.157

*Product Code

1. Based on the latest ingredient analysis information. Since nutrient composition of natural ingredients varies, analysis will differ accordingly.
2. Nutrients expressed as percent of ration except where otherwise indicated. Moisture content is assumed to be 10.0% for the purpose of calculations.
3. NDF = approximately cellulose, hemi-cellulose and lignin.
4. ADF = approximately cellulose and lignin.
5. Physiological Fuel Value (kcal/gm) = Sum of decimal fractions of protein, fat and carbohydrate (use Nitrogen Free Extract) x 4, 9, 4 kcal/gm respectively.

LabDiet
www.labdiet.com

Appendix 3. Low calcium rabbit diet

Modified LabDiet 5321 w/ Reduced Calcium — 5S4T

DESCRIPTION

Modified LabDiet® Laboratory Rabbit Diet 5321with Reduced Calcium (0.50 to 0.55% Ca).

Storage conditions are particularly critical to TestDiet® products, due to the absence of antioxidants or preservative agents. To provide maximum protection against possible changes during storage, store in a dry, cool location. Storage under refrigeration (2° C) is recommended. Maximum shelf life is six months. (If long term studies are involved, storing the diet at -20° C or colder may prolong shelf life.) Be certain to keep in air tight containers.

*Product Forms Available**	*Catalog #*
3/16" Pellet	1812909

**Other Forms Available On Request*

INGREDIENTS

Dehydrated Alfalfa Meal, Wheat Middlings, Ground Corn, Ground Oats, Dehulled Soybean Meal, Ground Soybean Hulls, Cane Molasses, Salt, 5S4T Vitamin & Mineral Premix, Soybean Oil, DL-Methionine, Dicalcium Phosphate, Choline Chloride.

FEEDING DIRECTIONS

Feed ad libitum. Plenty of fresh, clean water should be available at all times.

CAUTION:
Perishable - store upon receipt.
For laboratory animal use only; not for human consumption.

1/14/2008

NUTRITIONAL PROFILE [1]

Protein, %	***17.0***
Arginine, %	0.90
Histidine, %	0.40
Isoleucine, %	0.90
Leucine, %	1.29
Lysine, %	0.80
Methionine, %	0.37
Cystine, %	0.23
Phenylalanine, %	0.82
Tyrosine, %	0.53
Threonine, %	0.62
Tryptophan, %	0.21
Valine, %	0.87
Alanine, %	0.81
Aspartic Acid, %	1.78
Glutamic Acid, %	3.27
Glycine, %	0.75
Proline, %	1.30
Serine, %	0.82
Taurine, %	0.00
Fat (ether extract), %	***2.8***
Fat (acid hydrolysis), %	***4.1***
Cholesterol, ppm	0
Linoleic Acid, %	1.32
Linolenic Acid, %	0.25
Arachidonic Acid, %	0.00
Omega-3 Fatty Acids, %	0.25
Total Saturated Fatty Acids, %	0.52
Total Monounsaturated Fatty Acids, %	0.61
Polyunsaturated Fatty Acids, %	1.23
Fiber (max), %	***14.7***
Neutral Detergent Fiber[2], %	30.6
Acid Detergent Fiber[3], %	17.9
Nitrogen-Free Extract (by difference), %	***48.9***
Starch, %	25.51
Glucose, %	0.33
Fructose, %	0.89
Sucrose, %	2.39
Lactose, %	0.00
Total Digestible Nutrients, %	**65.4**
Energy (kcal/g) [4]	**2.89**

From:	kcal	%
Protein	0.680	23.6
Fat (ether extract)	0.252	8.7
Carbohydrates	1.955	67.7

Minerals	
Ash, %	**6.6**
Calcium, %	0.51
Phosphorus, %	0.44
Phosphorus (available), %	0.20
Potassium, %	1.20
Magnesium, %	0.39
Sulfur, %	0.24
Sodium, %	0.30
Chloride, %	0.65
Fluorine, ppm	3.3
Iron, ppm	276
Zinc, ppm	120
Manganese, ppm	122
Copper, ppm	18
Cobalt, ppm	1.26
Iodine, ppm	1.61
Chromium, ppm	0.69
Selenium, ppm	0.43

Vitamins	
Carotene, ppm	30.7
Vitamin A, IU/g	20
Vitamin D-3 (added), IU/g	1.1
Vitamin E, IU/kg	48
Vitamin K (as menadione), ppm	2.9
Thiamin Hydrochloride, ppm	6
Riboflavin, ppm	5.5
Niacin, ppm	54
Pantothenic Acid, ppm	19
Folic Acid, ppm	8.5
Pyridoxine, ppm	4.50
Biotin, ppm	0.3
Vitamin B-12, mcg/kg	7
Choline Chloride, ppm	1,600
Ascorbic Acid, ppm	0

1. Based on the latest ingredient analysis information. Since nutrient composition of natural ingredients varies, analysis will differ accordingly. Nutrients expressed as percent of ration on an As-Fed basis except where otherwise indicated. Moisture content is assumed to be 10.0% for the purpose of calculations.
2. NDF = approximately cellulose, hemi-cellulose and lignin.
3. ADF = approximately cellulose and lignin.
4. Energy (kcal/gm) - Sum of decimal fractions of protein, fat and carbohydrate x 4,9,4 kcal/gm respectively.

ISO 9001:2000

TestDiet
www.testdiet.com